Global maps of soil temperature

Reference:
Lembrechts Jonas, van den Hoogen Johan, Aalto Juha, Ashcroft Michael B., De Frenne Pieter, Kemppinen Julia, Kopecký Martin, Luoto Miska, Maclean Ilya M.D., Crowther Thomas W., ...- Global maps of soil temperature
EcoEvoRxiv, 2021, 65 p.
Full text (Publisher's DOI): https://doi.org/10.32942/OSF.IO/PKSQW
To cite this reference: https://hdl.handle.net/10067/1833250151162165141

Global maps of soil temperature

Running head: Global maps of soil temperature

Jonas J. Lembrechts[1,*,x], Johan van den Hoogen[2,*], Juha Aalto[3,4], Michael B. Ashcroft[5,6], Pieter De Frenne[7], Julia Kemppinen[8], Martin Kopecký[9,10], Miska Luoto[4], Ilya M. D. Maclean[11], Thomas W. Crowther[2], Joseph J. Bailey[12], Stef Haesen[13], David H. Klinges[14,15], Pekka Niittynen[4], Brett R. Scheffers[16], Koenraad Van Meerbeek[13], Peter Aartsma[17], Otar Abdalaze[18], Mehdi Abedi[19], Rien Aerts[20], Negar Ahmadian[19], Antje Ahrends[21], Juha M. Alatalo[22], Jake M. Alexander[23], Camille Nina Allonsius[24], Jan Altman[9], Christof Ammann[25], Christian Andres[26], Christopher Andrews[27], Jonas Ardö[28], Nicola Arriga[29], Alberto Arzac[30], Valeria Aschero[31,32], Rafael L. Assis[33], Jakob Johann Assmann[34,35], Maaike Y. Bader[36], Khadijeh Bahalkeh[19], Peter Barančok[37], Isabel C. Barrio[38], Agustina Barros[39], Matti Barthel[26], Edmund W. Basham[14], Marijn Bauters[40], Manuele Bazzichetto[41], Luca Belelli Marchesini[42], Michael C. Bell[43], Juan C. Benavides[44], José Luis Benito Alonso[45], Bernd J. Berauer[46,47], Jarle W. Bjerke[48], Robert G. Björk[49,50], Mats P. Björkman[49,50], Katrin Björnsdóttir[51], Benjamin Blonder[52], Pascal Boeckx[40], Julia Boike[53,54], Stef Bokhorst[20], Bárbara N. S. Brum[55], Josef Brůna[9], Nina Buchmann[26], Pauline Buysse[56], José Luís Camargo[57], Otávio C. Campoe[58], Onur Candan[59], Rafaella Canessa[60,61], Nicoletta Cannone[62], Michele Carbognani[63], Jofre Carnicer[64,65], Angélica Casanova-Katny[66], Simone Cesarz[67,68], Bogdan Chojnicki[69,69], Philippe Choler[70,71], Steven L. Chown[72], Edgar F. Cifuentes[73], Marek Čiliak[74], Tamara Contador[75,76], Peter Convey[77], Elisabeth J. Cooper[78], Edoardo Cremonese[79], Salvatore R. Curasi[80], Robin Curtis[11], Maurizio Cutini[81], C. Johan Dahlberg[82,83], Gergana N. Daskalova[84], Miguel Angel de Pablo[85], Stefano Della Chiesa[86], Jürgen Dengler[87,88,67], Bart Deronde[89], Patrice Descombes[90], Valter Di Cecco[91], Michele Di Musciano[92], Jan Dick[27], Romina D. Dimarco[93,94], Jiri Dolezal[9,95], Ellen Dorrepaal[96], Jiří Dušek[97], Nico Eisenhauer[67,68], Lars Eklundh[28], Brian Enquist[98], Todd E. Erickson[99,100], Brigitta Erschbamer[101], Werner Eugster[26], Robert M. Ewers[102], Dan A. Exton[103], Nicolas Fanin[104], Fatih Fazlioglu[59], Iris Feigenwinter[26], Giuseppe Fenu[105], Olga Ferlian[67,68], M. Rosa Fernández Calzado[106], Eduardo Fernández-Pascual[107], Manfred Finckh[108], Rebecca Finger Higgens[109], T'ai G. W. Forte[63], Erika C. Freeman[110], Esther R. Frei[111,112], Eduardo Fuentes-Lillo[113,1,114], Rafael A. García[113,115], María B. García[116], Charly Géron[117], Mana Gharun[26], Dany Ghosn[118], Khatuna Gigauri[119], Anne Gobin[120,121], Ignacio Goded[29], Mathias Goeckede[122], Felix Gottschall[67,68], Keith Goulding[123], Sanne Govaert[7], Bente Jessen Graae[124], Sarah Greenwood[125], Caroline Greiser[82], Achim Grelle[126], Benoit Guénard[127], Mauro Guglielmin[128], Joannès Guillemot[129,130], Peter Haase[131,132], Sylvia Haider[133,67], Aud H. Halbritter[134], Maroof Hamid[135], Albin Hammerle[136], Arndt Hampe[137], Siri V. Haugum[134,138], Lucia Hederová[9], Bernard Heinesch[139], Carole Helfter[140], Daniel Hepenstrick[87], Maximiliane Herberich[141], Mathias Herbst[142], Luise Hermanutz[143], David S. Hik[144], Raúl Hoffrén[145], Jürgen Homeier[146], Lukas Hörtnagl[26], Toke T. Høye[147], Filip Hrbacek[148], Kristoffer Hylander[82], Hiroki Iwata[149], Marcin Antoni Jackowicz-Korczynski[150,28], Hervé Jactel[151], Järvi Järveoja[152], Janusz Olejnik[153], Szymon Jastrzębowski[154], Anke Jentsch[47,155], Juan J. Jiménez[156], Ingibjörg S. Jónsdóttir[157], José João L. L. Souza[158], Tommaso Jucker[159], Alistair S. Jump[160], Radoslaw Juszczak[69], Róbert Kanka[37], Vít Kašpar[9,161], George Kazakis[118], Julia Kelly[162], Anzar A. Khuroo[135], Leif Klemedtsson[49], Marcin Klisz[154], Natascha Kljun[162], Alexander Knohl[163], Johannes Kobler[164], Jozef Kollár[37], Olaf Kolle[165], Martyna M. Kotowska[146], Bence Kovács[166], Juergen Kreyling[167], Andrea Lamprecht[168], Simone I. Lang[169], Christian Larson[170], Keith Larson[171], Kamil Laska[148,172], Guerric le Maire[129,130], Rachel I. Leihy[173], Luc Lens[174], Bengt Liljebladh[49], Annalea Lohila[175,176], Juan Lorite[106,177], Benjamin Loubet[56], Joshua Lynn[134], Martin Macek[9], Roy Mackenzie[75], Enzo Magliulo[178], Regine Maier[26], Francesco Malfasi[62], František Máliš[179], Matěj Man[9], Giovanni Manca[29], Antonio Manco[180], Tanguy Manise[139], Paraskevi Manolaki[181,182,183], Felipe Marciniak[55], Marianna Nardino[184], Radim Matula[10,185], Ana Clara Mazzolari[32], Sergiy Medinets[186,187,188], Volodymyr Medinets[186], Camille Meeussen[7], Sonia Merinero[82], Rita de Cássia Guimarães Mesquita[189], Katrin Meusburger[190], Filip J. R. Meysman[191], Sean T. Michaletz[192], Ann Milbau[193], Dmitry Moiseev[194], Pavel Moiseev[194], Andrea Mondoni[195], Ruth Monfries[21], Leonardo Montagnani[196], Mikel Moriana-Armendariz[78], Umberto Morra di Cella[197], Martin Mörsdorf[198], Jonathan R. Mosedale[199], Lena Muffler[146], Miriam Muñoz-Rojas[200,99], Jonathan A. Myers[201], Isla H.

Myers-Smith[84], Laszlo Nagy[202], Ilona Naujokaitis-Lewis[203], Emily Newling[204], Lena Nicklas[101], Georg Niedrist[205], Armin Niessner[206], Mats B. Nilsson[152], Signe Normand[34,35], Marcelo D. Nosetto[207,208], Yann Nouvellon[129,130], Martin A. Nuñez[209,94], Romà Ogaya[210,211], Jérôme Ogée[104], Joseph Okello[40,212,213], Jørgen Eivind Olesen[214], Øystein Opedal[215], Simone Orsenigo[216], Andrej Palaj[37], Timo Pampuch[217], Alexey V. Panov[218], Meelis Pärtel[219], Ada Pastor[220,182], Aníbal Pauchard[113,115], Harald Pauli[168], Marian Pavelka[97], William D. Pearse[221,222], Matthias Peichl[152], Loïc Pellissier[223,224], Rachel M. Penczykowski[225], Josep Penuelas[210,211], Matteo Petit Bon[169,78,9], Alessandro Petraglia[63], Shyam S. Phartyal[226], Gareth K. Phoenix[227], Casimiro Pio[228], Andrea Pitacco[229], Camille Pitteloud[223,224], Roman Plichta[185], Francesco Porro[195], Miguel Portillo-Estrada[1], Jérôme Poulenard[230], Rafael Poyatos[65,231], Anatoly S. Prokushkin[218,30], Radoslaw Puchalka[232,233], Mihai Pușcaș[234,235,236], Dajana Radujković[1], Krystal Randall[237], Amanda Ratier Backes[133,67], Sabine Remmele[206], Wolfram Remmers[238], David Renault[41,239], Anita C. Risch[240], Christian Rixen[111], Sharon A. Robinson[241], Bjorn J.M. Robroek[242], Adrian V. Rocha[243], Christian Rossi[244,245], Graziano Rossi[195], Olivier Roupsard[246,247,248], Alexey V. Rubtsov[30], Patrick Saccone[168], Clotilde Sagot[249], Jhonatan Sallo Bravo[250,251], Cinthya C. Santos[252], Judith M. Sarneel[253], Tobias Scharnweber[217], Jonas Schmeddes[167], Marius Schmidt[254], Thomas Scholten[255], Max Schuchardt[47], Naomi Schwartz[256], Tony Scott[123], Julia Seeber[205,257], Ana Cristina Segalin de Andrade[252], Tim Seipel[170], Philipp Semenchuk[258], Rebecca A. Senior[259], Josep M. Serra-Diaz[260], Piotr Sewerniak[261], Ankit Shekhar[26], Nikita V. Sidenko[218], Lukas Siebicke[163], Laura Siegwart Collier[143,262], Elizabeth Simpson[221], David P. Siqueira[263], Zuzana Sitková[264], Johan Six[26], Marko Smiljanic[217], Stuart W. Smith[124,265], Sarah Smith-Tripp[266], Ben Somers[267], Mia Vedel Sørensen[124], Bartolomeu Israel Souza[268], Arildo Souza Dias[269,252], Marko J. Spasojevic[270], James D. M. Speed[271], Fabien Spicher[272], Angela Stanisci[273], Klaus Steinbauer[168], Rainer Steinbrecher[274], Michael Steinwandter[205], Michael Stemkovski[221], Jörg G. Stephan[275], Christian Stiegler[163], Stefan Stoll[238,276], Martin Svátek[185], Miroslav Svoboda[10], Torbern Tagesson[28,277], Andrew J. Tanentzap[110], Franziska Tanneberger[278], Jean-Paul Theurillat[279,280], Haydn J. D. Thomas[84], Andrew D. Thomas[281], Katja Tielbörger[61], Marcello Tomaselli[63], Urs Albert Treier[34,35], Mario Trouillier[217], Pavel Dan Turtureanu[234,282,236], Rosamond Tutton[283], Vilna A. Tyystjärvi[4,3], Masahito Ueyama[284], Karol Ujházy[179], Mariana Ujházyová[74], Domas Uogintas[285], Anastasiya Vladimirovna Urban[218,185], Josef Urban[185,30], Marek Urbaniak[153], Tudor-Mihai Ursu[286], Francesco Primo Vaccari[287], Stijn Van de Vondel[288], Liesbeth van den Brink[61], Maarten Van Geel[289], Vigdis Vandvik[134], Pieter Vangansbeke[7], Andrej Varlagin[290], G.F. (Ciska) Veen[291], Elmar Veenendaal[292], Susanna E. Venn[293], Hans Verbeeck[294], Erik Verbrugggen[1], Frank G.A. Verheijen[295], Luis Villar[296], Luca Vitale[297], Pascal Vittoz[298], Maria Vives-Ingla[65], Jonathan von Oppen[34,35], Josefine Walz[96], Runxi Wang[127], Yifeng Wang[283], Robert G. Way[283], Ronja E. M. Wedegärtner[124], Robert Weigel[146], Jan Wild[9,161], Matthew Wilkinson[43], Martin Wilmking[217], Lisa Wingate[104], Manuela Winkler[168], Sonja Wipf[244], Georg Wohlfahrt[136], Georgios Xenakis[299], Yan Yang[300], Zicheng Yu[301,302], Kailiang Yu[303], Florian Zellweger[112], Jian Zhang[304,305], Zhaochen Zhang[304], Peng Zhao[152], Klaudia Ziemblińska[153], Reiner Zimmermann[206,306], Shengwei Zong[307], Viacheslav I. Zyryanov[218], Ivan Nijs[1], Jonathan Lenoir[272,+,x]

* These authors contributed equally to this work

[x] Corresponding authors

[+] These authors contributed equally to this work

** See end of manuscript for affiliations

Corresponding authors

Jonas Lembrechts (Jonas.lembrechts@uantwerpen.be, https://orcid.org/0000-0002-1933-0750).

Jonathan Lenoir (jonathan.lenoir@u-picardie.fr, https://orcid.org/0000-0003-0638-9582).

Abstract

Research in global change ecology relies heavily on global climatic grids derived from estimates of air temperature in open areas at around 2 m above the ground. These climatic grids thus fail to reflect conditions below vegetation canopies and near the ground surface, where critical ecosystem functions are controlled and most terrestrial species reside. Here we provide global maps of soil temperature and bioclimatic variables at a 1-km² resolution for 0–5 and 5–15 cm depth. These maps were created by calculating the difference (i.e., offset) between *in-situ* soil temperature measurements, based on time series from over 1200 1-km² pixels (summarized from 8500 unique temperature sensors) across all of the world's major terrestrial biomes, and coarse-grained air temperature estimates from ERA5-Land (an atmospheric reanalysis by the European Centre for Medium-Range Weather Forecasts). We show that mean annual soil temperature differs markedly from the corresponding 2 m gridded air temperature, by up to 10°C (mean = 3.0 ± 2.1°C), with substantial variation across biomes and seasons. Over the year, soils in cold and/or dry biomes are substantially warmer (3.6 ± 2.3°C warmer than gridded air temperature), whereas soils in warm and humid environments are on average slightly cooler (0.7 ± 2.3°C cooler). The observed substantial and biome-specific offsets underpin that the projected impacts of climate and climate change on biodiversity and ecosystem functioning are inaccurately assessed when air rather than soil temperature is used, especially in cold environments. The global soil-related bioclimatic variables provided here are an important step forward for any application in ecology and related disciplines. Nevertheless, we highlight the need to fill remaining global gaps by collecting more *in-situ* measurements of microclimate conditions to further enhance the spatiotemporal resolution of global soil temperature products for ecological applications.

Keywords: microclimate, bioclimatic variables, soil temperature, global maps, temperature offset, soil-dwelling organisms, near-surface temperatures

Introduction

With the rapidly increasing availability of big data on species distributions, functional traits and ecosystem functioning (Bond-Lamberty & Thomson, 2018, Bruelheide *et al.*, 2018, Kissling *et al.*, 2018, Kattge *et al.*, 2019, Lenoir *et al.*, 2020), we can now study biodiversity and ecosystem responses to global changes in unprecedented detail (Senior *et al.*, 2019, Steidinger *et al.*, 2019, Van Den Hoogen *et al.*, 2019, Antão *et al.*, 2020). However, despite this increasing availability of ecological data, most spatially-explicit studies of ecological, biophysical and biogeochemical processes still make use of the same global gridded temperature data (Soudzilovskaia *et al.*, 2015, Van Den Hoogen *et al.*, 2019, Du *et al.*, 2020). Most of these gridded air temperature datasets are based on long-term climatologies of rather coarse spatiotemporal resolutions: monthly and annual means, or bioclimatic derivatives, based on 30-yr time series averaged within 1 km to 50 km grid cells. Additionally, these coarse temperature grids are constructed based on measurements from standard meteorological stations that record free-air temperature inside well-ventilated protective shields placed up to 2 m above-ground in open, shade-free habitats, where abiotic conditions may differ substantially from those actually experienced by most organisms (World Meteorological Organization, 2008, Lembrechts *et al.*, 2020).

Ecological patterns and processes often relate more directly to below-canopy soil temperature rather than to well-ventilated air temperature inside a weather station. Near-surface, rather than air, temperature better predicts ecosystem functions like biogeochemical cycling (e.g., organic matter decomposition, soil respiration and other aspects of the global carbon balance) (Schimel *et al.*, 2004, Pleim & Gilliam, 2009, Portillo-Estrada *et al.*, 2016, Hursh *et al.*, 2017, Gottschall *et al.*, 2019, Davis *et al.*, 2020, Perera-Castro *et al.*, 2020). Similarly, the use of soil temperature in correlative analyses or predictive models may improve predictions of climate impacts on organismal physiology and behaviour, as well as on population and community dynamics and species distributions (Körner & Paulsen, 2004, Schimel *et al.*, 2004, Ashcroft *et al.*, 2008, Kearney *et al.*, 2009, Scherrer *et al.*, 2011, Opedal *et al.*, 2015, Berner *et al.*, 2020, Zellweger *et al.*, 2020). Given the key role of soil-related processes for both aboveground and belowground parts of the ecosystem and their feedbacks to the atmosphere (Crowther *et al.*, 2016), adequate soil temperature data are critical for a broad range of fields of study, such as ecology, biogeography, biogeochemistry, agronomy, soil science and climate system dynamics. Nevertheless, existing global soil temperature products such as those from ERA5-Land (Copernicus Climate Change Service (C3S), 2019), with a resolution of 0.08 × 0.08 degrees (≈ 9 × 9 km at the equator), remain too coarse for most ecological applications.

The direction and magnitude of the – often multi-degree – difference or *offset* between *in-situ* soil temperature and coarse-gridded air temperature products result from a combination of two factors: (i) the (vertical) microclimatic difference between air and soil temperature, and (ii) the (horizontal) mesoclimatic difference between air temperature in flat, cleared areas (i.e., where meteorological stations are located) and air temperature within different vegetation types (e.g., below a dense canopy of trees) or topographies (e.g., within a ravine or on a ridge) (Lembrechts *et al.*, 2020, De Frenne *et al.*, 2021). In essence, the offset is thus the combination of both the vertical and horizontal differences that result from factors affecting the energy budget at the Earth's surface, principally radiative energy: the ground absorbs radiative energy, which is transferred to the air by convective heat exchange, evaporation and spatial variation in net radiation, and lower convective conductance near the Earth's surface results in horizontal and vertical variation in temperature (Richardson, 1922, Geiger, 1950). Both these vertical and horizontal differences in temperature vary significantly across the globe and in time as a result of environmental conditions affecting the radiation budget (e.g., as a result of topographic orientation, canopy cover or surface albedo), convective heat exchange and evaporation (e.g., foliage density, variation in the degree of wind shear caused by surface friction) and the capacity for the soil to store and conduct heat (e.g., water content and soil structure and texture) (Geiger, 1950, Zhang *et al.*, 2008, Way & Lewkowicz, 2018, De Frenne *et al.*, 2019).

While the physics of soil temperatures have long been well-understood (Richardson, 1922, Geiger, 1950), the creation of high-resolution global gridded soil temperature products has not been feasible before, amongst others due to the absence of detailed global *in-situ* soil temperature measurements (Lembrechts & Lenoir, 2019, Lembrechts *et al.*, 2020). Recently, however, the call for microclimate temperature data with spatiotemporal resolutions relevant to the studied organism and, most importantly, values representative of *in-situ* conditions (i.e., microhabitat) as experienced by these organisms has become more urgent (Bramer *et al.*, 2018), while global data availability has rapidly increased (Lembrechts *et al.*, 2020). In this paper, we mainly address the point on the representativeness of *in-situ* conditions by generating global gridded maps of below-canopy and near-surface soil temperature at 1-km² resolution (in line with most existing global air temperature products). These maps are representative of the habitat conditions experienced by organisms living under vegetation canopies, in the topsoil or near the soil surface. They were created using the abovementioned offset between gridded air temperature data and *in-situ* soil temperature measurements. We expect these soil temperature maps to be substantially more representative of actual microclimatic conditions than existing products – even though still at a relatively coarse spatial resolution of 1-km² and summarizing multi-decadal averages – as they capture relevant near- and below-ground abiotic conditions where ecosystem functions and processes operate (Daly, 2006, Bramer *et al.*, 2018, Körner & Hiltbrunner, 2018). Indeed, the offset between free-air (macroclimate) and soil (microclimate) temperature, and between cleared areas and other habitats, can easily reach up to ±10°C annually, even at the coarse 1-km² spatial resolution used here (Zhang *et al.*, 2018, Lembrechts *et al.*, 2019, Wild *et al.*, 2019).

To create the global gridded soil temperature maps introduced above, we used over 8500 time series of soil temperature measured *in-situ* across the world's major terrestrial biomes, compiled and stored in the SoilTemp database (Lembrechts *et al.*, 2020) (Fig. 1a, Supplementary Material Fig. S1) and averaged into 1200 (or 1000 for the second soil layer) unique 1-km² pixels. First, to illustrate the magnitude of the studied effect, we visualized the global and biome-specific patterns in the mean annual offset between *in-situ* soil temperature (topsoil: 0–5 cm and second layer: 5–15 cm depth) and coarse-scale interpolated air temperature from ERA5-Land (soil temperature minus air temperature, hereafter called the *temperature offset,* sensu (De Frenne *et al.*, 2021); elsewhere called the *surface offset* (Smith & Riseborough, 1996, Smith & Riseborough, 2002)) using the average within 1 × 1 km grid cells. Next, we used a machine learning approach with 31 environmental explanatory variables (including macroclimate, soil, topography, reflectance, vegetation and anthropogenic variables) to model the spatial variation in monthly temperature offsets at a 1 × 1 km resolution for all continents except Antarctica (as absent in many of the used predictor variable layers). Using these offsets, we then calculated relevant soil-related bioclimatic variables (SBIO), mirroring the existing global bioclimatic variables for air temperature.

Finally, we compare our new global soil temperature product with a similar one calculated using coarser-resolution soil temperature data from ERA5-Land (Copernicus Climate Change Service (C3S), 2019).

Methods

Data acquisition

Analyses are based on SoilTemp, a global database of microclimate time series (Lembrechts *et al.*, 2020). We compiled soil temperature measurements from 9362 unique sensors (mean duration 2.9 years, median duration 1.0 year, ranging from 1 month to 41 years) from 60 countries, using both published and unpublished data sources (Fig. 1, Supplementary Material Fig. S1). Each sensor corresponds to one independent time series.

We used time series spanning a minimum of one month, with a temporal resolution of four hours or less. Sensors of any type were included (Supplementary Material Table S1), as long as they measured *in situ*. Sensors in experimentally manipulated plots, i.e., plots in which microclimate has been manipulated, were excluded. Most data (> 90%) came from low-cost rugged microclimate loggers such as iButtons (Maxim Integrated, USA) or TMS4-sensors (Wild *et al.*, 2019), with measurement errors of around 0.5–1°C (note that we are using °C over K throughout, for ease of understanding), while in a minority of cases sensors with higher meteorological specifications such as industrial or scientific grade thermocouples and thermistors (measurement errors of less than 0.5°C) were used. Contributing datasets mostly consisted of short-term regional networks of microclimate measurements, yet also included a set (< 5%) of soil temperature sensors from long-term research networks equipped with weather stations (e.g., Pastorello *et al.*, 2017). By combining these two types of data, a much higher spatial density of sensors and broader distribution of microhabitats could be obtained than by using weather station data only.

About 68% of sensors measured in time intervals located between 2010 and 2020 and 93% between 2000 and 2020; we thus focus on the latter period in our analyses. Additionally, given the relatively short time frame covered by most individual sensors, we were not able to test for systematic differences in the temperature offset between old and recent data sets, and thus we did not correct for this in our models. We strongly urge future studies to assess such temporal dynamics in the offset, once long-term microclimate data have become sufficient and more available.

For each of the individual 9362 time series, we calculated monthly mean, minimum (5% percentile of all monthly values) and maximum (95% percentile) temperature, after checking all time series for plausibility and erroneous data. These monthly values, while perhaps not fully intercomparable between the northern and southern hemisphere, are those that have traditionally been used to calculate bioclimatic variables (Fick & Hijmans, 2017). Months with more than one day of missing data, either at the beginning or end of the measurement period, or due to logger malfunctioning during measurement, were excluded, resulting in a final subset of 380 676 months of soil temperature time series that were used for further analyses. For each sensor with more than twelve months of data, we calculated moving averages of annual mean temperature, using each consecutive month as a starting month and calculating the mean temperature including the next eleven months. We used these moving averages to make maximal use of the full temporal extent covered by each sensor, because each time series spanned a different time period, often including parts of calendar years only. Next, these moving averages were further summarized to one mean annual average per 1-km² pixel (see below, under '*Global and biome-level analyses*').

The selected dataset contained sensors installed strictly belowground, measuring temperature at depths between 0 and 200 cm below the ground surface. Sensors recording several measurements at the same site but located at different (vertical) depths were included separately (the 9362 unique sensors thus came from 7251 unique loggers).

Sensors were grouped in different soil depth categories (0–5, 5–15, 15–30, 30–60, 60–100, 100–200 cm, Supplementary Material Table S2) to incorporate the effects of soil temperature dampening. We limited our analyses to the topsoil (0–5 cm) and the second soil layer (5–15 cm), as we currently lack sufficient global coverage to make trustworthy models at deeper soil depths (8519 time series, about 91%, came from the two upper depth layers). Due to uncertainty in identification of these soil depths between studies (e.g., due to litter layers), no finer categorisation is used.

We tested for potential bias in temporal resolution (i.e., measurement interval) by calculating mean, minimum and maximum temperature for a selection of 2000 months for data measured every 15 minutes, and the same data aggregated to 30, 60, 90, 120 and 240 minutes. Monthly mean, minimum and maximum temperature calculated with any of the aggregated datasets differed on average less than 0.2°C from the ones with the highest temporal resolution. We were thus confident that pooling data with different temporal resolutions of 4 hours or finer would not significantly affect our results.

Temperature offset calculation

For each monthly value at each sensor location (see Supplementary Material Table S3 for number of data points per month), we extracted the corresponding monthly means of the 2 m air temperature from the European Centre for Medium-Range Weather (ECMWF) Forecast's 5th reanalysis (ERA5) (from 1979–1981) and ERA5-Land from 1981–2020 (Copernicus Climate Change Service (C3S), 2019), hereafter called ERA5L. The latter dataset models the global climate with a spatial resolution of 0.08 × 0.08 degrees (≈ 9 × 9 km at the equator) with an hourly resolution, converted into monthly means using daily means for the whole month. Similarly, monthly minima and maxima were obtained from TerraClimate (Abatzoglou *et al.*, 2018) for the period 2000 to 2020 at a 0.04 × 0.04 degrees (≈ 4 × 4 km at the equator) resolution. Monthly means for TerraClimate were not available, we therefore estimated them by averaging the monthly minima and maxima. Finally, we also obtained monthly mean temperatures from CHELSA (Karger *et al.*, 2017a, Karger *et al.*, 2017b) for the period 2000 to 2013 at a 30 × 30 arc second (≈ 1 × 1 km at the equator) resolution. In our modelling exercises (see section *'Integrative modelling'* below), we opted to use the mean temperature offsets as calculated based on ERA5L rather than on CHELSA. While CHELSA's higher spatial resolution is definitely an advantage, its time period (stopping in 2013) insufficiently overlapped with the time period covered by our *in-situ* measurements (2000 to 2020), so temperature offsets based on the CHELSA dataset were only used for comparative purposes. We used TerraClimate to model offsets in monthly minimum and maximum temperature.

We calculated moving annual averages of the gridded air temperature data similar to those we computed for soil temperature. These were used to create annual temperature offset values following the same approach as above.

The offset between the *in situ* measured soil temperature in the SoilTemp database and the 2 m free-air temperature obtained from the air-temperature grids (ERA5L, TerraClim and CHELSA, hereafter called 'gridded air temperature') was calculated by subtracting the monthly or annual mean air temperature from the monthly or annual mean soil temperature. Positive offset values indicate a measured soil temperature higher than gridded air temperature, while negative offset values represent cooler soils. Similarly, monthly minimum and maximum air temperature were subtracted from minimum and maximum soil temperature, respectively. Monthly minima and maxima of the soil temperature were calculated as, respectively, the 5% lowest and highest instantaneous measurement in that month, to correct for outliers, which can be especially pronounced at the soil surface (Speak *et al.*, 2020). As a result, patterns in minima and maxima are more conservative estimates than if we had used the absolute lowest and highest values.

Importantly, the temperature offset calculated here is a result of three key groups of drivers: (1) height effects (2 m versus 0–15 cm below the soil surface); (2) environmental or habitat effects (e.g., spatial variability in vegetation, snow or topography); and (3) spatial scale effects (resolution of gridded air temperature) (Lembrechts *et al.*, 2020). We investigated the potential role of scale effects by comparing gridded air temperature data sources with different resolutions (ERA5L, TerraClimate and CHELSA, see below). Height effects and environmental effects are however not disentangled here, as the offset we propose incorporates both the difference between air and soil temperature (vertically), as well as the difference between free-air macroclimate and *in situ* microclimate (horizontally) in one measure (Lembrechts *et al.*, 2020). While it can be argued that it would be better to treat both vertical and horizontal effects separately, this would require a similar database of coupled *in-situ* air and soil temperature measurements, which is not yet available. Using *in situ* measured air temperature could also solve spatial mismatches (i.e., spatially averaged air temperature represents the whole 1 to 81 km^2 pixel, depending on pixel size, not only the exact location of the sensor). However, coupled air and soil temperature measurements are not only rare, but the air temperature measurements also have large measurement errors, especially in open habitats. These errors can be up to several degrees in open habitats when using non-standardized sensors, loggers and shielding (Maclean *et al.*, 2021). Hence, using *in situ* measured air temperature without correcting for these measurement errors would be misleading.

Global and biome-level analyses

For the purpose of visualization, annual offsets were first averaged in hexagons with a resolution of approximately 70 000 km^2, using the dggridR-package in R (Barnes *et al.*, 2017) (Fig. 1). Next, we plotted mean, minimum and maximum annual soil temperature as a function of corresponding gridded air temperature from ERA5, TerraClimate and CHELSA and used generalized additive models (GAMs, package mgcv; Wood, 2012) to visualise deviations from the 1:1-line (i.e., temperature offsets deviating from zero, Supplementary Figs. S4-5).

All annual and monthly values within each soil depth category and falling within the same 1-km^2 pixel were aggregated as a mean, resulting in a total of c. 1200 unique pixels at 0–5 cm, and c. 1000 unique pixels at 5–15 cm each month, across the globe (Supplementary Material Table S3). This averaging includes summarizing the data over space, i.e., multiple sensors within the same 1-km^2 pixel, and time, i.e., data from multi-year time series from a certain sensor, to reduce spatial and temporal autocorrelation and sampling bias. We assigned these 1-km^2 averages to the corresponding Whittaker biome of their georeferenced location, using the package *plotbiomes* in R (Fig. 1 c, d, Supplementary Material Table S4-5 (Stefan & Levin, 2018)). We ranked biomes based on their offset and compared this with the mean annual precipitation in each biome (Fig. 1b). This was done separately for each air temperature data source (ERA5L, TerraClimate and CHELSA), soil depth (0–5 cm, 5–15 cm) and timeframe (ERA5L 1979–2020, 2000–2020), as well as for the offset between monthly minimum and maximum soil temperature and the minimum and maximum gridded air temperature from TerraClimate. Our analyses showed that patterns were robust to variation in spatial resolution, sensor depth, climate interpolation method and temporal scale (Supplementary Material Figs. S2–5).

Acquisition of global predictor variables

To create spatial predictive models of the offset between *in-situ* soil temperature and gridded air temperature, we first sampled a stack of global map layers at each of the logger locations within the dataset. These layers included long-term macroclimatic conditions, soil texture and physiochemical information, vegetation, radiation and topographic indices as well as anthropogenic variables. Details of all layers, including descriptions, units, and source information, are described in Supplementary Data S1. In short, information about soil texture, structure and physiochemical properties was obtained from SoilGrids (version 1 (Hengl *et al.*, 2017)), limited to the upper soil layer (top 5 cm). Long-term averages of macroclimatic conditions (i.e., monthly mean, maximum and minimum temperature, monthly precipitation) was obtained from CHELSA (version 2017 (Karger *et al.*, 2017a)), which includes climate data averaged across 1979–2013, and from WorldClim (version 2 (Fick & Hijmans, 2017)). Monthly snow probability is based on a pixel-wise frequency of snow occurrence (snow cover >10%) in MODIS daily snow cover products (MOD10A1 & MYD10A1 (Hall *et al.*, 2002)) in 2001–2019. Spectral vegetation indices (i.e., averaged MODIS NDVI product MYD13Q1) and surface reflectance data (i.e., MODIS MCD43A4) were obtained from the Google Earth Engine Data Catalog (developers.google.com/earth-engine/datasets) and averaged from 2015 to 2019. Landcover and topographic information were obtained from EarthEnv (Amatulli *et al.*, 2018). Aridity index (AI) and potential evapotranspiration (PET) layers were obtained from CGIAR (Zomer *et al.*, 2008). Anthropogenic information (population density) was obtained from the EU JRC (ghsl.jrc.ec.europa.eu/ghs_pop2019.php). Aboveground biomass data were obtained from GlobBiomass (Santoro, 2018). Resolved ecoregion classifications were used to categorize sampling locations into biomes (Dinerstein *et al.*, 2017). With this set of predictor variables, we included information on all different categories of drivers of soil temperature. An important variable that had to be excluded was snow depth, due to the lack of a relevant 1-km^2 resolution global product. The final set of predictor variables included 24 'static' variables and eight monthly layers (i.e., maximum, mean and minimum temperature, precipitation, cloud cover, solar radiation, water vapour pressure, and snow cover). As cloud cover estimates were not available for high-latitude regions in the Northern Hemisphere in January and December due to a lack of daylight, we excluded cloud cover as an explanatory variable for these months (i.e., 'EarthEnvCloudCover_MODCF_monthlymean_XX', with XX representing the months in two-digit form Supplementary Data S1).

All variable map layers were reprojected and resampled to a unified pixel grid in EPSG:4326 (WGS84) at 30 arc-sec resolution (≈ 1 × 1 km at the equator). Areas covered by permanent snow or ice (e.g., the Greenland ice cap or glaciated mountain ranges, identified using SoilGrids) were excluded from the analyses. Antarctic sampling points were excluded from the modelling data set owing to the limited coverage of several covariate layers in the region.

Integrative modelling

To generate global maps of monthly temperature offsets (Fig. 2), we trained random forest (RF) models for each month, using the temperature offsets as the response variables and the global variable layers as predictors. We used a geospatial RF modelling pipeline as developed by van den Hoogen *et al.* (2021). RF models are particularly valuable here due to their capacity to uncover nonlinear relationships (e.g., due to increased decoupling of soil from air temperature in colder and thus snow-covered areas) and their ability to capture complex interactions among covariates (e.g., between snow and vegetation cover) (Olden *et al.*, 2008).

We performed a grid search procedure to tune the RF models across a range of 122 hyperparameter settings (variables per split: 2–12, minimum leaf population: 2–12). During this procedure, we assessed each model's performance using k-fold cross-validation (k = 10; folds assigned randomly, stratified per biome), for each of the 122 models. The models' mean and standard deviation values were the basis for choosing the best of all evaluated models. This procedure was repeated for each month separately for the two soil depth layers (0–5 cm, 5–15 cm), for offsets in mean, minimum and maximum temperature. The importance of explanatory variables was assessed using the variable importance and ordered by mean variable importance across all models. This variable importance adds up the decreases in the impurity criterion (i.e., the measure on which the local optimal condition is chosen) at each split of a node for each individual variable over all trees in the forest (van den Hoogen *et al.*, 2021).

Soil bioclimatic variables

The resulting global maps of the annual and monthly offsets between mean, minimum and maximum soil and air temperature were used to calculate relevant bioclimatic variables following the definition used in CHELSA, BIOCLIM, ANUCLIM and WorldClim (Xu & Hutchinson, 2011, Booth *et al.*, 2014, Fick & Hijmans, 2017, Karger *et al.*, 2017a) (Fig. 3–4). We calculated 11 soil bioclimatic layers (SBIO, Table 1). First, we calculated monthly soil mean, maximum and minimum temperature by adding monthly temperature offsets to the respective CHELSA monthly mean, maximum and minimum temperature (Karger *et al.*, 2017a). Next, we used these soil temperature layers to compute the SBIO layers (O'Donnell & Ignizio, 2012). Wettest and driest quarters were identified for each pixel based on CHELSA's monthly values.

Table 1: Overview of soil bioclimatic variables as calculated in this study.

Bioclimatic variable	Meaning
SBIO1	annual mean temperature
SBIO2	mean diurnal range (mean of monthly (max temp - min temp))
SBIO3	isothermality (SBIO2/SBIO7) (×100)
SBIO4	temperature seasonality (standard deviation ×100)
SBIO5	max temperature of warmest month
SBIO6	min temperature of coldest month
SBIO7	temperature annual range (SBIO5-SBIO6)
SBIO8	mean temperature of wettest quarter
SBIO9	mean temperature of driest quarter
SBIO10	mean temperature of warmest quarter
SBIO11	mean temperature of coldest quarter

Model uncertainty

To assess the uncertainty in the monthly models, we performed a stratified bootstrapping procedure, with total size of the bootstrap samples equal to the original training data (van den Hoogen *et al.*, 2021). Using biomes as a stratification category, we ensured the samples included in each of the bootstrap training collections were proportionally representative of each biome's total area. Next, we trained RF models (with the same hyperparameters as selected during the grid-search procedure) using each of 100 bootstrap iterations. Each of these trained RF models was then used to classify the covariate layer stack, to generate per-pixel 95% confidence intervals and standard deviation for the modelled monthly offsets (Fig. 5a, Supplementary Material Fig. S6a). The mean R^2 value of the RF models for the monthly mean temperature offset was 0.70 (from 0.64 to 0.78) at 0–5 cm and 0.76 (0.63–0.85) at 5 to

15 cm across all twelve monthly models. Mean RMSE of the models was 2.20°C (1.94–2.51°C) at 0–5 cm, and 2.06°C (1.67–2.35°C) at 5–15 cm.

Importantly, model uncertainty as reported in Fig. 5a and Supplementary Material Fig. S6a comes on top of existing uncertainties in (1) *in-situ* soil temperature measurements and (2) the ERA5L macroclimate models as used in our models. However, both of those are usually under 1°C (Copernicus Climate Change Service (C3S), 2019, Wild *et al.*, 2019).

To assess the spatial extent of extrapolation, which is necessary due to the incomplete global coverage of the training data, we first performed a Principal Component Analysis (PCA) on the full environmental space covered by the monthly training data, including all explanatory variables as used in the models, and then transformed the composite image into the same PC spaces as of the sampled data (Van Den Hoogen *et al.*, 2019). Next, we created convex hulls for each of the bivariate combinations from the first 10 to 12 PCs, covering at least 90% of the sample space variation, with the number of PCs depending on the month. Using the coordinates of these convex hulls, we assessed whether each pixel fell within or outside each of these convex hulls, and calculated the percentage of bivariate combinations for which this was the case (Fig. 5b, Supplementary Material Fig. S6b). This process was repeated for each month, and for each of the two soil depths separately.

These uncertainty maps are important because one should be careful with extrapolation beyond the range of conditions covered by the environmental variables included in the original calibration dataset, especially in the case of non-linear patterns such as modelled here. The maps are provided as spatial masks to remove or reduce the weighting of the pixels for which predictions are beyond the range of values covered by the models during calibration. To assess this further, we used a spatial leave-one-out cross-validation analysis to test for spatial autocorrelation in the data set (Supplementary Material Fig. S7) (van den Hoogen *et al.*, 2021). This approach trains a model for each sample in the data set on all remaining samples, excluding data points that fall within an increasingly large buffer around that focal sample. Results show lowest confidence for May to September at 5–15 cm, likely driven by uneven global coverage of data points.

Finally, we compared the modelled mean annual temperature (SBIO1, topsoil layer) with a similar product based on monthly ERA5L topsoil (0–7 cm) temperature with a spatial resolution of 0.1 × 0.1 degrees (Copernicus Climate Change Service (C3S), 2019). The corresponding SBIO1 based on ERA5L was calculated using the means of the monthly averages for each month over the period 1981 to 2016, and averaging these 12 monthly values into one annual product. We then visualized spatial differences between SBIO1 and ERA5, as well as differences across the macroclimatic gradient, to identify mismatches between both datasets.

All geospatial modelling was performed using the Python API in Google Earth Engine (Gorelick *et al.*, 2017). The R statistical software, version 4.0.2 (R Core Team, 2020), was used for data visualisations. All maps were plotted using the Mollweide projection (which preserves relative areas) to avoid large distortions at high latitudes.

Sources of uncertainty

There is a temporal mismatch between the period covered by CHELSA (1979-2013) and our *in-situ* measurements (2000-2020), which prevented us from directly using CHELSA climate to calculate the temperature offsets used in our models. This temporal mismatch might affect the offsets calculated here because the relationship between temperature offset and macroclimate will change through time as the climate warms. However, we are confident that our results are sufficiently robust to withstand this mismatch, given that we found high consistency in offset patterns between the different timeframes and air temperature datasets examined (Supplementary Material Figs. S2–5). Nevertheless, we strongly urge future research to disentangle these potential temporal dynamics, especially given the increasing rate at which the climate is warming (Xu *et al.*, 2018, GISTEMP Team, 2021).

Similarly, a potential bias could result from the mismatch in method and resolution between ERA5L – used to calculate the temperature offsets – and CHELSA, which was used to create the bioclimatic variables. However, even though temperature offsets have slightly larger variation when based on the coarser-grained ERA5L-data than on the finer-grained CHELSA-data, Supplementary Material Figs. S2–5 show that relationships between soil and air temperature are largely consistent in all biomes and across the whole global temperature gradient. Therefore, the larger offsets created additional random scatter, yet no consistent bias.

Finally, we acknowledge that the 1-km² resolution gridded products might not be representative of conditions at the *in-situ* measurement locations within each pixel. This issue could be particularly significant for different vegetation types (here proxied at the pixel level using total aboveground biomass (unit: tons/ha i.e., Mg/ha, for the year 2010; Santoro, 2018) and NDVI (MODIS NDVI product MYD13Q1, averaged over 2015–2019)). To verify this, we compared a pixel's estimated aboveground biomass with the dominant *in-situ* habitat (forest versus open) surrounding the sensors in that pixel (Supplementary Table S6). Importantly, all sensors installed in forests fell indeed in pixels with more than 1 ton/ha aboveground biomass. Similarly, 75% or more of sensors in open terrain fell in pixels with biomass estimates of less than 1 ton/ha. Only in the temperate woodland biome was the match between *in-situ* habitat estimates and pixel-level aboveground biomass lower, with less than 95% of sensors in forested locations correctly placed in pixels with more than 1 ton/ha biomass, and less than 50% of open terrain sensors in pixels with less than 1 ton/ha biomass. While our predictions will thus not be accurate for locations within a pixel that largely deviate from average conditions (e.g., open terrain in pixels identified as largely forested, or vice versa), they should be largely representative for those pixel-level averages.

Results

Biome-wide patterns in the temperature offset

We found positive and negative temperature offsets of up to 10°C between *in situ* measured mean annual topsoil temperature and gridded air temperature (mean = 3.0 ± 2.1°C standard deviation, Fig. 1, 0–5 cm depth; 5–15 cm is available in Supplementary Material Figs. S2, 5). The magnitude and direction of these temperature offsets varied considerably within and across biomes. Mean annual topsoil temperature was on average 3.6 ± 2.3°C higher than gridded air temperature in cold and/or dry biomes, namely tundra, boreal forests, temperate grasslands and subtropical deserts. In contrast, offsets were slightly negative in warm and wet biomes (tropical savannas, temperate forests and tropical rainforests) where soils were, on average, 0.7 ± 2.7°C cooler than gridded air temperature (Fig. 1b, Supplementary Material

Figs. S2 and 5; note, however, the lower spatial coverage in these biomes in Fig. 1a, c, d, Supplementary Material Table S4). Temperature offsets in annual minimum and maximum temperature amounted to c. 10°C maximum. While annual soil temperature minima were on average higher than corresponding gridded air temperature minima in all biomes, temperature offsets of annual maxima followed largely the same biome-related trends as seen for the annual means, albeit with the higher variability expected for temperature extremes (Supplementary Material Figs. S2g, h, S4g, h). Using different air temperature data sources did not alter the annual temperature offset and biome-related patterns (see Methods and Supplementary Material Figs. S2–5).

Soils in the temperate seasonal forest biome were on average 0.8°C (± 2.2°C) cooler than air temperature within 1-km^2 grid cells of forested habitats, and 1.0°C (± 4.0°C) warmer than the air within 1-km^2 grid cells of non-forested habitats, resulting in a biome-wide average of 0.5°C (Supplementary Material Table S7). Similar patterns were observed in other biomes.

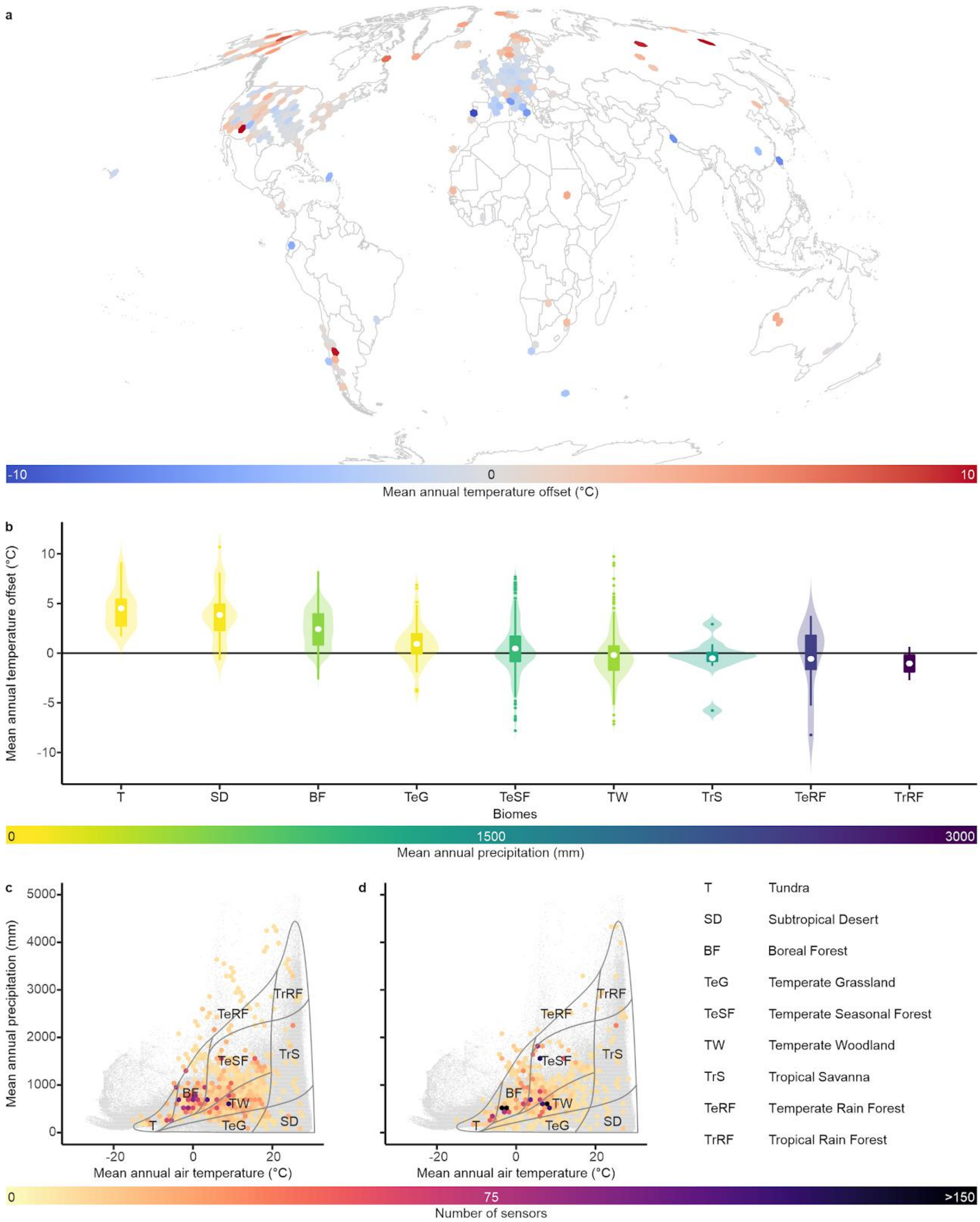

Figure 1: Temperature offsets between soil and air temperature differed significantly among biomes. *(a) Distribution of in-situ measurement locations across the globe, coloured by the mean annual temperature offset (in °C) between in situ measured soil temperature (topsoil, 0–5 cm depth) and gridded air temperature (ERA5L). Offsets were averaged per hexagon, each with a size of approximately 70,000 km². Mollweide projection. (b) Mean annual temperature offsets per Whittaker biome (adapted from Whittaker 1970, based on geographic location of sensors averaged at 1 km²; 0–5 cm depth), ordered by mean temperature offset and coloured by mean annual precipitation. (c–d) Distribution of sensors in 2D climate space for the topsoil (c, 0–5 cm depth, N = 4530) and the second*

layer (d, 5–15 cm depth, N = 3989). Colours of hexagons indicate the number of sensors at each climatic location, with a 40 × 40 km resolution. Grey dots in the background represent the global variation in climatic space (obtained by sampling 1 000 000 random locations from the CHELSA world maps). Overlay with grey lines depicts a delineation of Whittaker biomes.

Temporal and spatial variation in temperature offsets

Our random forest modelling approach highlighted a strong seasonality in monthly temperature offsets, especially towards higher latitudes (Fig. 2). High-latitude soils were found to be several degrees warmer than the air (monthly offsets of up to 25°C) during their respective winter months, and cooler (up to 10°C) in summer months, both at 0–5 cm (Fig. 2) and 5–15 cm (Supplementary Material Fig. S8) soil depths. In the tropics and subtropics, soils in dry biomes (e.g., in the Sahara desert or southern Africa) were predicted to be warmer than air throughout most of the year, whilst soils in mesic biomes (e.g., tropical biomes in South America, central Africa and Southeast Asia) were modelled to be consistently cooler, at both soil depths. These global gridded products were then used to create temperature-based global bioclimatic variables for soils (SBIO, Fig. 3, Supplementary Material Fig. S9).

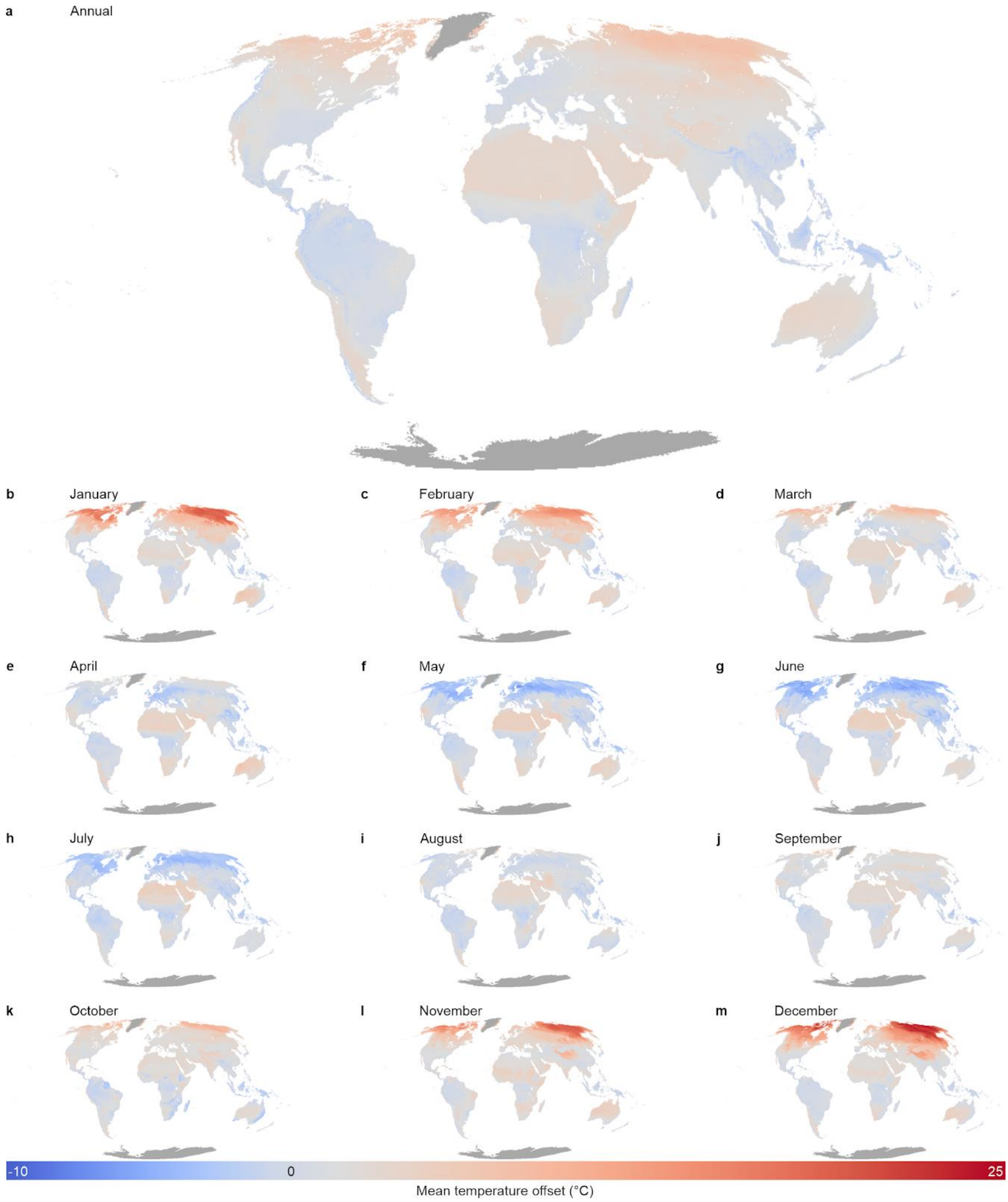

Figure 2: Global modelled temperature offsets between soil and air temperature show strong spatiotemporal variation across months. *Modelled annual (a) and monthly (b–m) temperature offset (in °C) between in situ measured soil temperature (topsoil, 0–5 cm) and gridded air temperature. Positive (red) values indicate soils that are warmer than the air. Dark grey represents regions outside the modelling area.*

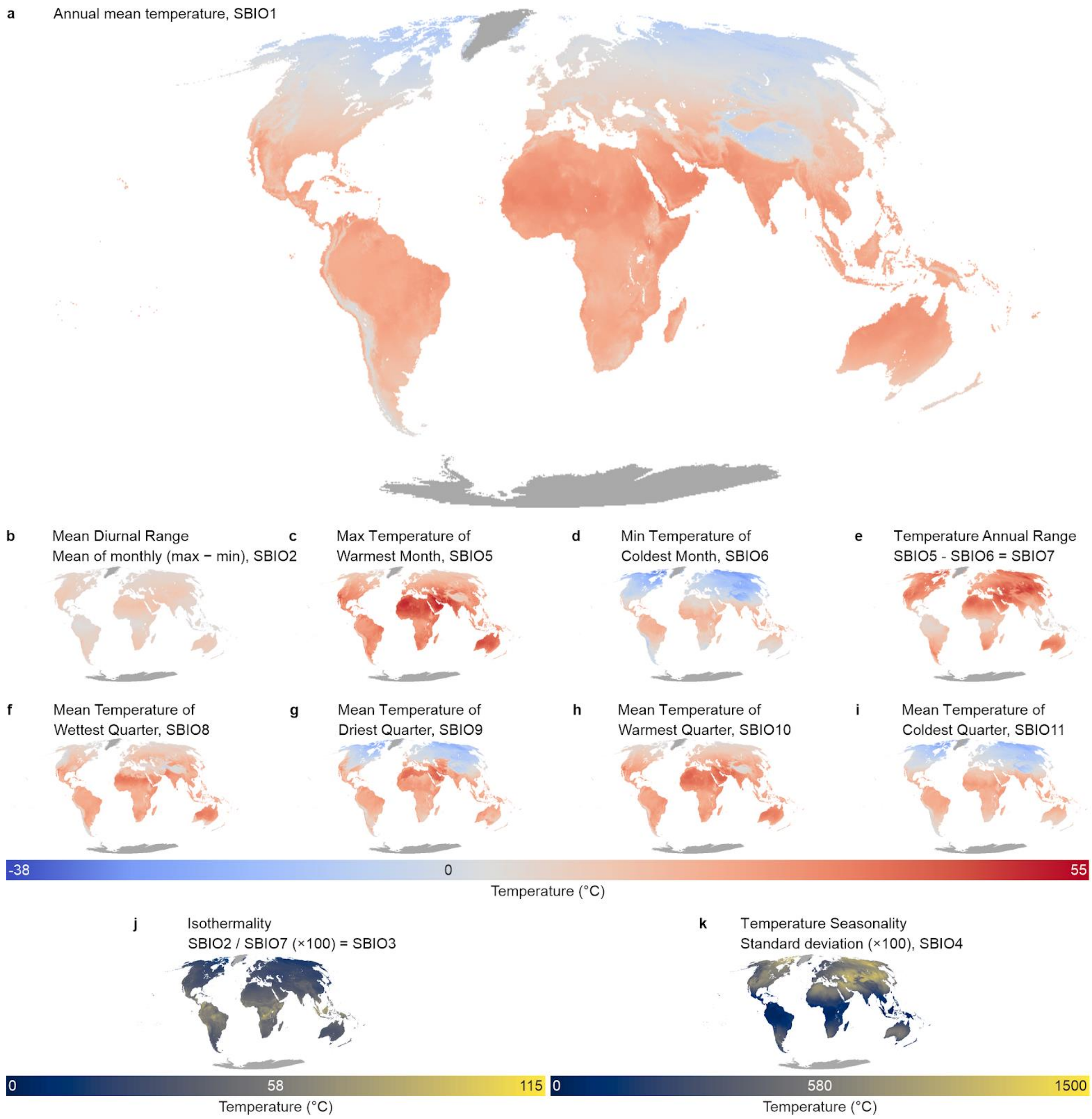

Figure 3: Soil bioclimatic variables. *Global maps of bioclimatic variables for topsoil (0–5 cm depth) climate, calculated using the maps of monthly soil climate (see Fig. 2), and the bioclimatic variables for air temperature from CHELSA.*

Global variation in soil temperature

We observed 17% less spatial variation in mean annual soil temperature globally (expressed by the standard deviation) than in air temperature, largely driven by the positive offset between soil and air temperature in cold environments (Fig. 4). Importantly, our machine learning models slightly (up to 1°C, or around 10% of variation) underestimated temperature offsets at both extremes of the temperature gradient at the 1-km² resolution (Supplementary Material Fig. S10) and likely even more in comparison with finer-resolution products. Estimates of the reduction in variation across space are thus conservative, especially in the coldest biomes. The reduction in spatial temperature variation was observed in all cold and cool biomes, with tundra and boreal forests having both a significant positive mean temperature offset and a reduction of 20% and 22% in variation, respectively (Fig. 4c). In the warmest biomes (e.g., tropical savanna and subtropical desert), however, we found an increase in variation of, on average, 10%.

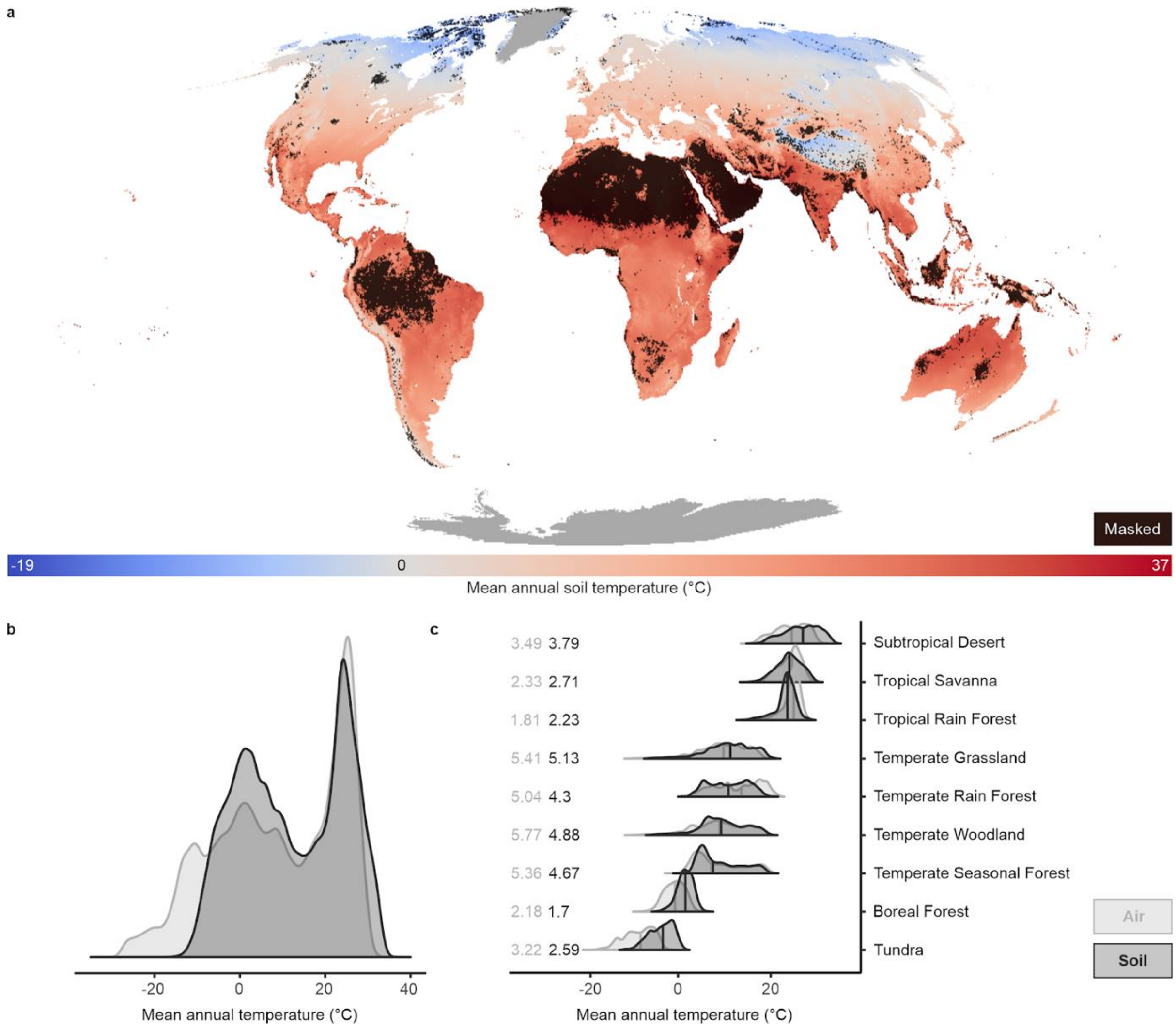

Figure 4: Mean annual soil temperature shows significantly lower spatial variability than air temperature. *(a) Global map of mean annual topsoil temperature (SBIO1, 0–5 cm depth, in °C), created by adding the monthly offset between soil and air temperature for the period 2000–2020 (Fig. 2) to the monthly air temperature from CHELSA. A black mask is used to exclude regions where our models are extrapolating (i.e., interpolation values in Fig. 5 are < 0.9, 18% of pixels). Dark grey represents regions outside the modelling area. (b–c) Density plots of mean annual soil temperature across the globe (b) and for each Whittaker biome separately (c) for SBIO1 (dark grey, soil temperature),*

compared with BIO1 from CHELSA (light grey, air temperature), created by extracting 1 000 000 random points from the 1-km² gridded bioclimatic products. The numbers in (c) represent the standard deviations of air temperature (light grey) and soil temperature (dark grey). Biomes are ordered according to the median annual soil temperature values from the highest temperature (subtropical desert) to the lowest (tundra).

Our bootstrap approach to validate modelled monthly offsets indicated high consistency among the outcomes of 100 bootstrapped models (Fig. 5, Supplementary Material Fig. S6a), with standard deviations in most months and across most parts of the globe around or below ±1°C. One exception to this was the temperature offset at high latitudes of the northern hemisphere during winter months (standard deviation up to ±5°C in the 0–5 cm layer). Predictive performance was comparable across biomes, although with large variation in data availability (Supplementary Material Fig. S11).

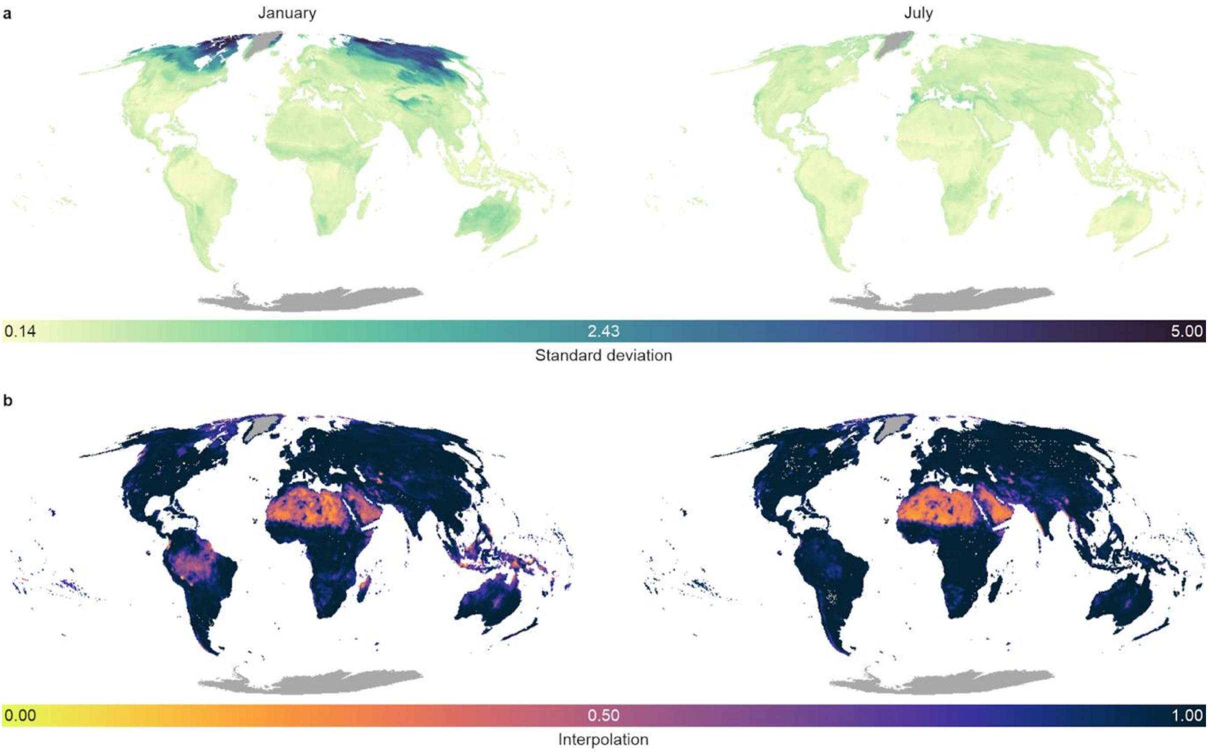

***Figure 5**: **Models of the temperature offset between soil and air temperature have low standard deviations and good global coverage.** Analyses for the temperature offset between in situ measured topsoil (0–5 cm depth) temperature and gridded air temperature. (a) Standard deviation (in °C) over the predictions from a cross-validation analysis that iteratively varied the set of covariates (explanatory data layers) and model hyperparameters across 100 models and evaluated model strength using 10-fold cross-validation, for January (left) and July (right), as examples of the two most contrasting months. (b) The fraction of axes in the multidimensional environmental space for which the pixel lies inside the range of data covered by the sensors in the database. Low values indicate increased extrapolation.*

The importance of explanatory variables in the RF models was largely consistent across months. Macroclimatic variables such as incoming solar radiation as well as long-term averages in air temperature and precipitation were by far the most influential explanatory variables in the spatial models of the monthly temperature offset (Supplementary Material Figs. S12, 13).

We highlight that the current availability of *in-situ* soil temperature measurements is significantly lower in the tropics (Supplementary Material Table S5), where our model had to extrapolate temperatures beyond the range used to calibrate the model (Fig. 5b, Supplementary Material Fig. S6b).

Finally, our comparison with a mean annual soil temperature product derived from the coarse-resolution ERA5L topsoil temperature showed that spatial variability, e.g., driven by topographic heterogeneity, is much better captured here than in the coarser resolution of the ERA5L-based product (Fig. 6c-e). Nevertheless, our predictions at the coarse scale showed to be condensed within a 5°C range of values from the ERA5L-predictions, for more than 95% of pixels globally. Noteworthy, our predictions resulted in consistently cooler soil temperature predictions than topsoil conditions provided by ERA5L across large areas, such as the boreal and tropical forest biomes (Fig. 6a, b). Additionally, our models predicted lower values for SBIO1 than ERA5L in all regions with mean annual soil temperature below 0°C, except for a few locations around Greenland and Svalbard (Fig. 6a, b).

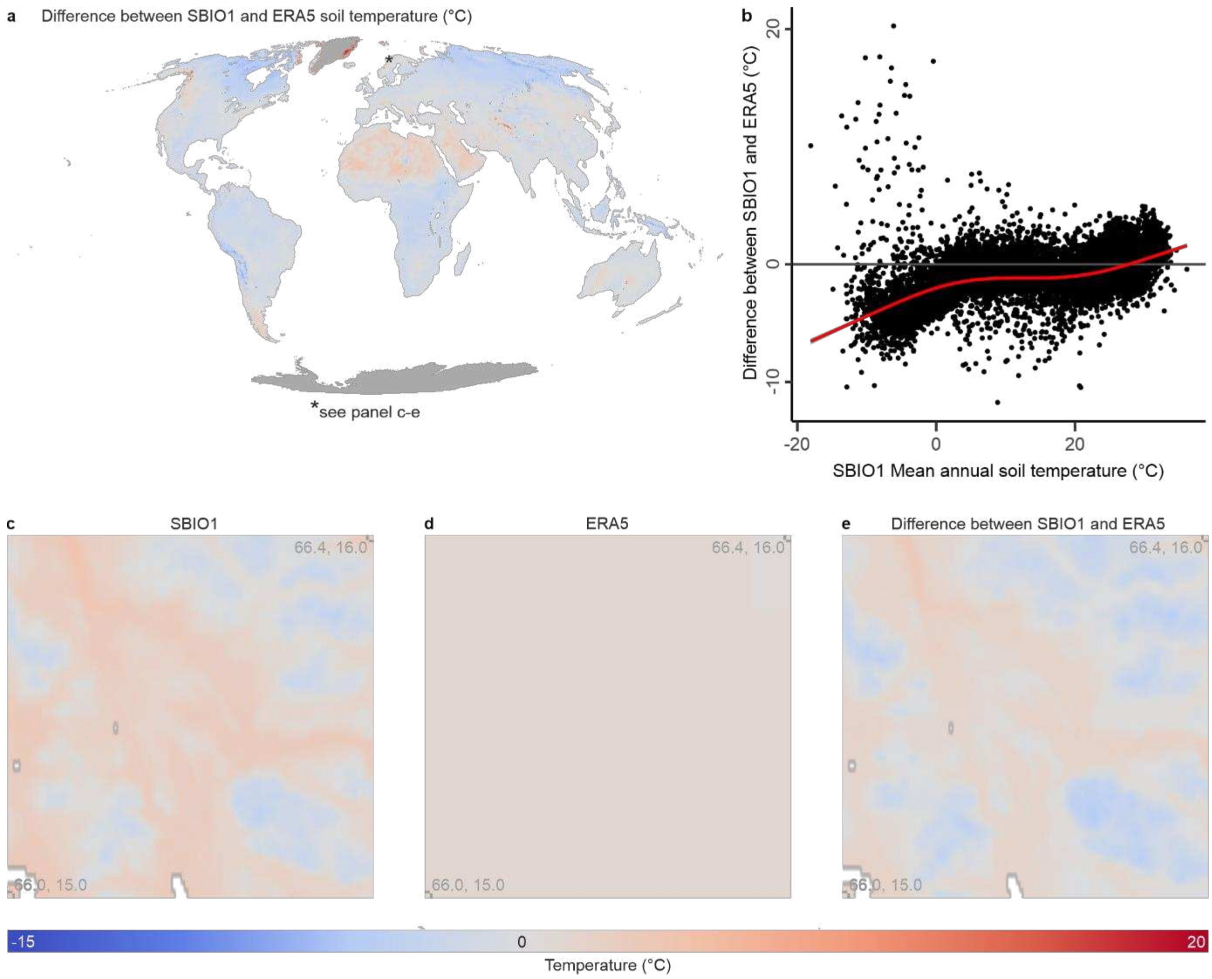

***Figure 6**: The mean annual soil temperature (SBIO1, 1 x 1 km resolution) modelled here is consistently cooler than ERA5L (9 x 9 km) soil temperature in forested areas.* *(a) Spatial representation of the difference between SBIO1 based on our model and based on ERA5L soil temperature data. Negative values (blue colours) indicate areas where our model predicts cooler soil temperature. Dark grey areas (Greenland and Antarctica) are excluded from our models. Asterisk in Scandinavia indicates the highlighted area in panels d to f (see below). (b) Distribution of the difference between SBIO1 and ERA5L along the macroclimatic gradient (represented by SBIO1 itself) based on a random subsample of 50 000 points from the map in a). Red line from a Generalized Additive Model (GAM) with k=4. (c-e) High-resolution zoomed panels of an area of high elevational contrast in Norway (from 66.0-66.4° N, 15.0-16.0° E) visualizing SBIO1 (c), ERA5L (d) and their difference (e), to highlight the higher spatial resolution as obtained with SBIO1.*

Discussion

Global patterns in soil temperature

We observed large spatiotemporal heterogeneity in the global offset between soil and air temperature, often in the order of several degrees annually and up to more than 20°C during winter months at high latitudes. These values are in line with empirical data from regional studies (Zhang *et al.*, 2018, Lembrechts *et al.*, 2019, Obu *et al.*, 2019). Both annual and monthly offsets showed clear discrepancies between cold and dry versus warm and wet biomes. The modelled monthly offsets covaried strongly negatively with both long-term averages in free-air temperature and solar radiation, linking to the well-known decoupling of soil from air temperature due to snow (for cold extremes in cold and cool biomes) (Grundstein *et al.*, 2005). However, the secondary importance of variables related to precipitation and soil structure hints to the additional distinction between wet and dry biomes at the warm end of the temperature gradient, where buffering due to shading, evapotranspiration and the specific heat of water (mostly against warm extremes in warm and wet biomes) results in cooler soil temperature (Geiger, 1950, Grundstein *et al.*, 2005, Hennon *et al.*, 2010, Wang & Dickinson, 2012, De Frenne *et al.*, 2013, Grünberg *et al.*, 2020), a less important process in warm and dry biomes (Wang & Dickinson, 2012, Greiser *et al.*, 2018, Zhou *et al.*, 2021). As such, these results highlight strong macroclimatic impacts on the soil microclimate across the globe (see also De Frenne *et al.*, 2019), yet with soil temperature importantly non-linearly related to air temperature at the global scale. This confirms that the latter is not sufficient as a proxy for temperature conditions near or in the soil. With our soil-specific global bioclimatic products, we have provided the means to correct for these important region-specific, non-linear differences between soil and air temperature at an unprecedented spatial resolution.

Drivers of the temperature offset

Our empirical modelling approach enabled us to accurately map global patterns in soil temperature. In doing so we did not aim to disentangle the mechanisms governing the temperature offset: such an endeavour would require modelling the biophysics of energy exchange at the soil surface across biomes (Kearney *et al.*, 2019, Maclean *et al.*, 2019, Maclean & Klinges, 2021). Importantly, many of the predictor variables used in our study (e.g., long-term averages in macroclimatic conditions or solar radiation) are unlikely to represent direct causal relationships underlying the temperature offset, but may rather indirectly relate to many ensuing factors that affect the functioning of ecosystems at fine spatial scales which, in turn, feedback on local temperature offsets, such as energy and water balances, snow cover, wind intensity and vegetation cover (De Frenne *et al.*, 2021). For example, while increased solar radiation itself would theoretically result in soils warming more than the air, high solar radiation at the global scale often coincides with high vegetation cover blocking radiation input to the soil, thus correlating with relatively cooler soils (De Frenne *et al.*, 2021). Our results highlight, however, that the complex relationship between microclimatic soil temperature and macroclimatic air temperature is predictable across large spatial extents thanks to broad scale patterns, even if this is governed by a multitude of local-scale factors involving fine spatiotemporal resolutions. Nevertheless, the predictive quality of our models was lower in high latitude regions, where high variation in the *in situ* measured offsets – likely driven by the interactions between snow, local topography and vegetation – reduced predictive power of the models at the 1-km² resolution (Greiser *et al.*, 2018, Way & Lewkowicz, 2018, Grünberg *et al.*, 2020, Myers-Smith *et al.*, 2020, Niittynen *et al.*, 2020).

Implications for microclimate warming

Our results highlight clear biome-specific differences in mean annual temperature between air and soil temperatures, as well as a significant reduction in the spatial variation in temperature in the soil or near the soil surface, especially in cold and cool biomes (Fig. 4). These patterns remain even despite the presence of often strongly opposing monthly offset trends (Fig. 2). The observed correlation between long-term averages in macroclimatic conditions and the annual temperature offset illustrates that soil temperature is unlikely to warm at the same rate as air temperature when macroclimate warms. Indeed, one degree of air temperature warming could result in either a bigger or smaller soil temperature change, depending on where along the macroclimatic gradient this is happening. These effects might be seen in cold biome soils most strongly, as they not only experience the largest (positive) temperature offsets and reductions in climate range compared to air temperature (Fig. 4b, c), but they are also expected to experience the strongest magnitude of macroclimate warming (Cooper, 2014, Overland *et al.*, 2014, Chen *et al.*, 2021, GISTEMP Team, 2021). As a result, mean annual temperatures in cold climate soils can be expected to warm slower than the corresponding macroclimate as offsets shrink with increasing macroclimate warming.

Contrastingly, predicted climate warming in hot and dry biomes could be amplified in the topsoil, where we show soils to become increasingly warmer than the air at higher temperatures. Similarly, changes in precipitation regimes – and thus soil moisture – can significantly alter the relationship between air and soil temperature, with critical implications for soil moisture-atmosphere feedbacks, especially in hot biomes (Zhou *et al.*, 2021). Indeed, as precipitation decreases, offsets could turn more positive and soil temperatures might warm even faster than the observed macroclimate warming. Therefore, future research should not only use soil temperature data as provided here to study belowground ecological processes (De Frenne *et al.*, 2013, Lembrechts *et al.*, 2020), it should also urgently investigate future scenarios of soil climate warming in light of changing air temperature and precipitation, at ecologically relevant spatial and temporal resolutions to incorporate the non-linear relationships exposed so far (Lembrechts & Nijs, 2020).

Within-pixel heterogeneity

We chose to use a 1-km² resolution spatial grid to model mismatches between soil and air temperature, aggregating all values from different microhabitats within the same 1-km² grid cell (e.g., sensors in forested versus open patches) as well as all daily and diurnal variation within a month. We are aware that higher spatiotemporal resolutions would likely reveal the importance of locally heterogeneous variables. Finer-scale factors that affect the local radiation balance and wind (e.g., topography, snow and vegetation cover, urbanization) at the landscape to local scales and those that directly affect neighbouring locations (e.g. topographic shading and cold-air drainage, Whiteman, 1982, Ashcroft & Gollan, 2012, Lembrechts *et al.*, 2020) would probably have emerged as more important drivers at regional scales and with higher spatiotemporal resolutions than those used here (Supplementary Material Fig. S12). The latter is illustrated by the multi-degree Celsius difference in mean annual temperature between forested and non-forested locations within the same biome (Supplementary Material Table S7), as well as the lower accuracy obtained during winter months at high latitudes, where and when fine-scale spatial heterogeneity in snow cover and depth probably lowers models' predictability at the 1-km² resolution. *In-situ* measurements were largely from areas with a representative vegetation type, supporting the reliability of our predictions for the dominant habitat type within a pixel. However, improved accuracy at high latitudes will depend on the future development of high-resolution snow depth and/or snow water equivalent estimates (Luojus *et al.*, 2010).

The SoilTemp database (Lembrechts *et al.*, 2020) will facilitate the necessary steps towards mapping soil temperature at higher spatiotemporal resolutions in the future, with its georeferenced time series of *in situ* measured soil and near-surface temperature and associated metadata. Nevertheless, when compared to existing soil temperature products such as those from ERA5L (Copernicus Climate Change Service (C3S), 2019), we emphasize that the increased resolution of our data products already provides a major technical advance, even though substantial finer within-pixel variation is still lost through spatiotemporal aggregation.

Conclusions

The spatial (biome-specific) and temporal (seasonally variable) offsets between air and soil temperature quantified here likely bias predictions of current and future climate impacts on species and ecosystems (Körner & Paulsen, 2004, Kearney *et al.*, 2009, Cooper, 2014, Opedal *et al.*, 2015, Graae *et al.*, 2018, Zellweger *et al.*, 2020, Bergstrom *et al.*, 2021). Temperature in the topsoil rather than in the air ultimately defines the distribution and performance of most terrestrial species, as well as many ecosystem functions at or below the soil surface (Pleim & Gilliam, 2009, Portillo-Estrada *et al.*, 2016, Hursh *et al.*, 2017, Gottschall *et al.*, 2019). As many ecosystem functions are highly correlated with temperature (yet often non-lineary, Johnston *et al.*, 2021), soil temperature rather than air temperature should in those instances be the preferred predictor for estimating their rates and temperature thresholds (Rosenberg *et al.*, 1990, Coûteaux *et al.*, 1995, Schimel *et al.*, 1996). Correcting for the non-linear relationship between air and soil temperature identified here is thus vital for all fields investigating abiotic and biotic processes relating to terrestrial environments (White *et al.*, 2020). Indeed, soil temperature, macroclimate and land-use change will interact to define the future climate as experienced by organisms, and high-resolution soil temperature data is needed to tackle current and future challenges.

By making our global soil temperature maps and the underlying monthly offset data openly available, we offer gridded soil temperature data for climate research, ecology, agronomy and other life and environmental sciences. Future research has the important task of further improving the spatial and temporal resolution of global microclimate products as microclimate operates at much higher temporal resolutions, with temporal variation over hours, days, seasons and years (Potter *et al.*, 2013, Bütikofer *et al.*, 2020), as well as to confirm accuracy of predictions in undersampled regions in the underlying maps (Lembrechts *et al.*, 2021). However, we are convinced that the maps presented here bring us one step closer to having accessible climate data exactly where it matters most for many terrestrial organisms (Ashcroft *et al.*, 2014, Niittynen & Luoto, 2018, Lembrechts & Lenoir, 2019). We nevertheless highlight that there is still a long way to go towards global soil microclimate data with an optimal spatiotemporal resolution. We therefore urge all scientists to submit their microclimate time series to the SoilTemp database to fill data gaps and help to increase the spatial resolution until it matches with the scale at which ecological processes take place (Bütikofer *et al.*, 2020, Lembrechts *et al.*, 2020).

Data availability

All monthly data to train the models and reproduce the figures, sampled covariate data, and models are available at https://doi.org/10.5281/zenodo.4558663. Soil bioclim layers SBIO1-11 are also directly available in Google Earth Engine under projects/crowtherlab/soil_bioclim/soil_bioclim_0_5cm and projects/crowtherlab/soil_bioclim/soil_bioclim_5_15cm.

Code availability

All source code is available at https://doi.org/10.5281/zenodo.4558663.

Acknowledgements

JJL areceived funding from the Research Foundation Flanders (grant nr. 12P1819N) The project received funding from the Research Foundation Flanders (grants nrs, G018919N, W001919N). JA received funding from the University of Helsinki, Faculty of Science (MICROCLIM, grant nr. 7510145) and Academy of Finland Flagship (grant no. 337552). PDF, CM and PV received funding from the European Research Council (ERC) under the European Union's Horizon 2020 research and innovation programme (ERC Starting Grant FORMICA 757833). JK received funding from the Arctic Interactions at the University of Oulu and Academy of Finland (318930, Profi 4), Maa- ja vesitekniikan tuki ry., Tiina and Antti Herlin Foundation, Nordenskiöld Samfundet and Societas pro Fauna et Flora Fennica. MK received funding from the Czech Science Foundation (grant nr. 20-28119S) and the Czech Academy of Sciences (grant nr. RVO 67985939). TC received funding from DOB Ecology. National Geographic Society grant no. 9480-14 and WW-240R-17. MA recieved funding from CISSC (program ICRP (grant nr:2397) and INSF (grant nr: 96005914). The Royal Botanic Garden Edinburgh is supported by the Scottish Government's Rural and Environment Science and Analytical Services Division. JMA received funding from the Funding Org. Qatar

Petroleum (grant nr. QUEX-CAS-QP-RD-18/19). JMA received funding from the European Union's Horizon 2020 research and innovation program (grant no. 678841) and from the Swiss National Science Foundation (grant no. 31003A_176044). JA was supported by research grants LTAUSA19137 (program INTER-EXCELLENCE, subprogram INTER-ACTION) provided by Czech Ministry of Education, Youth and Sports and 20-05840Y of the Czech Science Foundation. AA was supported by the Ministry of Science and Higher Education of the Russian Federation (grant FSRZ-2020-0014). SN, UAT, JJA, and JvO received funding from the Independent Research Fund Denmark (7027-00133B). LvdB, KT, MYB and RC acknowledge funding from the German Research Foundation within the Priority Program SPP-1803 "EarthShape: Earth Surface Shaping by Biota" (grant TI 338/14-1&2 and BA 3843/6-1). PB was supported by grant project VEGA of the Ministry of Education of the Slovak Republic and the Slovak Academy of Sciences No. 2/0132/18. Forest Research received funding from the Forestry Commission (climate change research programme). JCB acknowldeges the support of Universidad Javeriana. JLBA received funding from the Dirección General de Cambio Climático del Gobierno de Aragón; JLBA acknowledges fieldwork assistance by Ana Acín, the Ordesa y Monte Perdido National Park, and the Servicio de Medio Ambiente de Soria de la Junta de Castilla y León. RGB and MPB received funding from BECC - Biodiversity and Ecosystem services in a Changing Climate. MPB received funding from The European Union's Horizon 2020 research and innovation program under the Marie Skłodowska-Curie Grant Agreement No. 657627 and The Swedish Research Council FORMAS – future research leaders No. 2016-01187. JB received funding from the Czech Academy of Sciences (grant nr. RVO 67985939). NB received funding from the SNF (grant numbers 40FA40_154245, 20FI21_148992, 20FI20_173691, 407340_172433) and from the EU (contract no. 774124). ICOS EU research infrastructure. EU FP7 NitroEurope. EU FP7 ECLAIRE. The authors from Biological Dynamics of Forest Fragments Project, PDBFF, Instituto Nacional de Pesquisas da Amazônia, Brazil were supported by the MCTI/CNPq/FNDCT – Ação Transversal n°68/2013 – Programa de Grande Escala da Biosfera-Atmosfera na Amazônia – LBA; Project "Como as florestas da Amazônia Central respondem às variações climáticas? Efeitos sobre dinâmica florestal e sinergia com a fragmentação florestal.". to The EUCFLUX Cooperative Research Program and Forest Science and Research Institute-IPEF. NC acknowledges funding by Stelvio National Park. JC was funded by the Spanish government grant CGL2016-78093-R. ANID-FONDECYT 1181745 AND INSTITUTO ANTARTICO CHILENO (INACH FR-0418). SC received funding from the German Research Foundation (grant no. DFG– FZT 118, 202548816). The National Science Foundation, Poland (grant no. UMO-2017/27/B/ST10/02228), within the framework of the "Carbon dioxide uptake potential of sphagnum peatlands in the context of atmospheric optical parameters and climate changes"(KUSCO2) project. SLC received funding from the South African National Research Foundation and the Australian Research Council. FM, MČ, KU and MU received funding from Slovak Research and Development Agency (no. APVV-19-0319). Instituto Antartico Chileno (INACH_RT-48_16), Iniciativa Científica Milenio Núcleo Milenio de Salmónidos Invasores INVASAL, Institute of Ecology and Biodiversity (IEB), CONICYT PIA APOYO CCTE AFB170008. PC is supported by NERC core funding to the BAS 'Biodiversity, Evolution and Adaptation Team. EJC received funding from the Norwegian Research Council (grant n umber 230970). GND was supported by NERC E3 doctoral training partnership grant (NE/L002558/1) at the University of Edinburgh and the Carnegie Trust for the Universities of Scotland. Monitoring stations on Livingston Island, Antarctica were funded by different research projects of the Gobern of Spain (PERMAPLANET CTM2009-10165-E; ANTARPERMA CTM2011-15565-E; PERMASNOW CTM2014-52021-R), and the PERMATHERMAL arrangement between the University of Alcalá and the Spanish Polar Committee. GN received funding from the Autonomous Province of Bolzano (ITA). The infrastructure, part of the UK Environmental Change Network, was funded historically in part by ScotNature.and and NERC National Capability LTS-S: UK-SCAPE; NE/R016429/1). JD was supported by the Czech Science Foundation (GA17-19376S) and MSMT (LTAUSA18007). ED received funding from the Kempe Foundation (JCK-1112 and JCK-1822). The infrastructure was supported by the Ministry of Education, Youth and Sports of the Czech Republic within the National Sustainability Programme I (NPU I), grant number LO1415 and by the project for national infrastructure support CzeCOS/ICOS Reg.No. LM2015061. NE received funding from the German Research Foundation (DFG– FZT 118, 202548816). BE received funding from the GLORIA-EU project no EVK2-CT2000-00056, the Autonomous Province of Bolzano (ITA), from the Tiroler Wissenschaftsfonds and from the University of Innsbruck. RME was supported by funding to the SAFE Project from the Sime Darby Foundation. OF received funding from the German Research Foundation (DFG– FZT 118, 202548816). EFP was supported by the Jardín Botánico Atlántico (SV-20-GIJON-JBA). MF was funded by the German Federal Ministry of Education and Research (BMBF) in the context of The Future Okavango (Grant No. 01LL0912) and SASSCAL (01LG1201M; 01LG1201N) projects. RAG received funding from Fondecyt 11170516 and CONICYT PIA AFB170008. MBG received funding from National Parks (DYNBIO, #1656/2015) and The Spanish Research Agency (VULBIMON, #CGL2017-90040-R). MG received funding from the Swiss National Science Foundation (ICOS-CH Phase 2 20FI20_173691). FG received funding from the German Research Foundation (DFG– FZT 118, 202548816). KG and TS received funding from the UK Biotechnology and Biological Research Council (grant = 206/D16053). SG was supported by the Research Foundation Flanders (FWO) (project G0H1517N). KJ and PH received funding from the EU Horizon2020 INFRAIA project eLTER-PLUS (871128), the project LTER-CWN (FFG, F&E Infrastrukturförderung, project number 858024) and the Austrian Climate Research Program (ACRP7 – CentForCSink – KR14AC7K11960). SH and ARB received funding through iDiv funded by the German Research Foundation (DFG– FZT 118, 202548816). LH received funding from the Czech Science Foundation (grant nr. 20-28119S) and the Czech Academy of Sciences (grant nr. RVO 67985939). MH received funding from the Baden-Württemberg Ministry of Science, Research and Arts via the project DRIeR (Drought impacts, processes and resilience: making the in-visible visible). LH received funding from International Polar Year, Weston Foundation, and ArcticNet. DH received funding from Natural Sciences and Engineering Council (Canada) (RGPIN-06691). TTH received funding from Independent Research Fund Denmark (grant no. 8021-00423B) and Villum Foundation (grant no. 17523). Ministry of Education, Youth and Sports of the Czech Republic (projects LM2015078, VAN2020/01 and CZ.02.1.01/0.0/0.0/16_013/0001708). KH and CG received funding from Bolin Centre for Climate Research, Stockholm University and from the Swedish research council Formas [grant n:o 2014-00530 to KH]. JJ received funding from the Funding Org. Swedish Forest Society Foundation (grant nr. 2018-485-Steg 2 2017) and Swedish Research Council FORMAS (grant nr. 2018-00792). Project LAS III 77/2017/B entitled: \"Estimation of net carbon dioxide fluxes exchanged between the forest ecosystem on post-agricultural land and between the tornado-damaged forest area and the atmosphere using spectroscopic and numerical methods\", source of funding: General Directorate of State Forests, Warsaw, Poland. AJ received funding from the German Federal Ministry of Education and Research BMBF (Grant Nr. FKZ 031B0516C SUSALPS) and the Oberfrankenstiftung (Grant Nr. OFS FP00237). ISJ received funding from the Energy Research Fund (NÝR-11 - 2019, NÝR-18 - 2020). TJ was supported by a UK NERC Independent Research Fellowship (grant number: NE/S01537X/1). RJ received funding from National Science Centre of Poland (grant number: 2016/21/B/ST10/02271) and Polish National Centre for Research and Development (grant number: Pol-Nor/203258/31/2013). VK received funding from the Czech Academy of Sciences (grant nr. RVO 67985939). AAK received funding from MoEFCC, Govt of India (AICOPTAX project F. No. 22018/12/2015/RE/Tax). NK received funding from FORMAS, VR, support from the research infrastructure ICOS. BK received funding from the Nati onal Research, Development and Innovation Fund of Hungary (grant nr. K128441). Ministry of Education, Youth and Sports of the Czech Republic (projects LM2015078 and CZ.02.1.01/0.0/0.0/16_013/0001708). Project B1-RNM-163-UGR-18-Programa Operativo FEDER 2018, partially funded data collection. Norwegian Research Council (NORKLIMA grants #184912 and #244525) awarded to Vigdis Vandvik. MM received funding from the Czech Science Foundation (grant nr. 20-28119S) and the Czech Academy of Sciences (grant nr. RVO 67985939). Project CONICYT-PAI 79170119 awarded to Roy Mackenzie. This work was partly funded by project MIUR PON Cluster OT4CLIMA. RM received funding from the SNF project number 407340_172433. FM received funding from the Stelvio National Park. PM received funding from AIAS-COFUND fellowship programme supported by the Marie Skłodowska- Curie actions under the European Union's Seventh Framework Pro-gramme for Research, Technological development and Demonstration (grant agreement no 609033) and the Aarhus University Research Foundation, Denmark. RM received funding from the Ministry of Education, Youth and Sports of the Czech Republic (project LTT17033). SM and VM received funding from EU FP6 NitroEurope (grant nr. 17841), EU FP7 ÉCLAIRE (grant nr. 282910), the Ministry of Education and Science of Ukraine (projects nr. 505, 550, 574, 602), GEF-UNEP funded "Toward INMS" project (grant nr. NEC05348) and ENI CBC BSB PONTOS (grant nr. BSB 889). STM received funding from New Frontiers in Research Fund-Exploration (grant nr. NFRF-2018-02043) and NSERC Discovery. MMR received funding from the Australian Research Council Discovery Early Career Research Award (grant nr. DE180100570). JAM received funding from the National Science Foundation (DEB 1557094), International Center for Advanced Renewable Energy and Sustainability (I-CARES) at Washington University in St. Louis, ForestGEO, and Tyson Research Center. IM-S was funded by the UK Natural Environment Research Council through the ShrubTundra Project (NE/M016323/1). MBN received funding from FORMAS, VR, Kempe Foundations support from the research infrastructures ICOS and SITES. MDN received funding from CONICET (grant nr. PIP 112-201501-00609). Spanish Minsitry of Science grant PID2019-110521GB-I00 and Catalan government grant 2017-1005. French National Research Agency (ANR) in the frame of the Cluster of Excellence COTE (project HydroBeech, ANR-10-LABX-45). VLIR-OUS, under the Institutional University Coorperation programme (IUC) with Mountains of the Moon University. Max Planck Society (Germany), RFBR, Krasnoyarsk Territory and Krasnoyarsk Regional Fund of Science, project number 20-45-242908. Estonian Research Council (PRG609), and the European Regional Development Fund (Centre of Excellence EcolChange). Canada-Denmark Arctic Research Station Early Career Scientist Exchange Program, from Polar knowledge Canada (POLAR) and the Danish Agency for Science and Higher Education. Fondecyt 1180205 and CONICYT PIA AFB170008. MP received funding from the Funding Org. Knut and Alice Wallenberg Foundation (grant nr. 2015.0047), and acknowledges funding from the Swedish Research Council (VR) with contributing research institutes to both the SITES and ICOS Sweden infrastructures. Spanish Minsitry of Science grant PID2019-110521GB-I00, fundación Ramón Areces ELEMENTAL-CLIMATE project, and Catalan government grant 2017-1005. MPB received funding from the Svalbard Environmental Protection Fund (grant project number 15/128) and the Research Council of Norway (Arctic Field Grant, project number 269957). RP received funding from the Ministry of Education, Youth and Sports of the Czech Republic (grant INTER-TRANSFER nr. LTT20017). LTSER Zone Atelier Alpes; Fédération FREE-Alpes. RP received funding from a Humboldt Fellowship for Experienced Researchers. RPu received founding from the Polish National Science Centre (grant project number 2017/27/B/NZ8/00316). ODYSSEE project (ANR-13-ISV7-0004, PN-II-ID-JRP-RO-FR-2012). KR was supported through an Australian Government Research Training Program Scholarship. Fieldwork was supported by the Global Challenges program at the University of Wollongong, the ARC the Australian Antarctic Division and INACH. Project SUBANTECO IPEV 136 (French Polar Institute Paul-Emile Victor), Zone Atelier CNRS Antarctique et Terres Australes, SAD Région Bretagne (Project INFLICT), BiodivERsa 2019-2020 BioDivClim call 'ASICS' (ANR-20-EBI5-0004). SAR received funding from the Australian Research Council. NSF grant #1556772 to the University of Notre Dame. Pavia University (Italy). OR received funding from EU-LEAP-Agri (RAMSES II), EU-DESIRA (CASSECS), EU-H2020 (SustainSahel), AGROPOLIS and TOTAL Foundations (DSCATT), CGIAR (GLDC). AR was supported by the Russian Science Foundation (Grant 18-74-10048). Parc national des Ecrins. JS received funding from Vetenskapsrådet grant nr (No: 2014-04270), ALTER-net multi site grant, River LIFE project (LIFE08 NAT/S/000266), Flexpeil. Helmholtz Association long-term research program TERENO (Terrestrial Environmental Observatories). PS received funding from the Polish Ministry of Science and Higher Education (grant nr. N N305 304840). AS recieved funding from the ETH Research grant (grant number ETH-27 19-1). LSC recevied funding from NSERC Canada Graduate Scholarship (Doctoral) Program; LSC was also supported by ArcticNet-NCE. Conselho Nacional de Desenvolvimento Científico e Tecnológico (141513/2017-9); Fundação Carlos Chagas Filho de Amparo à Pesquisa do Estado do Rio de Janeiro (E26/200.84/2019). ZS received funding from the SRDA (nr. APVV-16-0325) and from the ERDF (grant nr. ITMS 313011S735, CE LignoSilva). JS, MB, and CA received funding from core budget of ETH Zurich. State excellence Program M-V \"WETSCAPES\". AfricanBioServices project funded by the EU Horizon 2020 grant number 641918. The authors from KIT/IMK-IFU acknowldege the funding received within the German Terrestrial Environmental Observatories (TERENO) research program of the Helmholtz Association and from the Bavarian Ministry of the Environment and Public Health (UGV06080204000). Deutsche Forschungsgemeinschaft (DFG, German Research Foundation), project number 192626868, in the framework of the collaborative German-Indonesian research project CRC 990 (SFB): "EFForTS, Ecological and Socioeconomic Functions of Tropical Lowland Rainforest Transformation Systems (Sumatra, Indonesia)". MS received funding from the Ministry of Education, Youth and Sports of the Czech Republic (grant nr. INTER-TRANSFER LTT19018). TT received funding from the Swedish National Space Board (SNSB Dnr 95/16) and the CASSECS project supported by the European Union. HJDT received funding from the UK Natural Environment Research Council (NERC doctoral training partnership grant NE/L002558/1). German Science Foundation (DFG) GraKo 2010 \"Response\". PDT received funding from the MEMOIRE project (PN-III-P1-1.1-PD2016-0925). Arctic Challenge for Sustainability II (ArCS II; JPMXD1420318865). JU received funding from Czech Science Foundation (grant nr. 21-11487S). TU received funding from the Romanian Ministry of Education and Research (CCCDI - UEFISCDI -project PN-III-P2-2.1-PED-2019-4924 and PN2019-2022/19270201-Ctr. 25N BIODIVERS 3-BIOSERV). LvdB, KT, MYB and RC acknowledge funding from the German Research Foundation within the Priority Program SPP-1803 "EarthShape: Earth Surface Shaping by Biota" (grant TI 338/14-1&2 and BA 3843/6-1). AV acknowledge funding from RSF, project 21-14-00209. GFV received funding from the Dutch Research Council NWO (Veni grant, no. 863.14.013). Australian Research Council Discovery Early Career Research Award DE140101611. FGAV received funding from the Portuguese Science Foundation (FCT) under CEECIND/02509/2018, CESAM (UIDP/50017/2020+UIDB/50017/2020), FCT/MCTES through national funds, and the co-funding by the FEDER, within the PT2020 Partnership Agreement and Compete 2020. Ordesa y Monte Perdido National Park. MVI received funding from the Spanish Ministry of Science and Innovation through a doctoral grant (FPU17/05869). JW received funding from the Czech Science Foundation (grant nr. 20-28119S) and the Czech Academy of Sciences (grant nr. RVO 67985939). CR and SW received funding from the Swiss Federal Office for the Environment (FOEN) and the de Giacomi foundation. YY received funding from the National Natural Science

Foundation of China (Grant no. 41861134039 and 41941015). ZY received funding from the National Natural Science Foundation of China (grant nr. 41877458). FZ received funding from the Swiss National Science Foundation (grant nr. 172198 and 193645). PZ received funding from the Funding Org. Knut and Alice Wallenberg Foundation (grant no. 2015.0047). JL received funding from: (i) the Agence Nationale de la Recherche (ANR), under the framework of the young investigators (JCJC) funding instrument (ANR JCJC Grant project N°ANR-19-CE32-0005-01: IMPRINT); (ii) the Centre National de la Recherche Scientifique (CNRS) (Défi INFINITI 2018: MORFO); and the Structure Fédérative de Recherche (SFR) Condorcet (FR CNRS 3417: CREUSE).

Fieldwork in the Arctic got facilitated by funding from the EU INTERACT program. SN, UAT, JJA, and JvO would like to thank the field team of the Vegetation Dynamics group for their efforts and hard work. We acknowledge Dominique Tristan for letting access to the field. for the logistic support the crew of INACH and Gabriel de Castilla Station team on Deception Island. We thank the Inuvialuit and Kluane First Nations for the opportunity to work on their land. MAdP acknowledges fieldwork assistance and logistics support to Unidad de Tecnología Marina CSIC, and the crew of Juan Carlos I and Gabriel de Castilla Spanish Antarctic Stations, as well as to the different colleagues from UAH that helped on the instruments maintainance. ERF acknowledges fieldwork assistance by Martin Heggli. MBG acknowledges fieldwork and technical assistance by P Abadía, C Benedé, P Bravo, J Gómez, M Grasa, R Jimenez, H Miranda, B Ponz, J Revilla and P Tejero, and the Ordesa and Monte Perdido National Park staff. LH acknowledges field assistance by John Jacobs, Andrew Trant, Robert Way, Darroch Whitaker; I acknowledge the IInuit of Nunatsiavut, and the Cooperative Man- agement Board of Torngat Mountains National Park for their support of this project and acknowledge that the field research was conducted on their traditional lands. We thank our many bear guides, especially Boonie, Eli, Herman, John, and Maria Merkuratsuk. AAK acknowledges field support of Akhtar Malik, Rameez Ahmad. Part of microclimatic records from Saxony was funded by the Saxon Switzerland National Park Administration. Tyson Research Center. JP acknowledges field support of Emmanuel Malet (Edytem) and Rangers of Reserves Naturelles de Haute-Savoie (ASTERS). practical help: Roel H. Janssen, N. Huig, E. Bakker, Schools in the tepåseförsöket, Forskar fredag, Erik Herberg. The support by the Bavarian Forest National Park administration is highly appreciated. Liesbeth acknowledges CONAF and onsite support from the park rangers from PN Pan de Azucar, PN La Campana, PN Nahuelbuta and from communidad agricola Quebrada de Talca. JL and FS acknowledge Manuel Nicolas and all forest officers from the Office National des Forêts (ONF) who are in charge of the RENECOFOR network and who provided help and local support for the installation and maintenance of temperature loggers in the field.

Author contributions

JJL and JL conceptualized the project, JJL, JvdH, MBA, PDF, MK, ML, IMDM, TWC, IN and JL designed the paper, the SoilTemp consortium acquired the data, JJL, JVDH, JK, and PN analysed the data, JJL, JvdH, JA, MBA, PDF, JK, MK, ML, IMDM, TWC, JJB, SH, DHK, PN, BRS and KVM interpreted the analyses. All authors significantly revised the manuscript and approved it for submission.

The authors declare no competing interests.

Affiliations

1) Research Group PLECO (Plants and Ecosystems), University of Antwerp, 2610 Wilrijk, Belgium, 2) Department of Environmental Systems Science, Institute of Integrative Biology, ETH Zürich, Zürich, Switzerland, 3) Finnish Meteorological Inst., P.O. Box 503, FI-00101 Helsinki, Finland, 4) Dept of Geosciences and Geography, Gustaf Hällströmin katu 2a, FIN–00014 Univ. of Helsinki, Finland, 5) Centre for Sustainable Ecosystem Solutions, School of Biological Sciences, University of Wollongong, Wollongong, Australia, 6) Australian Museum, Sydney, Australia, 7) Forest & Nature Lab, Department of Environment, Ghent University, Geraardsbergsesteenweg 267, 9090 Melle-Gontrode, Belgium, 8) Geography Research Unit, University of Oulu, Oulu, Finland, 9) Institute of Botany of the Czech Academy of Sciences, Zámek 1, CZ-25243, Průhonice, Czech Republic, 10) Faculty of Forestry and Wood Sciences, Czech University of Life Sciences Prague, Kamýcká 129, CZ-165 21, Prague 6 - Suchdol, Czech Republic, 11) Environment and Sustainability Institute, University of Exeter, Penryn Campus, Penryn, UK, TR10 9FE, 12) Department of Geography, York St John University, Lord Mayor's Walk, York, YO31 7EX, United Kingdom, 13) Department of Earth and Environmental Sciences, KU Leuven, Celestijnenlaan 200E, 3001 Leuven, Belgium, 14) School of Natural Resources and Environment, University of Florida, Gainesville, FL 32611, USA, 15) Smithsonian Environmental Research Center, Edgewater MD 21037 USA, 16) Department of Wildlife Ecology and Conservation, University of Florida, Gainesville, FL 32611, USA, 17) Department of Natural Sciences and Environmental Health, University of South-Eastern Norway, Gullbringvegen 36, NO-3800, Bø, Norway, 18) Alpine Ecosystems Research Program, Institute of Ecology, Ilia State University, Tbilisi, Georgia, 19) Department of Range Management, Faculty of Natural Resources and Marine Sciences, Tarbiat Modares University, Noor, Mazandaran Province, I. R. Iran, 20) Department of Ecological Science, Vrije Universiteit Amsterdam, The Netherlands., 21) Royal Botanic Garden Edinburgh, 20A Inverleith Row, EH3 5LR, Edinburgh, UK, 22) Environmental Science Center, Qatar University, Doha, Qatar, 23) Department of Environmental Systems Science, Institute of Integrative Biology, ETH Zurich, Universitätsstrasse 16, CH-8092 Zürich, Switzerland, 24) Research group ECOBE, University of Antwerp, 2610 Wilrijk, Belgium, 25) Department of Agroecology and Environment, Agroscope Research Institute, Reckenholzstrasse 191, 8046 Zürich, Switzerland, 26) Department of Environmental Systems Science, ETH Zurich, Universitaetstrasse 2, 8092 Zurich, Switzerland, 27) UK Centre for Ecology & Hydrology, Bush Estate, Penicuik, Midlothian, EH26 0QB, United Kingdom, 28) Department of Physical Geography and Ecosystem Science, Lund University, Sölvegatan 12, 223 62 Lund, Sweden, 29) European Commission, Joint Research Centre (JRC), Ispra, Italy, 30) Siberian Federal University, 660041 Krasnoyarsk, Russia, 31) Instituto Argentino de Nivología, Glaciología y Ciencias Ambientales (IANIGLA), CONICET, CCT-Mendoza; Facultad de Ciencias Exactas y Naturales, Universidad Nacional de Cuyo, 32) Instituto Argentino de Nivologiá, Glaciologiá y Ciencias Ambientales (IANIGLA), CONICET, CCT-Mendoza, 33) Natural History Museum, University of Oslo, 0318, Oslo, Norway, 34) Section for Ecoinformatics & Biodiversity, Department of Biology, Aarhus University, Aarhus C, Denmark, 35) Center for Biodiversity Dynamics in a Changing World, Department of Biology, Aarhus University, Aarhus C, Denmark, 36) Ecological Plant Geography,

Faculty of Geography, University of Marburg, Deutschhausstrasse 10, 35032, Marburg, Germany, 37) Institute of Landscape Ecology Slovak Academy of Sciences, Štefánikova 3, 81499 Bratislava, Slovakia, 38) Faculty of Environmental and Forest Sciences, Agricultural University of Iceland, Árleyni 22, 112 Reykjavík, Iceland, 39) Instituto Argentino de Nivología, Glaciología y Ciencias Ambientales (IANIGLA), CONICET, CCT-Mendoza, 40) Isotope Bioscience Laboratory - ISOFYS, Ghent University, Coupure Links 653, 9000 Gent, Belgium, 41) Université de Rennes, CNRS, EcoBio (Ecosystèmes, biodiversité, évolution) - UMR 6553, F-35000 Rennes, France, 42) Department of Sustainable Agro-ecosystems and Bioresources, Research and Innovation Centre, Fondazione Edmund Mach, Via E. Mach 1, 38010 San Michele all'Adige, Italy, 43) Forest Research, Alice Holt Lodge, Wrecclesham, Farnham, UK, 44) Department of Ecology, Pontificia Universidad Javeriana, Bogota, Colombia, 45) Jolube Consultor Botánico. C/Mariano R de Ledesma, 4. E-22700 Jaca, Huesca, SPAIN, 46) Institute of Landscape and Plant Ecology, Department of Plant Ecology, University of Hohenheim, Ottilie-Zeller_weg 2, 70599 Stuttgart, Germany, 47) Disturbance Ecology, BayCEER, University of Bayreuth, Universitätsstr. 30, 95447 Bayreuth, Germany, 48) Norwegian Institute for Nature Research, FRAM - High North Research Centre for Climate and the Environment, P.O. Box 6606 Langnes, N-9296 Tromsø, Norway, 49) Department of Earth Sciences, University of Gothenburg, P.O. Box 460, SE-40530 Gothenburg, Sweden, 50) Gothenburg Global Biodiversity Centre, P.O. Box 461, SE-405 30 Gothenburg, Sweden, 51) Department of Biological and Environmental Sciences, University of Gothenburg, P.O. Box 461, 43 Gothenburg SE-405 30, Sweden, 52) Department of Environmental Science, Policy, and Management, University of California, Berkeley, CA 94720 USA, 53) Alfred Wegener Institute Helmholtz Center for Polar and Marine Research, Telegrafenberg A45, 14473 Potsdam, Germany, 54) Geography Department, Humboldt-Universität zu Berlin, Germany, 55) Pós-Graduação em Ciências de Florestas Tropicais, Instituto Nacional de Pesquisas da Amazônia, Manaus, Brasil, CEP: 69060-001, 56) UMR ECOSYS INRAE, AgroParisTech, Uinversité Paris Saclay, France, 57) Biological Dynamics of Forest Fragments Project, BDFFP, Instituto Nacional de Pesquisas da Amazônia, Av. André Araujo, 2936 - Petrópolis, Manaus, Amazonas, 69067-375, Brazil, 58) Department of Forest Sciences, Federal University of Lavras, 37.200-900, Lavras, MG, Brazil, 59) Faculty of Arts and Sciences, Department of Molecular Biology and Genetics, Ordu University, 52200, Ordu, Turkey, 60) Ecological Plant Geography, Faculty of Geography, University of Marburg, Deutschhausstrasse 10, 35032, Marburg, Germany., 61) Plant Ecology Group, Department of Evolution and Ecology, University of Tübingen, Auf der Morgenstelle 5, 72076 Tübingen, Germany, 62) Department of Science and High Technology, Insubria University, Via Valleggio 11, 22100 Como, Italy, 63) Department of Chemistry, Life Sciences and Environmental Sustainability, University of Parma, Parco Area delle Scienze 11/A, 43124 Parma, Italy, 64) Department of Evolutionary Biology, Ecology and Environmental Sciences, Biodiversity Research Institute (IRBio), University of Barcelona, 08028 Barcelona, Catalonia, Spain, 65) CREAF, E08193 Bellaterra (Cerdanyola del Vallès), Catalonia, Spain, 66) Laboratorio de Ecofisiología vegetal y Cambio Climático and Núcleo de Estudios Ambientales (NEA), Universidad Católica de Temuco, Campus Luis Rivas del Canto, Rudecindo Ortega 02950, Temuco, Chile., 67) German Centre for Integrative Biodiversity Research (iDiv) Halle-Jena-Leipzig, Leipzig, Germany, 68) Institute of Biology, Leipzig University, Leipzig, Germany, 69) Laboratory of Bioclimatology, Department of Ecology and Environmental Protection, Poznan University of Life Siences, ul. Piatkowska 94, 60-649, Poznan, Poland, 70) Univ. Grenoble Alpes, Univ. Savoie Mont Blanc, CNRS, LECA, F-38000 Grenoble, France, 71) Univ. Grenoble Alpes, Univ. Savoie Mont Blanc, CNRS, LTSER Zone Atelier Alpes, F-38000 Grenoble, France, 72) Securing Antarctica's Environmental Future, School of Biological Sciences, Monash University, Victoria 3800, Australia, 73) Forest Ecology and Conservation Group, Department of Plant Sciences, University of Cambridge, Cambridge CB23EA, UK, 74) Faculty of Ecology and Environmental Sciences, Technical University in Zvolen, T. G. Masaryka 24, 960 01 Zvolen, Slovakia, 75) Sub-Antarctic Biocultural Conservation Program, Universidad de Magallanes, Pdte. Manuel Bulnes 01855, Punta Arenas, Magallanes y la Antártica Chilena, 76) Núcleo Milenio de Salmónidos Invasores, INVASAL, Concepción, Chile, 77) British Antarctic Survey, NERC, High Cross, Madingley Road, Cambridge CB3 0ET, United Kingdom, 78) Department of Arctic and Marine Biology, Faculty of Biosciences Fisheries and Economics, UiT-The Arctic University of Norway, N-9037 Tromsø, Norway, 79) Climate Change Unit, Environmental Protection Agency of Aosta Valley, Italy, 80) Department of Biological Sciences, University of Notre Dame, Notre Dame, IN 46556, USA, 81) Department of Science, University of Roma Tre, 00146 Rome, Italy, 82) Department of Ecology, Environment and Plant Sciences and Bolin Centre for Climate Research, Stockholm University, 106 91 Stockholm, Sweden, 83) the County Administrative Board of Västra Götaland, SE-403 40 Gothenburg, Sweden, 84) School of GeoSciences, University of Edinburgh, King's Buildings, Edinburgh, EH9 3FF, United Kingdom, 85) Department of Geology, Geography and Environment. University of Alcalá. 28805 Alcalá de Henares, Madrid, Spain., 86) Chair of Geoinformatics, Technische Universität Dresden, Dresden Germany, 87) Vegetation Ecology, Institute of Natural Resource Sciences, ZHAW Zurich University of Applied Sciences, Grüental, 8820 Wädenswil, Switzerland, 88) Plant Ecology, Bayreuth Center of Ecology and Environmental Research (BayCEER), University of Bayreuth, Universitätsstr. 30, 95447 Bayreuth, Germany, 89) VITO-TAP, Boeretang 200, 2400-Mol, Belgium, 90) Swiss Federal Research Institute WSL, 8903 Birmensdorf, Switzerland, 91) Majella Seed Bank, Majella National Park, Colle Madonna, 66010 Lama dei Peligni, Italy, 92) Department of Life, Health and Environmental Sciences, University of L'Aquila, Piazzale Salvatore Tommasi 1, 67100 L'Aquila, Italy, 93) Grupo de Ecología de Poblaciones de Insectos, IFAB (INTA - CONICET), Modesta Victoria 4450, Bariloche, Argentina, 94) Department of Biology and Biochemistry, University of Houston, Houston, Texas, 77204 USA, 95) Faculty of Science, Department of Botany, University of South Bohemia, Na Zlaté Stoce 1, 37005 České Budějovice, Czech Republic, 96) Climate Impacts Research Centre, Department of Ecology and Environmental Sciences, Umeå University, Abisko, Sweden, 97) Global Change Research Institute, Academy of Sciences of the Czech Republic, 98) Department of Ecology & Evolutionary Biology, University of Arizona, USA, 99) School of Biological Sciences, The University of Western Australia, Crawley, WA 6009, Australia, 100) Kings Park Science, Department of Biodiversity, Conservation & Attractions, Kings Park, 6005 WA, Australia, 101) Department of Botany, Faculty of Biology, University of Innsbruck, Sternwartestraße 15, 6020 Innsbruck, Austria, 102) Imperial College London, Silwood Park Campus, Ascot SL5 7PY, UK, 103) Operation Wallacea, Wallace House, Old Bolingbroke, Lincolnshire, PE23 4EX, UK, 104) INRAE, Bordeaux Sciences Agro, UMR 1391 ISPA, F-33140 Villenave d'Ornon, France, 105) Department of Life and Environmental Sciences, University of Cagliari, Viale Sant'Ignazio da Laconi 13, 09123, Cagliari, Italy., 106) Department of Botany, University of Granada, 18071, Granada, Spain, 107) IMIB – Biodiversity Research Institute, University of Oviedo, Mieres, Spain, 108) Institute for Plant Science and Microbiology, University of Hamburg, Ohnhorststr. 18, 22609 Hamburg, Germany, 109) Dartmouth College, Hanover, NH, USA, 110) Ecosystems and Global Change Group, Department of Plant Sciences, University of Cambridge, Cambridge, CB2 3EA, United Kingdom, 111) WSL Institute for Snow and Avalanche Research SLF, 7260 Davos, Switzerland, 112) Swiss Federal Research Institute for Forest, Snow and Landscape Research WSL, 8903 Birmensdorf, Switzerland, 113) Laboratorio de Invasiones Biológicas (LIB), Facultad de Ciencias Forestales, Universidad de Concepción, Concepción, Chile, 114) School of Education and Social Sciences, Adventist University of Chile, Chile, 115) Instituto de Ecología y Biodiversidad (IEB), Santiago, Chile, 116) Pyrenean Institute of Ecology (CSIC), Av. Montañana 1005, 50059

Zaragoza, Spain, 117) Biodiversity and Landscape, TERRA research centre, Gembloux Agro-Bio Tech, University of Liège, Gembloux, 5032, Belgium ; Research Group PLECO (Plants and Ecosystems), University of Antwerp, 2610 Wilrijk, Belgium, 118) Department of Geo-information in Environmental Management, Mediterranean Agronomic Institute of Chania, PO Box 85, 73100 Chania, Greece, 119) Georgian Institute of Public Affairs, department of Environmental management ad policy, Tbilisi, Georgia, 120) Flemish Institute for Technological Research, 2400 Mol, Belgium, 121) Department of Earth and Environmental Science, Faculty of BioScience Engineering, KULeuven, Belgium, 122) Max Planck Institute for Biogeochemistry, Department of Biogeochemical Signals, Jena, Germany, 123) Sustainable Agricultural Sciences Department, Rothamsted Research, Harpenden, AL5 2JQ, UK, 124) Department of Biology, Norwegian University of Science and Technology, 7491 Trondheim, Norway, 125) Biodiversity, Wildlife and Ecosystem Health, Biomedical Sciences, University of Edinburgh, Edinburgh, EH8 9JZ, UK, 126) Department of Ecology, Swedish University of Agricultural Sciences, Box 7042, S-750 07 Uppsala, 127) School of Biological Sciences, The University of Hong Kong, Pok Fu Lam Road, Hong Kong SAR, China, 128) Department of Theoretical and Applied Sciences, Insubria University, Via Dunant 3, 21100 Varese, Italy, 129) CIRAD, UMR Eco&Sols, 34060 Montpellier, France, 130) Eco&Sols, Univ Montpellier, CIRAD, INRAE, IRD, Montpellier SupAgro, 34060 Montpellier, France, 131) Senckenberg Research Institute and Natural History Museum Frankfurt, 63571 Gelnhausen, Germany, 132) Faculty of Biology, University of Duisburg-Essen, 45141 Essen, Germany, 133) Institute of Biology / Geobotany and Botanical Garden, Martin Luther University Halle-Wittenberg, Halle (Saale), Germany, 134) Department of Biological Sciences and Bjerknes Centre for Climate Research, University of Bergen, N-5020 Bergen, Norway, 135) Centre for Biodiversity & Taxonomy, Department of Botany, University of Kashmir, Srinagar - 190006, J&K, India, 136) Department of Ecology, University of Innsbruck, 6020 Innsbruck, Austria, 137) INRAE, Univ. Bordeaux, BIOGECO, F-33610 Cestas, France, 138) Museumsenteret i Hordaland, Lyngheisenteret, Alver, Norway, 139) TERRA Teaching and Research Center, Faculty of Gembloux Agro-Bio Tech, University of Liege, Passage des déportés, 2, 5030 Gembloux, Belgium, 140) UK Centre for Ecology & Hydrology, Penicuik, EH26 0QB, Scotland, UK., 141) Institute for Botany, University of Natural Resources and Life Sciences Vienna (BOKU), Gregor-Mendel-Straße 33/I, 1180 Vienna, Austria, 142) Centre for Agrometeorological Research (ZAMF), German Meteorological Service (DWD), Bundesallee 33, 38116 Braunschweig, Germany, 143) Dept of Biology, Memorial University, St. John's, NL, A1B 3X9. Canada, 144) Department of Biological Sciences, Simon Fraser University, Burnaby, BC, V5A 1S6, Canada, 145) Department of Geography, University of Zaragoza, Pedro Cerbuna 12, 50009 Zaragoza, Spain, 146) Plant Ecology, Albrecht-von-Haller-Institute for Plant Sciences, Georg-August University of Goettingen, Untere Karspuele 2, 37073 Goettingen, Germany, 147) Department of Bioscience and Arctic Research Centre, Aarhus University, Grenåvej 14, 8410 Rønde, Denmark, 148) Department of Geography, Masaryk University, Faculty of Science, Kotlarska 2, 611 37, Brno, Czech Republic, 149) Department of Environmental Science, Shinshu University, Matsumoto, Japan, 150) Department of Bioscience and Arctic Research Centre, Aarhus University, Frederiksborgvej 399, 4000 Roskilde, Denmark, 151) INRAE, University of Bordeaux, BIOGECO, F-33610 Cestas, France, 152) Department of Forest Ecology and Management, Swedish University of Agricultural Sciences, 90183 Umeå, Sweden, 153) Laboratory of Meteorology, Department of Construction and Geoengineering, Faculty of Environmental Engineering and Mechanical Engineering, Poznan University of Life Siences, ul. Piatkowska 94, 60-649, Poznan, Poland, 154) Forest Research Institute, Department of Silviculture and Forest Tree Genetics, Braci Lesnej Street, No 3, Sekocin Stary, 05-090 Raszyn, Poland, 155) Bayreuth Center of Ecology and Environmental Research, 156) ARAID/IPE-CSIC, Pyrenean Institute of Ecology, Avda. Llano de la Victoria, 16, Jaca 22700, Spain, 157) Life and Environmental Sciences, University of Iceland, Sturlugata 7, 102 Reykjavík, Iceland, 158) Soil Science Department, Federal University of Viçosa, Prof. Peter Henry Rolfs Ave., 36570-900, Viçosa-MG, Brazil, 159) School of Biological Sciences, University of Bristol, Bristol, United Kingdom, 160) Biological and Environmental Sciences, Faculty of Natural Sciences, University of Stirling, Scotland, FK9 4LA, 161) Faculty of Environmental Sciences, Czech University of Life Sciences Prague, Kamýcká 129, 165 21 Prague 6 - Suchdol, Czech Republic, 162) Centre for Environmental and Climate Science, Lund University, Sölvegatan 37, 223 62, Lund, Sweden, 163) University of Goettingen, Bioclimatology, Büsgenweg 2, 37077 Göttingen, Germany., 164) Environment Agency Austria, Spittelauer Lände 5, 1090 Vienna, Austria, 165) Max Planck Institute for Biogeochemistry, Jena, Thuringia, Germany, 166) Centre for Ecological Research, Institute of Ecology and Botany, H-2163 Vácrátót, Alkotmány út 2-4., Hungary, 167) Experimental Plant Ecology, Institute of Botany and Landscape Ecology, University of Greifswald, D-17487 Greifswald, Germany, 168) GLORIA Coordination, Institute for Interdisciplinary Mountain Research, Austrian Academy of Sciences (ÖAW) & Department of Integrative Biology and Biodiversity Research, University of Natural Resources and Life Sciences, Vienna (BOKU), Silbergasse 30/3, 1190 Vienna, Austria, 169) Department of Arctic Biology, The University Centre in Svalbard (UNIS), 9171 Longyearbyen, Svalbard, Norway, 170) Department of Land Resources and Environmental Sciences, Montana State University, Bozeman MT, USA, 59717, 171) Climate Impacts Research Centre, Department of Ecology and Environmental Sciences, Umeå University, Vetenskapens väg 38, 98107 Abisko, Sweden, 172) Centre for Polar Ecology, Faculty of Science, University of South Bohemia, Na Zlaté Stoce 3, CZ-370 05, České Budějovice, Czech Republic, 173) School of Biological Sciences, Monash University, Victoria 3800, Australia, 174) Terrestrial Ecology Unit, Dept. of Biology, Ghent University, B-9000 Gent, Belgium, 175) Finnish Meteorological Institute, Climate System Research, PoB503, 00101 Helsinki, Finland, 176) INAR Institute for Atmospheric and Earth System Research/Physics, Faculty of Science, POBox 68 FI-00014 University of Helsinki, Finland, 177) Interuniversity Institute for Earth System Research, University of Granada, Granada 18006 Spain, 178) CNR Institute for Agricultural and Forestry Systems in the Mediterranean, P.le Enrico Fermi 1 - Loc. del Granatello, 80055, Portici (Napoli) Italy, 179) Faculty of Forestry, Technical University in Zvolen, T.G.Masaryka 24, 960 01 Zvolen, Slovakia, 180) CNR Insitute for Agricultural and Forestry Systems in the Mediterranean, P.le Enrico Fermi 1 - Loc. del Granatello, 80055, Portici (Napoli) Italy, 181) School of Pure & Applied Sciences, Environmental Conservation & Management Programme Open University of Cyprus, PO Box 12794, 2252 Latsia, Nicosia, 182) Department of Biology - Aquatic Biology, Aarhus University, Ole Worms Allé 1, 8000 Aarhus C, Denmark, 183) Aarhus Institute of Advanced Studies, AIAS Høegh-Guldbergs Gade 6B, 8000 Aarhus, Denmark, 184) CNR Institute of BioEconomy, Via Gobetti 101, 40129 Bologna, Italy, 185) Department of Forest Botany, Dendrology and Geobiocoenology, Faculty of Forestry and Wood Technology, Mendel University in Brno, Zemedelska 1, 613 00 Brno, Czech Republic, 186) Regional Centre for Integrated Environmental Monitoring, Odesa National I.I. Mechnikov University, 7 Mayakovskogo lane, 65082 Odesa, Ukraine, 187) Department of Agroecology, Aarhus University, 20 Blichers Allé, 8830 Tjele, Denmark, 188) NGO New Energy, 11 Bakulina str., 61166 Kharkiv, Ukraine, 189) Biological Dynamics of Forest Fragments Project, Coordenação de Dinâmica Ambiental, Instituto Nacional de Pesquisas da Amazônia, Manaus, AM CEP 69067-375, Brazil., 190) Swiss Federal Institute for Forest, Snow and Landscape Research (WSL), CH-8903 Birmensdorf, Switzerland., 191) Department of Biology, University of Antwerp, Universiteitsplein 1, 2610 Wilrijk, Belgium, 192) Department of Botany and Biodiversity Research Centre, University of British Columbia, Vancouver, BC, Canada, 193) Province of Antwerp, Koningin Elisabethlei 22, 2018 Antwerpen, Belgium, 194) Institute of Plant and Animal Ecology of Ural Division of

Russian Academy of Science, 8 Marta st., 202, Ekaterinburg, Russia, 195) Department of Earth and Environmental Sciences, University of Pavia, Via S. Epifanio 14, Pavia, Italy, 196) Faculty of Science and Technology, Free University of Bolzano, Piazza Università 5, 39100 Bolzano, Italy, 197) Climate Change Unit, Environmental Protection Agency of Aosta Valley, Loc. La Maladière, 48, 11020 Saint-Christophe, Italy, 198) University of Freiburg, Chair of Geobotany, Schänzlestrasse 1, 79104 Freiburg, Germany, 199) Environment and Sustainability Institute, University of Exeter, Penryn Campus, Cornwall TR10 9FE, United Kingdom, 200) Centre for Ecosystem Science, School of Biological, Earth and Environmental Sciences, UNSW Sydney, NSW 2052, Sydney, Australia, 201) Department of Biology, Washington University in St. Louis, St. Louis, MO 63130, USA., 202) Department of Animal Biology, Institute of Biology, University of Campinas, Campinas, SP, CEP 13083-862, Brazil, 203) National Wildlife Research Centre, Environment and Climate Change Canada, Carleton University, 1125 Colonel by Drive, Ottawa, ON K1A 0H3, Canada, 204) School of Life and Environmental Sciences, Deakin University, Burwood, Victoria, Australia, 3125, 205) Institute for Alpine Environment, Eurac Research, Viale Druso 1, 39100 Bozen/Bolzano, Italy, 206) Institute of Biology, Dept. of Molecular Botany, University of Hohenheim, 70599 Stuttgart, Germany, 207) Instituto de Matemática Aplicada San Luis, IMASL, CONICET and Universidad Nacional de San Luis, Ejército de los Andes 950, D5700HHW San Luis, Argentina, 208) Cátedra de Climatología Agrícola (FCA-UNER), Ruta 11, km 10, Oro Verde, Entre Ríos, Argentina, 209) Grupo de Ecología de Invasiones, INIBIOMA, CONICET/ Universidad Nacional del Comahue, Av. de los Pioneros 2350, Bariloche 8400, Argentina, 210) CSIC, Global Ecology Unit CREAF- CSIC-UAB, Bellaterra, 08193, Catalonia, Spain., 211) CREAF, E08193, Cerdanyola del Vallès, Catalonia, Spain, 212) Mountains of the Moon University, P.O Box 837, Fort Portal, Uganda, 213) National Agricultural Research Organisation, Mbarara Zonal Agricultural Research and Development Institute, P.O Box 389, Mbarara , Uganda, 214) Department of Agroecology, Aarhus University, Blichers Allé 20, 8830 Tjele, Denmark, 215) Department of Biology, Lund University, SE-223 62 Lund, Sweden, 216) Department of Earth and Environmental Sciences, University of Pavia, Via S. Epifanio 14, 27100 Pavia, Italy, 217) Institute of Botany and Landscape Ecology, University Greifswald, D-17487 Greifswald, Germany, 218) V.N. Sukachev Institute of Forest SB RAS, Krasnoyarsk, Russia, 219) Institute of Ecology and Earth Sciences, University of Tartu, Lai 40, Tartu 51005, Estonia, 220) Department of Biology , Aarhus University, Ole Worms Allé 1, 8000 Aarhus C, Denmark, 221) Department of Biology and Ecology Center, Utah State University, 5305 Old Main Hill, Logan, UT 84322, USA, 222) Department of Life Sciences, Imperial College, Silwood Park Campus, Ascot, Berkshire SL5 7PY, UK, 223) Landscape Ecology, Institute of Terrestrial Ecosystems, Department of Environmental Systems Science, ETH Zürich, 8092 Zürich, Switzerland, 224) Unit of Land Change Science, Swiss Federal Research Institute WSL, 8903 Birmensdorf, Switzerland, 225) Department of Biology, Washington University in St. Louis, Campus Box 1137, 1 Brookings Drive, St. Louis, MO 63130 USA, 226) School of Ecology and Environment Studies, Nalanda University, Rajgir, India, 227) Department of Animal and Plant Sciences, University of Sheffield, Western Bank, Sheffield, S10 2TN, U.K., 228) CESAM & Department of Environment, University of Aveiro, 3810-193 Aveiro, Portugal, 229) Department of Agronomy, Food, Natural resources, Animals and Environment - University of Padua, 35020 Legnaro, Italy, 230) Univ. Savoie Mont Blanc, CNRS, Univ. Grenoble Alpes, EDYTEM, F-73000 Chambéry, France, 231) Universitat Autònoma de Barcelona, E08193 Bellaterra (Cerdanyola del\r\nVallès), Catalonia, Spain, 232) Department of Ecology and Biogeography, Faculty of Biological and Veterinary Sciences, Nicolaus Copernicus University, Toruń, Poland, 233) Centre for Climate Change Research, Nicolaus Copernicus University, Toruń, Poland, 234) A. Borza Botanic Garden, Babeș-Bolyai University, Cluj-Napoca, Romania, 235) Faculty of Biology and Geology, Department of Taxonomy and Ecology, Babeș-Bolyai University, Cluj-Napoca, Romania, 236) E. G. Racoviță Institute, Babeș-Bolyai University, Cluj-Napoca, Romania, 237) Centre for Sustainable Ecosystem Solutions, School of Earth, Atmospheric and Life Sciences, University of Wollongong, Wollongong, New South Wales, 2522, Australia, 238) University of Applied Sciences Trier, Environmental Campus Birkenfeld, 55761 Birkenfeld, Germany, 239) Institut Universitaire de France, 1 Rue Descartes, 75231 Paris cedex 05, France, 240) Swiss Federal Institute for Forest, Snow and Landscape Research WSL, Zuercherstrasse 111, 8903 Birmensdorf, Switzerland, 241) Securing Antarctica's Environmental Future, School of Earth, Atmospheric and Life Sciences, University of Wollongong, 2522 Australia, 242) Aquatic Ecology & Environmental Biology, Institute for Water and Wetland Research, Faculty of Science, Radboud University Nijmegen, AJ 6525 Nijmegen, The Netherlands., 243) University of Notre Dame, Department of Biological Sciences and the Environmental Change Initiative, 244) Swiss National Park, Chastè Planta-Wildenberg, 7530 Zernez, Switzerland, 245) Remote Sensing Laboratories, Dept. of Geography, University of Zurich, Winterthurerstrasse 190, 8057 Zurich, Switzerland, 246) CIRAD, UMR Eco&Sols, BP1386, CP18524, Dakar, Senegal, 247) Eco&Sols, Univ Montpellier, CIRAD, INRAE, IRD, Institut Agro, Montpellier, France, 248) LMI IESOL, Centre IRD-ISRA de Bel Air, BP1386, CP18524, Dakar, Senegal, 249) Parc national des Ecrins - Domaine de Charance - 05000 GAP - France, 250) Universidad Nacional de San Antonio Abad del Cusco, Cusco, Perú, 251) Centro de Investigación de la Biodiversidad Wilhelm L. Johannsen, Cusco, Perú, 252) Biological Dynamics of Forest Fragments Project, PDBFF, Instituto Nacional de Pesquisas da Amazônia, Av. André Araujo, 2936 - Petrópolis, Manaus, Amazonas, 69067-375, Brazil, 253) Department of Ecology and Environmental Science, Umeå University, 901 87 Umeå, Sweden, 254) Institute of Bio- and Geosciences (IBG-3): Agrosphere, Forschungszentrum Jülich GmbH, Jülich, Germany, 255) Chair of Soil Science and Geomorphology, Department of Geosciences, University of Tuebingen, 72070 Tuebingen, Germany, 256) Department of Geography, The University of British Columbia, Vancouver, BC V6T 1Z2, 257) Department of Ecology, University of Innsbruck, Technikerstrasse 25, 6020 Innsbruck, Austria, 258) Department of Botany and Biodiversity Research, Rennweg 14, 1030 Vienna, 259) Princeton School of Public and International Affairs, Princeton University, Princeton, NJ 08540, USA, 260) Université de Lorraine, AgroParisTech, INRAE, Silva, 54000 Nancy, France., 261) Department of Soil Science and Landscape Management, Faculty of Earth Sciences and Spatial Management, Nicolaus Copernicus University, Toruń, Poland, 262) Terra Nova National Park, Parks Canada Agency, Glovertown NL, A0G3Y0, 263) Universidade Estadual do Norte Fluminense Darcy Ribeiro, Campos dos Goytacazes, Rio de Janeiro, Brazil, 264) National Forest Centre, Forest Research Institute Zvolen, T. G. Masaryka 22, 96001 Zvolen, Slovakia, 265) Asian School of Environment, Nanyang Technological University, 42 Nanyang Ave, Singapore 639815, Singapore, 266) Department of Geography, University of British Columbia, 1984 West Mall, Vancouver, BC V6T 1Z2, 267) Department of Earth and Environmental Sciences, Celestijnenlaan 200E, 3001 Leuven, Belgium, 268) Universidade Federal da Paraíba, Departamento de Geociências. Cidade Universitária, João Pessoa - PB, CEP 58051-900, Brasil, 269) Goethe-Universität Frankfurt, Department of Physical Geography, Altenhöferallee 1, 60438 Frankfurt am Main, Germany, 270) Department of Evolution, Ecology, and Organismal Biology, University of California Riverside, Riverside, CA, 92521, USA, 271) Department of Natural History, NTNU University Museum, Norwegian University of Science and Technology, NO-7491 Trondheim Norway, 272) UR 'Ecologie et Dynamique des Systèmes Anthropisées' (EDYSAN, UMR 7058 CNRS-UPJV), Univ. de Picardie Jules Verne, Amiens, France, 273) EnvixLab, Dipartimento di Bioscienze e Territorio, Università degli Studi del Molise, Via Duca degli Abruzzi s.n.c., 86039 Termoli, Italy, 274) Institute of Meteorology and Climate Research (IMK), Department of Atmospheric Environmental Reserach (IFU), Karlsruhe Institute of Technology (KIT), Kreuzeckbahn Straße 19, 82467 Garmisch-Partenkirchen, Germany, 275) Swedish University of Agricultural Sciences, SLU Swedish Species Information Centre, Almas allé 8 E, 75651 Uppsala, Sweden, 276) University Duisburg-Essen, Faculty for Biology, Universitätsstr. 5, 45141 Essen, Germany, 277) Department of Geosciences and Natural Resource Management, University of Copenhagen, Øster Voldgade 10, DK-1350 Copenhagen, Denmark, 278) Experimental Plant Ecology, Institute of Botany and Landscape Ecology, University of Greifswald, partner in the Greifswald Mire Centre, D-17487 Greifswald, Germany, 279) Fondation J.-M. Aubert, 1938 Champex-Lac, Switzerland, 280) Département de Botanique et Biologie végétale, Université de Genève, Case postale 71, CH-1292 Chambésy, Switzerland, 281) Department of Geography and Earth Sciences, Aberystwyth University, Wales, UK, 282) Center for Systematic Biology, Biodiversity and Bioresources - 3B, Babeș-Bolyai University, Cluj-Napoca, Romania, 283) Northern Environmental Geoscience Laboratory, Department of Geography and Planning, Queen's University, 284) Graduate School of Life and Environmental Sciences, Osaka Prefecture University, 599-8531, Japan, 285) Nature Research Centre, Akademijos 2, 08412 Vilnius, Lithuania, 286) Institute of Biological Research Cluj-Napoca, National Institute of Research and Development for Biological Sciences, Bucharest, Romania, 287) CNR Institute for BioEconomy, Via Giovanni Caproni, 50144 Firenze, Italy, 288) The Ecosystem Management Research Group (ECOBE), University of Antwerp, 2610 Wilrijk (Antwerpen), Belgium, 289) Plant Conservation and Population Biology, Department of Biology, KU Leuven, Kasteelpark Arenberg 31, 3001 Heverlee, Belgium, 290) A.N. Severtsov Institute of Ecology and Evolution, Russian Academy of Sciences, 119071, Leninsky pr.33, Moscow, Russia, 291) Netherlands Institute of Ecology, Droevendaalsesteeg 10, 6708 PB, Wageningen, 292) Plant Ecology & Nature Conservation Group Wageningen University , Droevendaalse Steeg 3a 6708 PB Wageningen, 293) Centre for Integrative Ecology, School of Life and Environmental Sciences, Deakin University, Burwood, Victoria, Australia, 3125, 294) CAVElab - Computational and Applied Vegetation Ecology, Department of Environment, Ghent University, Coupure Links 653, 9000 Gent, Belgium, 295) Earth Surface Processes Team, Centre for Environmental and Marine Studies (CESAM), Dept. Environment and Planning, University of Aveiro, 3810-193, Aveiro, Portugal, 296) Instituto Pirenaico de Ecología, IPE-CSIC. Av. Llano de la Victoria, 16. 22700 Jaca (Huesca) Spain, 297) CNR - Institute for Agricultural and Forestry Systems in the Mediterranean, P.le Enrico Fermi 1- Loc. del Granatello, 80055, Portici, (Napoli), Italy, 298) Institute of Earth Surface Dynamics, Faculty of Geosciences and Environment, University of Lausanne, Géopolis, 1015 Lausanne, Switzerland, 299) Forest Research, Northern Research Station, Roslin, EH25 9SY, UK, 300) Institute of Mountain Hazards and Environment, Chinese Academy of Sciences, Chengdu, P.R. China, 301) Department of Earth and Environmental Sciences, Lehigh University, Bethlehem, PA 18015, United States, 302) Institute for Peat and Mire Research, School of Geographical Sciences, Northeast Normal University, Changchun, Jilin 130024, China, 303) High Meadows Environmental Institute, Princeton University, NJ 08544, USA, 304) Zhejiang Tiantong Forest Ecosystem National Observation and Research Station, School of Ecological and Environmental Sciences, East China Normal University, Shanghai 200241, China, 305) JJL received funding from the National Natural Science Foundation of China (grant nr. 32071538), 306) University of Bayreuth, Ecological-Botanical Gardens, Universitaetsstr. 30, Bayreuth, Germany, 307) Key Laboratory of Geographical Processes and Ecological Security in Changbai Mountains, Ministry of Education, School of Geographical Sciences, Northeast Normal University, Changchun 130024, China

References

Abatzoglou JT, Dobrowski SZ, Parks SA, Hegewisch KC (2018) TerraClimate, a high-resolution global dataset of monthly climate and climatic water balance from 1958–2015. Scientific data, **5**, 170191.

Amatulli G, Domisch S, Tuanmu M-N, Parmentier B, Ranipeta A, Malczyk J, Jetz W (2018) A suite of global, cross-scale topographic variables for environmental and biodiversity modeling. Scientific data, **5**, 180040.

Antão LH, Bates AE, Blowes SA, Waldock C, Supp SR, Magurran AE, Dornelas M, Schipper AM (2020) Temperature-related biodiversity change across temperate marine and terrestrial systems. Nature ecology & evolution, **4**, 927-933.

Ashcroft MB, Cavanagh M, Eldridge MDB, Gollan JR (2014) Testing the ability of topoclimatic grids of extreme temperatures to explain the distribution of the endangered brush-tailed rock-wallaby (*Petrogale penicillata*). Journal of biogeography, **41**, 1402-1413.

Ashcroft MB, Chisholm LA, French KO (2008) The effect of exposure on landscape scale soil surface temperatures and species distribution models. Landscape Ecology, **23**, 211-225.

Ashcroft MB, Gollan JR (2012) Fine-resolution (25 m) topoclimatic grids of near-surface (5 cm) extreme temperatures and humidities across various habitats in a large (200 x 300 km) and diverse region. International Journal of Climatology, **32**, 2134-2148.

Barnes R, Sahr K, Evenden G, Johnson A, Warmerdam F (2017) dggridR: discrete global grids for R. R package version 0.1.12.

Bergstrom DM, Wienecke BC, Van Den Hoff J, Hughes L, Lindenmayer DB, Ainsworth TD, Baker CM, Bland L, Bowman DM, Brooks ST (2021) Combating ecosystem collapse from the tropics to the Antarctic. Global change biology, **27**, 1692-1703.

Berner LT, Massey R, Jantz P, Forbes BC, Macias-Fauria M, Myers-Smith I, Kumpula T, Gauthier G, Andreu-Hayles L, Gaglioti BV (2020) Summer warming explains widespread but not uniform greening in the Arctic tundra biome. Nature Communications, **11**, 1-12.

Bond-Lamberty B, Thomson A (2018) A Global Database of Soil Respiration Data, Version 4.0. ORNL DAAC.

Booth TH, Nix HA, Busby JR, Hutchinson MF (2014) BIOCLIM: the first species distribution modelling package, its early applications and relevance to most current MAXENT studies. Diversity and Distributions, **20**, 1-9.

Bramer I, Anderson B, Bennie J, Bladon A, De Frenne P, Hemming D, Hill RA, Kearney MR, Körner C, Korstjens AH, Lenoir J, Maclean IMD, Marsh CD, Morecroft MD, Ohlemüller R, Slater HD, Suggitt AJ, Zellweger F, Gillingham PK (2018) Advances in monitoring and modelling climate at ecologically relevant scales. Advances in Ecological Research, **58**, 101-161.

Bruelheide H, Dengler J, Purschke O, Lenoir J, Jiménez-Alfaro B, Hennekens SM, Botta-Dukát Z, Chytrý M, Field R, Jansen F (2018) Global trait–environment relationships of plant communities. Nature ecology & evolution, **2**, 1906.

Bütikofer L, Anderson K, Bebber DP, Bennie JJ, Early RI, Maclean IM (2020) The problem of scale in predicting biological responses to climate. Global change biology, **26**, 6657-6666.

Chen L, Aalto J, Luoto M (2021) Significant shallow–depth soil warming over Russia during the past 40 years. Global and Planetary Change, **197**, 103394.

Cooper EJ (2014) Warmer shorter winters disrupt Arctic terrestrial ecosystems. Annual Review of Ecology, Evolution, and Systematics, **45**, 271-295.

Copernicus Climate Change Service (C3s) (2019) C3S ERA5-Land reanalysis. (ed Copernicus Climate Change Service).

Coûteaux M-M, Bottner P, Berg B (1995) Litter decomposition, climate and litter quality. Trends in ecology & evolution, **10**, 63-66.

Crowther TW, Todd-Brown KE, Rowe CW, Wieder WR, Carey JC, Machmuller MB, Snoek B, Fang S, Zhou G, Allison SD (2016) Quantifying global soil carbon losses in response to warming. Nature, **540**, 104-108.

Daly C (2006) Guidelines for assessing the suitability of spatial climate data sets. International Journal of Climatology, **26**, 707-721.

Davis E, Trant A, Hermanutz L, Way RG, Lewkowicz AG, Collier LS, Cuerrier A, Whitaker D (2020) Plant–Environment Interactions in the Low Arctic Torngat Mountains of Labrador. Ecosystems, 1-21.

De Frenne P, Lenoir J, Luoto M, Scheffers BR, Zellweger F, Aalto J, Ashcroft M, Christiansen D, Decocq G, De Pauw K, Govaert S, Greiser C, Gril E, Hampe A, Jucker T, Klinges D, Koelemeijer I, Lembrechts J, Marrec R, Meeussen C, Ogee J, Tyystjarvi V, Vangansbeke P, Hylander K (2021) Forest microclimates and climate change: importance, drivers and future research agenda. Global change biology, **In press**.

De Frenne P, Rodríguez-Sánchez F, Coomes DA, Baeten L, Verstraeten G, Vellend M, Bernhardt-Römermann M, Brown CD, Brunet J, Cornelis J (2013) Microclimate moderates plant responses to macroclimate warming. Proceedings of the National Academy of Sciences, **110**, 18561-18565.

De Frenne P, Zellweger F, Rodríguez-Sánchez F, Scheffers BR, Hylander K, Luoto M, Vellend M, Verheyen K, Lenoir J (2019) Global buffering of temperatures under forest canopies. Nature ecology & evolution, **3**, 744-749.

Dinerstein E, Olson D, Joshi A, Vynne C, Burgess ND, Wikramanayake E, Hahn N, Palminteri S, Hedao P, Noss R (2017) An ecoregion-based approach to protecting half the terrestrial realm. BioScience, **67**, 534-545.

Du E, Terrer C, Pellegrini AF, Ahlström A, Van Lissa CJ, Zhao X, Xia N, Wu X, Jackson RB (2020) Global patterns of terrestrial nitrogen and phosphorus limitation. Nature Geoscience, **13**, 221-226.

Fick SE, Hijmans RJ (2017) WorldClim 2: new 1-km spatial resolution climate surfaces for global land areas. International Journal of Climatology, **37**, 4302-4315.

Geiger R (1950) *The climate near the ground,* Cambridge, Massachusets, USA, Harvard University Press.

Gistemp Team (2021) GISS Surface Temperature Analysis (GISTEMP), version 4. NASA Goddard Institute for Space Studies.

Gorelick N, Hancher M, Dixon M, Ilyushchenko S, Thau D, Moore R (2017) Google Earth Engine: Planetary-scale geospatial analysis for everyone. Remote Sensing of Environment, **202**, 18-27.

Gottschall F, Davids S, Newiger-Dous TE, Auge H, Cesarz S, Eisenhauer N (2019) Tree species identity determines wood decomposition via microclimatic effects. Ecology and evolution, **9**, 12113-12127.

Graae BJ, Vandvik V, Armbruster WS, Eiserhardt WL, Svenning J-C, Hylander K, Ehrlén J, Speed JD, Klanderud K, Bråthen KA, Milbau A, Opedal OH, Alsos IG, Ejrnaes R, Bruun HH, Birks HJB, Westergaard KB, Birks HH, Lenoir J (2018) Stay or go–how topographic complexity influences alpine plant population and community responses to climate change. Perspectives in plant ecology, evolution and systematics, **30**, 41-50.

Greiser C, Meineri E, Luoto M, Ehrlén J, Hylander K (2018) Monthly microclimate models in a managed boreal forest landscape. Agricultural and Forest Meteorology, **250**, 147-158.

Grünberg I, Wilcox EJ, Zwieback S, Marsh P, Boike J (2020) Linking tundra vegetation, snow, soil temperature, and permafrost. Biogeosciences, **17**, 4261-4279.

Grundstein A, Todhunter P, Mote T (2005) Snowpack control over the thermal offset of air and soil temperatures in eastern North Dakota. Geophysical Research Letters, **32**.

Hall DK, Riggs GA, Salomonson VV, Digirolamo NE, Bayr KJ (2002) MODIS snow-cover products. Remote Sensing of Environment, **83**, 181-194.

Hengl T, De Jesus JM, Heuvelink GB, Gonzalez MR, Kilibarda M, Blagotić A, Shangguan W, Wright MN, Geng X, Bauer-Marschallinger B (2017) SoilGrids250m: Global gridded soil information based on machine learning. Plos One, **12**, e0169748.

Hennon PE, D'amore DV, Witter DT, Lamb MB (2010) Influence of forest canopy and snow on microclimate in a declining yellow-cedar forest of Southeast Alaska. Northwest Science, **84**, 73-87.

Hursh A, Ballantyne A, Cooper L, Maneta M, Kimball J, Watts J (2017) The sensitivity of soil respiration to soil temperature, moisture, and carbon supply at the global scale. Global change biology, **23**, 2090-2103.

Johnston AS, Meade A, Ardö J, Arriga N, Black A, Blanken PD, Bonal D, Brümmer C, Cescatti A, Dušek J (2021) Temperature thresholds of ecosystem respiration at a global scale. Nature ecology & evolution, **5**, 487-494.

Karger DN, Conrad O, Böhner J, Kawohl T, Kreft H, Soria-Auza RW, Zimmermann NE, Linder HP, Kessler M (2017a) Climatologies at high resolution for the earth's land surface areas. Scientific data, **4**, 170122.

Karger DN, Conrad O, Böhner J, Kawohl T, Kreft H, Soria-Auza RW, Zimmermann NE, Linder HP, Kessler M (2017b) Data from: Climatologies at high resolution for the earth's land surface areas. In: *Dryad Digital Repository.*

Kattge J, Bönisch G, Diaz S, Lavorel S, Prentice IC, Leadley P, Tautenhahn S, Werner G, Günther A (2019) TRY plant trait database-enhanced coverage and open access. Global change biology, **26**, 119-188.

Kearney M, Shine R, Porter WP (2009) The potential for behavioral thermoregulation to buffer "cold-blooded" animals against climate warming. Proceedings of the National Academy of Sciences, **106**, 3835-3840.

Kearney MR, Gillingham PK, Bramer I, Duffy JP, Maclean IM (2019) A method for computing hourly, historical, terrain-corrected microclimate anywhere on Earth. Methods in Ecology and Evolution, **11**, 38-43.

Kissling WD, Walls R, Bowser A, Jones MO, Kattge J, Agosti D, Amengual J, Basset A, Van Bodegom PM, Cornelissen JH (2018) Towards global data products of Essential Biodiversity Variables on species traits. Nature ecology & evolution, **2**, 1531-1540.

Körner C, Hiltbrunner E (2018) The 90 ways to describe plant temperature. Perspectives in plant ecology, evolution and systematics, **30**, 16-21.

Körner C, Paulsen J (2004) A world-wide study of high altitude treeline temperatures. Journal of biogeography, **31**, 713-732.

Lembrechts J, Aalto J, Ashcroft M, De Frenne P, Kopecký M, Lenoir J, Luoto M, Maclean IM, Consortium S, Nijs I (2020) SoilTemp: call for data for a global database of near-surface temperature. Global change biology, **26**, 6616-6629.

Lembrechts J, Lenoir J, Scheffers BR, De Frenne P (2021) Time for countrywide microclimate networks. Global Ecology and Biogeography.

Lembrechts JJ, Lenoir J (2019) Microclimatic conditions anywhere at any time! Global change biology.

Lembrechts JJ, Lenoir J, Roth N, Hattab T, Milbau A, Haider S, Pellissier L, Pauchard A, Ratier Backes A, Dimarco RD (2019) Comparing temperature data sources for use in species distribution models: From in-situ logging to remote sensing. Global Ecology and Biogeography, **28**, 1578-1596.

Lembrechts JJ, Nijs I (2020) Microclimate shifts in a dynamic world. Science, **368**, 711-712.

Lenoir J, Bertrand R, Comte L, Bourgeaud L, Hattab T, Murienne J, Grenouillet G (2020) Species better track climate warming in the oceans than on land. Nature ecology & evolution, **4**, 1044-1059.

Luojus K, Pulliainen J, Takala M, Derksen C, Rott H, Nagler T, Solberg R, Wiesmann A, Metsamaki S, Malnes E (2010) Investigating the feasibility of the GlobSnow snow water equivalent data for climate research purposes. In: *2010 IEEE International Geoscience and Remote Sensing Symposium.* IEEE.

Maclean IM, Duffy JP, Haesen S, Govaert S, De Frenne P, Vanneste T, Lenoir J, Lembrechts JJ, Rhodes MW, Van Meerbeek K (2021) On the measurement of microclimate. Methods in Ecology and Evolution.

Maclean IM, Klinges DH (2021) Microclimc: A mechanistic model of above, below and within-canopy microclimate. Ecological Modelling, **451**, 109567.

Maclean IM, Mosedale JR, Bennie JJ (2019) Microclima: An r package for modelling meso-and microclimate. Methods in Ecology and Evolution, **10**, 280-290.

Myers-Smith IH, Kerby JT, Phoenix GK, Bjerke JW, Epstein HE, Assmann JJ, John C, Andreu-Hayles L, Angers-Blondin S, Beck PS (2020) Complexity revealed in the greening of the Arctic. Nature Climate Change, **10**, 106-117.

Niittynen P, Heikkinen RK, Aalto J, Guisan A, Kemppinen J, Luoto M (2020) Fine-scale tundra vegetation patterns are strongly related to winter thermal conditions. Nature Climate Change, **10**, 1143-1148.

Niittynen P, Luoto M (2018) The importance of snow in species distribution models of arctic vegetation. Ecography, **41**, 1024-1037.

O'donnell MS, Ignizio DA (2012) Bioclimatic predictors for supporting ecological applications in the conterminous United States. US Geological Survey Data Series, **691**, 4-9.

Obu J, Westermann S, Bartsch A, Berdnikov N, Christiansen HH, Dashtseren A, Delaloye R, Elberling B, Etzelmüller B, Kholodov A (2019) Northern Hemisphere permafrost map based on TTOP modelling for 2000–2016 at 1 km2 scale. Earth-Science Reviews, **193**, 299-316.

Olden JD, Lawler JJ, Poff NL (2008) Machine learning methods without tears: a primer for ecologists. The Quarterly review of biology, **83**, 171-193.

Opedal OH, Armbruster WS, Graae BJ (2015) Linking small-scale topography with microclimate, plant species diversity and intra-specific trait variation in an alpine landscape. Plant Ecology & Diversity, **8**, 305-315.

Overland JE, Wang M, Walsh JE, Stroeve JC (2014) Future Arctic climate changes: Adaptation and mitigation time scales. Earth's Future, **2**, 68-74.

Pastorello G, Papale D, Chu H, Trotta C, Agarwal D, Canfora E, Baldocchi D, Torn M (2017) A new data set to keep a sharper eye on land-air exchanges. Eos, Transactions American Geophysical Union (Online), **98**.

Perera-Castro AV, Waterman MJ, Turnbull JD, Ashcroft MB, Mckinley E, Watling JR, Bramley-Alves J, Casanova-Katny A, Zuniga G, Flexas J (2020) It is hot in the sun: Antarctic mosses have high temperature optima for photosynthesis despite cold climate. Frontiers in Plant Science, **11**, 1178.

Pleim JE, Gilliam R (2009) An indirect data assimilation scheme for deep soil temperature in the Pleim–Xiu land surface model. Journal of Applied Meteorology and Climatology, **48**, 1362-1376.

Portillo-Estrada M, Pihlatie M, Korhonen JFJ, Levula J, Frumau AKF, Ibrom A, Lembrechts JJ, Morillas L, Horvath L, Jones SK, Niinemets U (2016) Climatic controls on leaf litter decomposition across European forests and grasslands revealed by reciprocal litter transplantation experiments. Biogeosciences, **13**, 1621-1633.

Potter KA, Woods HA, Pincebourde S (2013) Microclimatic challenges in global change biology. Global change biology, **19**, 2932-2939.

R Core Team (2020) R: a language and environment for statistical computing, R Foundation for Statistical Computing.

Richardson LF (1922) *Weather prediction by numerical process*, Cambridge university press.

Rosenberg NJ, Kimball B, Martin P, Cooper C (1990) From climate and CO2 enrichment to evapotranspiration. Climate change and US water resources., 151-175.

Santoro M (2018) GlobBiomass—Global datasets of forest biomass. PANGAEA10, **1594**.

Scherrer D, Schmid S, Körner C (2011) Elevational species shifts in a warmer climate are overestimated when based on weather station data. International journal of Biometeorology, **55**, 645-654.

Schimel DS, Braswell B, Mckeown R, Ojima DS, Parton W, Pulliam W (1996) Climate and nitrogen controls on the geography and timescales of terrestrial biogeochemical cycling. Global Biogeochemical Cycles, **10**, 677-692.

Schimel JP, Bilbrough C, Welker JM (2004) Increased snow depth affects microbial activity and nitrogen mineralization in two Arctic tundra communities. Soil Biology and Biochemistry, **36**, 217-227.

Senior RA, Hill JK, Edwards DP (2019) Global loss of climate connectivity in tropical forests. Nature Climate Change, **9**, 623-626.

Smith M, Riseborough D (1996) Permafrost monitoring and detection of climate change. Permafrost and Periglacial Processes, **7**, 301-309.

Smith M, Riseborough D (2002) Climate and the limits of permafrost: a zonal analysis. Permafrost and Periglacial Processes, **13**, 1-15.

Soudzilovskaia NA, Douma JC, Akhmetzhanova AA, Van Bodegom PM, Cornwell WK, Moens EJ, Treseder KK, Tibbett M, Wang YP, Cornelissen JH (2015) Global patterns of plant root colonization intensity by mycorrhizal fungi explained by climate and soil chemistry. Global Ecology and Biogeography, **24**, 371-382.

Stefan V, Levin S (2018) Plotbiomes: Plot Whittaker biomes with ggplot2. R package version 0.0. 0.9001.

Steidinger BS, Crowther TW, Liang J, Van Nuland ME, Werner GD, Reich PB, Nabuurs G-J, De-Miguel S, Zhou M, Picard N (2019) Climatic controls of decomposition drive the global biogeography of forest-tree symbioses. Nature, **569**, 404-408.

Van Den Hoogen J, Geisen S, Routh D, Ferris H, Traunspurger W, Wardle DA, De Goede RG, Adams BJ, Ahmad W, Andriuzzi WS (2019) Soil nematode abundance and functional group composition at a global scale. Nature, **572**, 194-198.

Van Den Hoogen J, Robmann N, Routh D, Lauber T, Van Tiel N, Danylo O, Crowther TW (2021) A geospatial mapping pipeline for ecologists. bioRxiv.

Wang K, Dickinson RE (2012) A review of global terrestrial evapotranspiration: Observation, modeling, climatology, and climatic variability. Reviews of Geophysics, **50**.

Way RG, Lewkowicz AG (2018) Environmental controls on ground temperature and permafrost in Labrador, northeast Canada. Permafrost and Periglacial Processes, **29**, 73-85.

White HJ, León-Sánchez L, Burton VJ, Cameron EK, Caruso T, Cunha L, Dirilgen T, Jurburg SD, Kelly R, Kumaresan D (2020) Methods and approaches to advance soil macroecology. Global Ecology and Biogeography, **29**, 1674-1690.

Whiteman CD (1982) Breakup of temperature inversions in deep mountain valleys: Part I. Observations. Journal of Applied Meteorology, **21**, 270-289.

Wild J, Kopecký M, Macek M, Šanda M, Jankovec J, Haase T (2019) Climate at ecologically relevant scales: A new temperature and soil moisture logger for long-term microclimate measurement. Agricultural and Forest Meteorology, **268**, 40-47.

Wood S (2012) mgcv: Mixed GAM Computation Vehicle with GCV/AIC/REML smoothness estimation.

World Meteorological Organization (2008) *Guide to Meteorological Instruments and Methods of Observation,* Geneva, WMO-No. 8.

Xu T, Hutchinson M (2011) ANUCLIM version 6.1 user guide. The Australian National University, Fenner School of Environment and Society, Canberra.

Xu Y, Ramanathan V, Victor DG (2018) Global warming will happen faster than we think. Nature.

Zellweger F, De Frenne P, Lenoir J, Vangansbeke P, Verheyen K, Bernhardt-Römermann M, Baeten L, Hédl R, Berki I, Brunet J, Van Calster H, Chudomelová M, Decocq G, Dirnböck T, Durak T, Heinken T, Jaroszewicz B, Kopecký M, Malis F, Macek M, Marek M, Naaf T, Nagel TA, Ortmann-Ajkai A, Petrik P, Pielech R, Reczynska K, Schmidt W, Standovár T, Swierkosz K,

Teleki B, Vild O, Wulf M, Coomes D (2020) Forest microclimate dynamics drive plant responses to warming. Science, **368**, 772-775.
Zhang Y, Sherstiukov AB, Qian B, Kokelj SV, Lantz TC (2018) Impacts of snow on soil temperature observed across the circumpolar north. Environmental Research Letters, **13**, 044012.
Zhang Y, Wang S, Barr AG, Black T (2008) Impact of snow cover on soil temperature and its simulation in a boreal aspen forest. Cold Regions Science and Technology, **52**, 355-370.
Zhou S, Williams AP, Lintner BR, Berg AM, Zhang Y, Keenan TF, Cook BI, Hagemann S, Seneviratne SI, Gentine P (2021) Soil moisture–atmosphere feedbacks mitigate declining water availability in drylands. Nature Climate Change, 1-7.
Zomer RJ, Trabucco A, Bossio DA, Verchot LV (2008) Climate change mitigation: A spatial analysis of global land suitability for clean development mechanism afforestation and reforestation. Agriculture, ecosystems & environment, **126**, 67-80.

Supplementary figures and tables

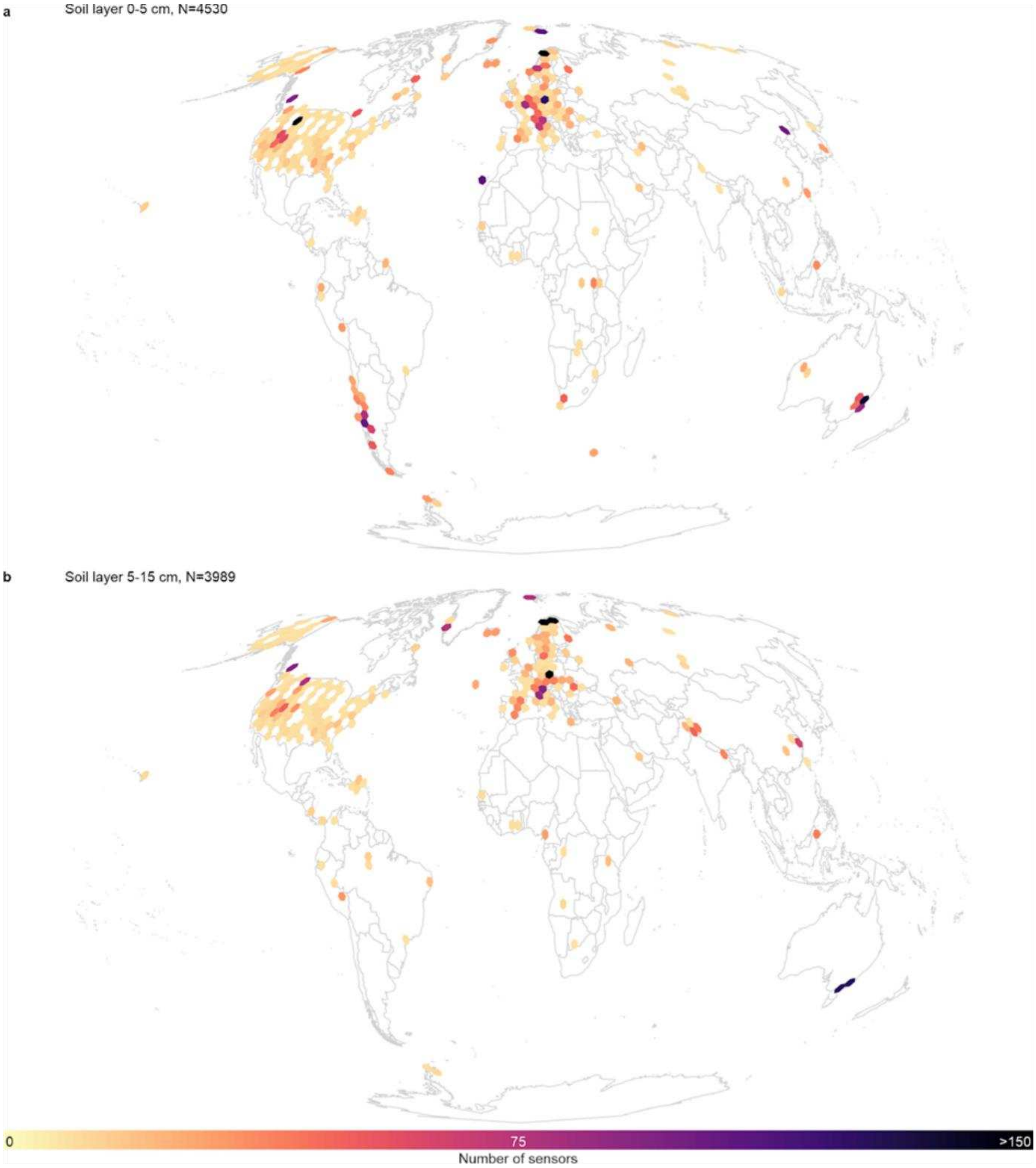

Fig. S1: Global distribution of the in-situ measurements. Distribution of all sensors in the topsoil (0–5 cm depth, (a), N = 4,530) and the second layer (5–15 cm depth, (b), N = 3,989). Background world map in Mollweide projection, hexagons with a resolution of approximately 70,000 km². Note that sensors appearing here and not in Fig. 1a or Fig. S3 covered time series of less than one year, and thus were only used in the monthly models (see methods for details).

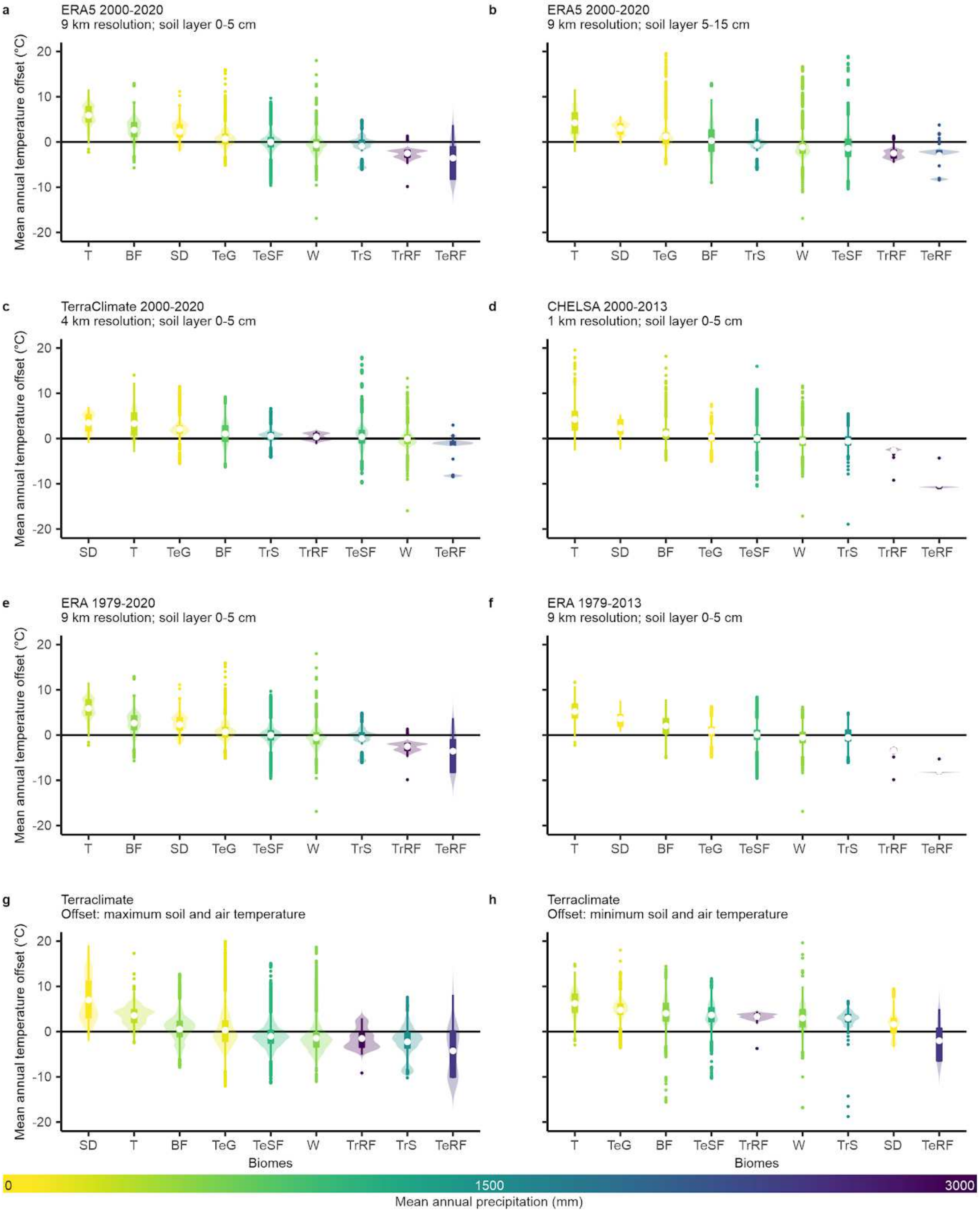

Fig. S2: Annual temperature offsets per biome (as in Fig. 1b), for the first (0–5 cm depth) and second soil layer (5–15 cm depth) and for different air temperature data sources and time periods. Box- and violin plots of the mean annual temperature offsets per Whittaker biome, ordered and coloured by mean annual precipitation. As a standard, we used ERA5L (2000-2020, 9 km resolution) and the topsoil (0–5 cm, (a), see also Fig. 1b). We compare now with the second soil layer (5–15 cm depth, b), with TerraClimate (2000-2020, 4 km resolution, c) and CHELSA (2000-2013, 1 km resolution, d), with ERA5L for the full period (1979-2020, e) and the period matching the bioclimatic variables (1979-2013, f). We also calculate offsets between maximum (95th percentile, g) soil and air temperature, and minimum (5th percentile, h) soil and air temperature, with maximum and minimum air temperature based on TerraClimate. Panels (c) to (h) all use the topsoil data (0–5 cm depth). All panels show relatively consistent results (i.e. strongly positive offsets in tundra, boreal forests, subtropical deserts and temperate grasslands, and weakly negative offsets in tropical savannas and temperate and tropical rainforests). Only annual soil temperature minima were on average higher than corresponding air temperature minima in all but one biomes.

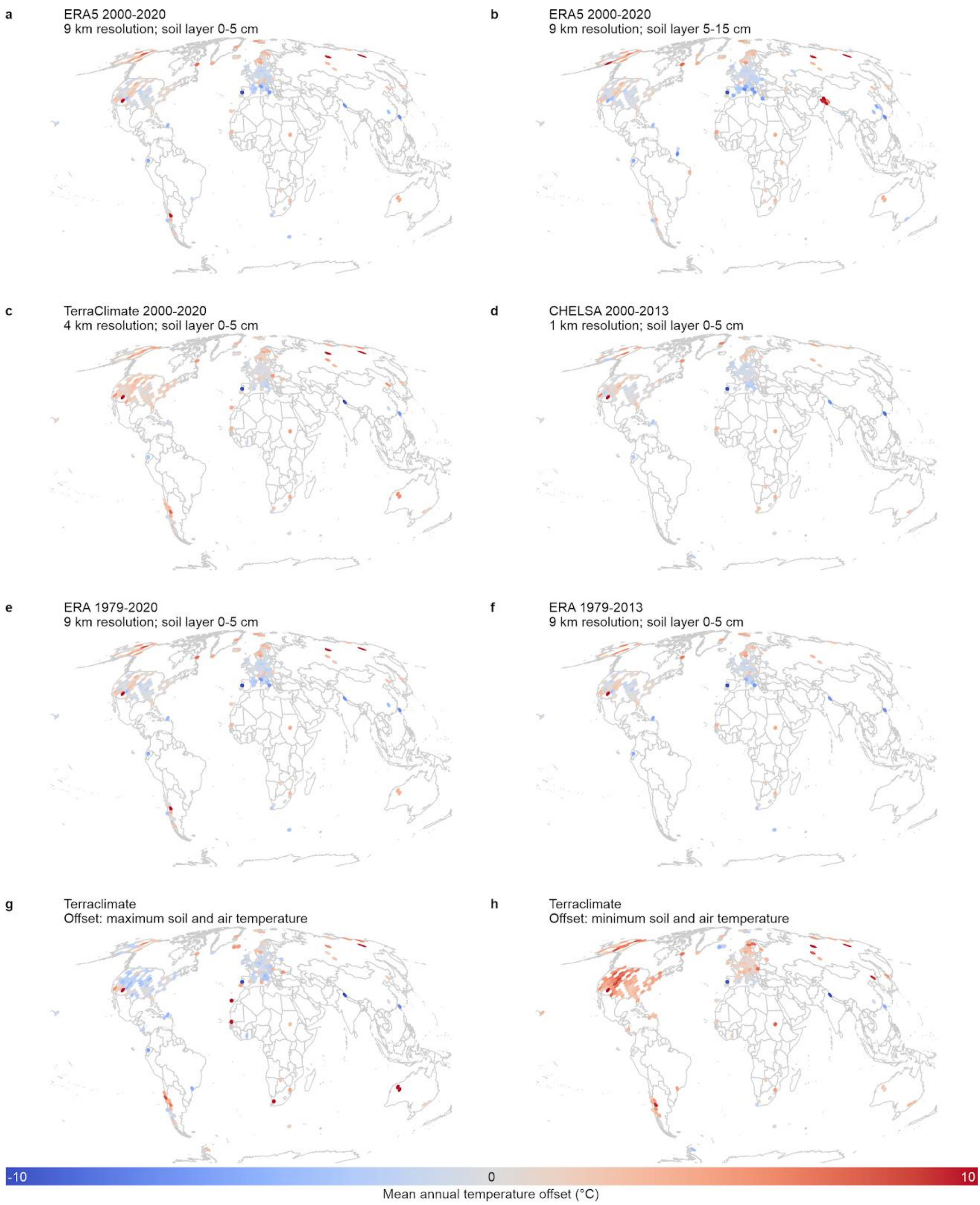

Fig. S3: Annual temperature offset maps (as in Fig. 1a), for the first (0–5 cm depth) and second soil layer (5–15 cm depth), for different air temperature data sources and time periods, and for maximum and minimum temperature. Distribution of sensors across the globe, coloured by the annual offset (in °C) between in-situ measured soil temperature and modelled air temperature. As a standard in Fig. 1a, we used ERA5L (2000-2020, 9 km² resolution) and the topsoil (0–5 cm, also here in a). We compare now with the second soil layer (5–15 cm depth, b), with TerraClimate (2000-2020, 4 km² resolution, c) and CHELSA (2000-2013, 1 km² resolution, d) for the topsoil layer, and with ERA5L for the full period (1979-2020,e) and the period matching the bioclimatic variables (1979-

2013, f). We also calculate offsets between maximum (95^{th} percentile, g) soil and air temperature, and minimum (5^{th} percentile, h) soil and air temperature, with maximum and minimum air temperature based on TerraClimate. Background world map in MollWeide projection, offsets averaged per hexagon with a resolution of approximately 70,000 km^2, made using the dggridR-package in R. Conclusions about consistency between methods similar as in Fig. S2.

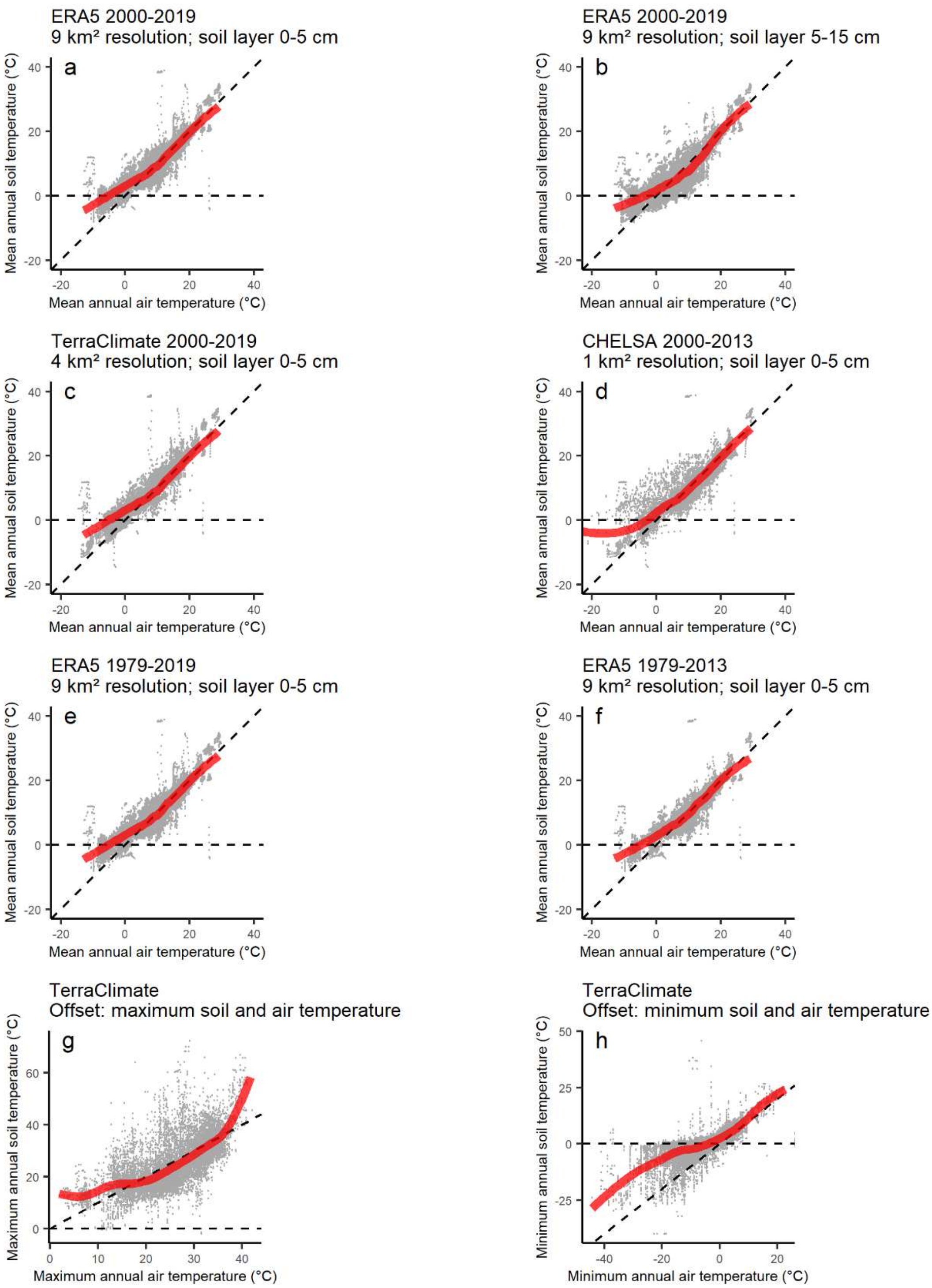

Fig. S4: Relationship between mean annual soil and air temperature at a 1 × 1 km resolution. Point cloud of in-situ mean annual soil temperature (°C) as a function of gridded mean annual air temperature for all in-situ measurements averaged at a 1 × 1 km resolution. As a standard, we used ERA5L (2000-2020, 9 km² resolution) and the topsoil (0–5 cm depth, a). We compare this first with the second soil layer (5–15 cm depth, b). We also compare with analyses for the top soil layer using TerraClimate (2000-2020, 4 km² resolution, c) and CHELSA (2000-2013, 1 km² resolution, d), and with ERA5L for the full period (1979-2020, e) and the period matching the bioclimatic variables (1979-2013, f). We also plot offsets between maximum (95^{th} percentile, g) soil and air temperature, and minimum (5^{th} percentile, h) soil and air temperature, with maximum and minimum air temperature based on

TerraClimate. Straight dashed line indicate a thermal offset of 0°C, and the 1:1-relationship between soil and air temperature, thick red lines the relationship based on generalized additive models, indicating in all cases warmer soil than air temperatures in cold extremes, yet slightly cooler soils at intermediate temperatures (except for h).

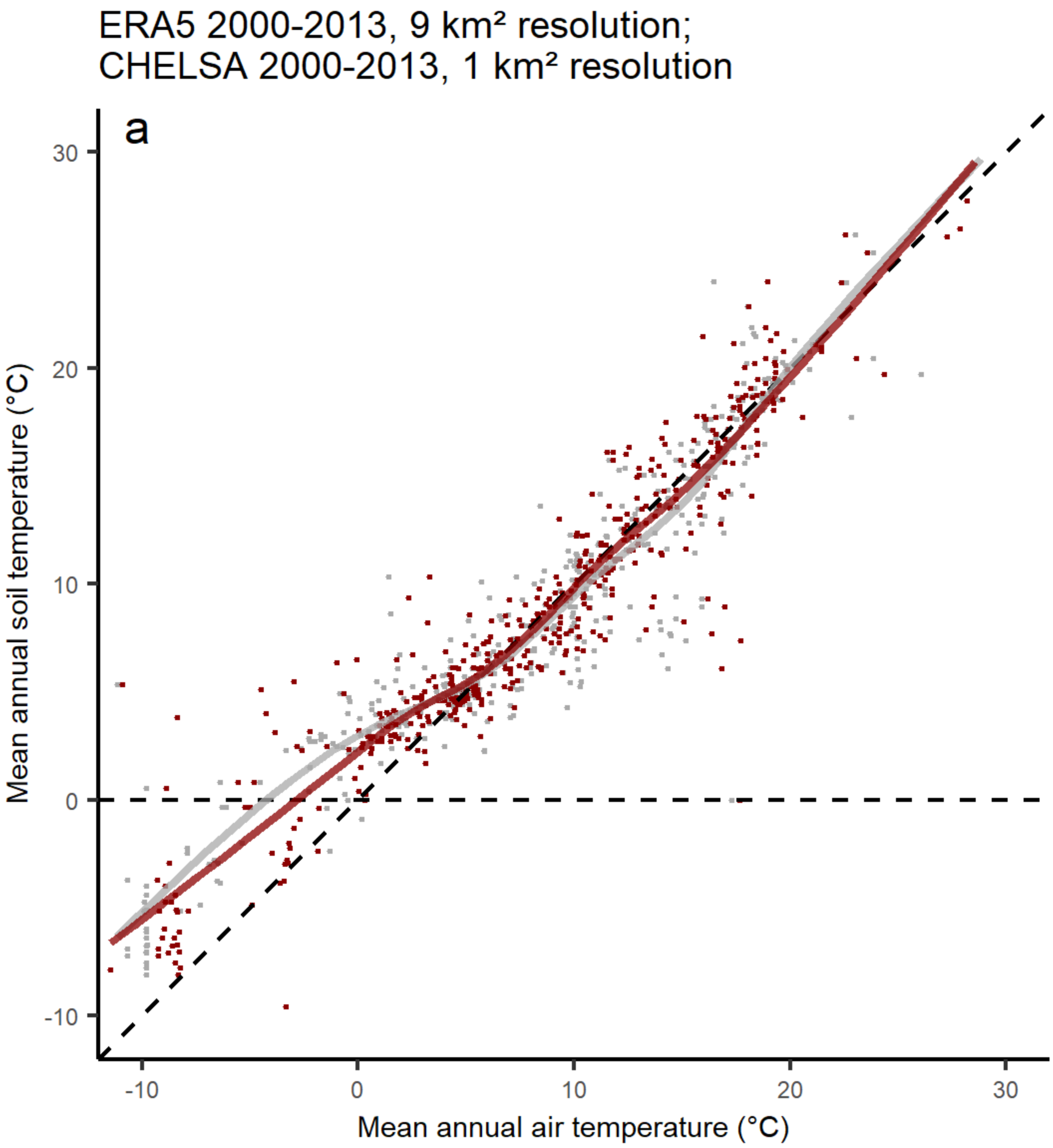

Fig. S5: Relationship between mean annual soil and air temperature for ERA5L (grey) versus CHELSA (red). Point cloud of in-situ mean annual soil temperature (°C) as a function of gridded mean annual air temperature for all in-situ measurements averaged at 1 km², between 2000 and 2013, for ERA5L (grey, 9-km² resolution) and CHELSA (dark red, 1 × 1 km resolution). Straight dashed line indicate a thermal offset of 0°C, and the 1:1-relationship between soil and air temperature, grey and red lines the relationship based on generalized additive models. As in Fig. S4, yet highlighting the strong overlap in pattern when using CHELSA vs ERA5L.

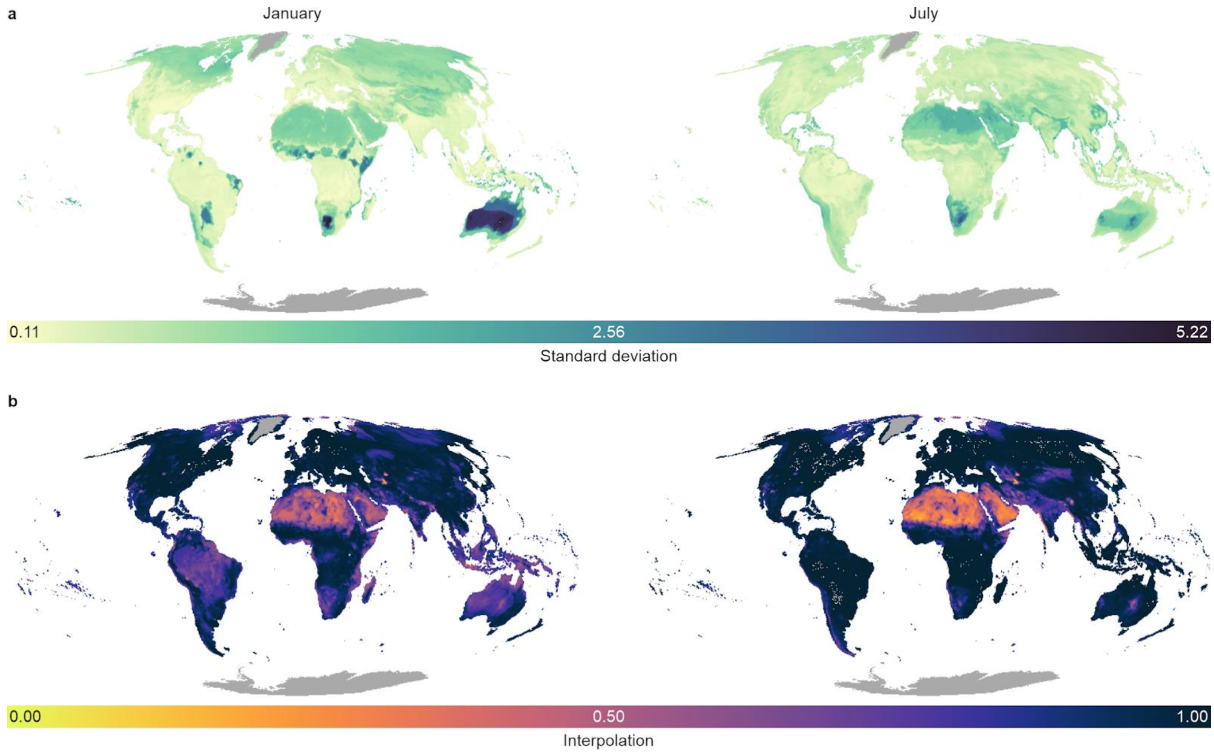

Fig. S6: Predictive performance of the temperature offset models in the second soil layer (5–15 cm depth). Analyses for the temperature offset between in-situ second soil layer (5–15 cm depth) temperature and free-air temperature. (a) Predicted standard deviation from a cross-validation analysis that iteratively varied the set of covariates (explanatory data layers) and model hyperparameters (i.e., number of variables per split; minimum leaf population) across 100 models and evaluated model strength using 10-fold cross-validation, for January (left) and July (right), as examples of the two most contrasting months. (b) The fraction of axes in the multidimensional environmental space for which the pixel lies inside the range of data covered by the sensors in the database. Pixels with low values indicate that the model has to extrapolate for many of the environmental layers for that specific pixel.

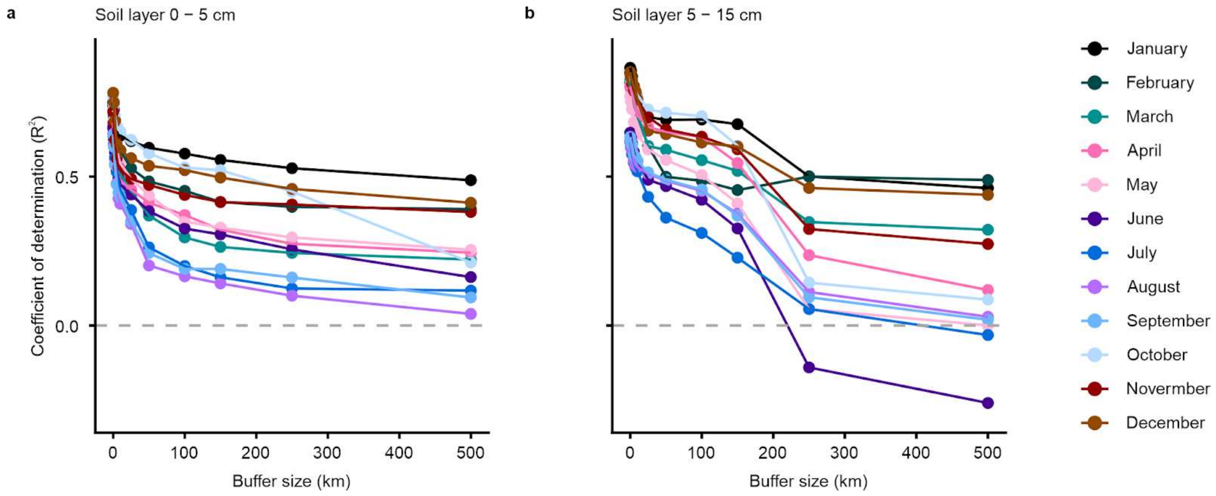

Fig. S7: spatial leave-one-out cross-validation. R^2 of all monthly models at the two soil depths using a spatial leave-one-out cross validation approach. This approach trains a model for each sample in the dataset on all remaining samples, with an increasingly large buffer around that focal sample. Note that a decrease in R^2 should be expected with increasing buffer size due to the removal of parts of the environmental gradient from the training dataset. Nevertheless, results show that spatial autocorrelation differs across the months, with uneven global data coverage likely causing lowest confidence for May to September at 5–15 cm depth, where use of data outside of the environmental gradient as covered by the data is thus particularlydiscouraged (see Fig 5b and Fig. S6b).

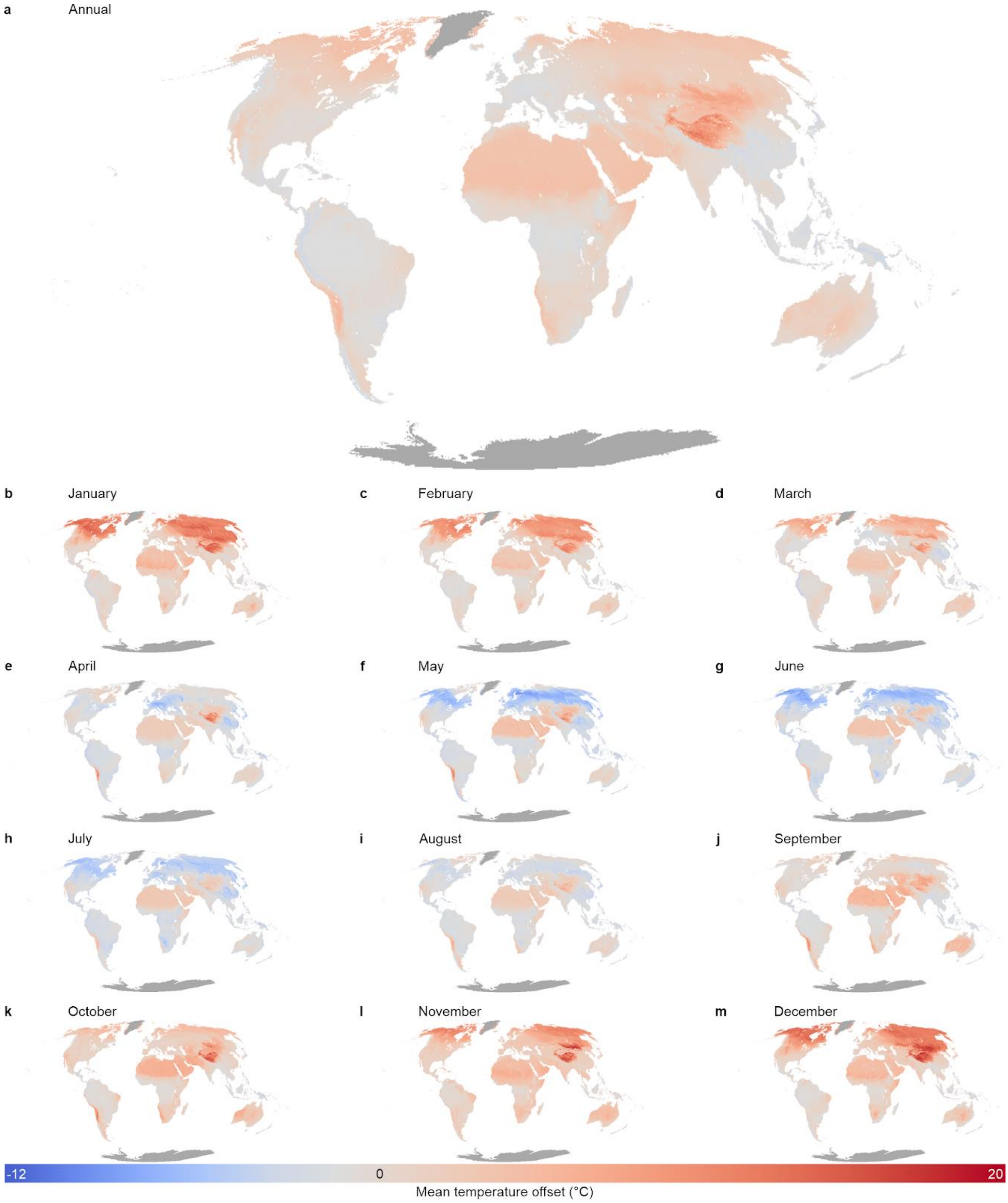

Fig. S8: Modelled mean temperature offset in the second soil layer (5–15 cm depth). Modelled annual (a) and monthly (b-m) temperature offset (in °C) between in-situ measured soil temperature (second soil layer, 5–15 cm depth) and modelled air temperature, in addition to the first soil layer (0–5 cm depth) used in Fig. 2.

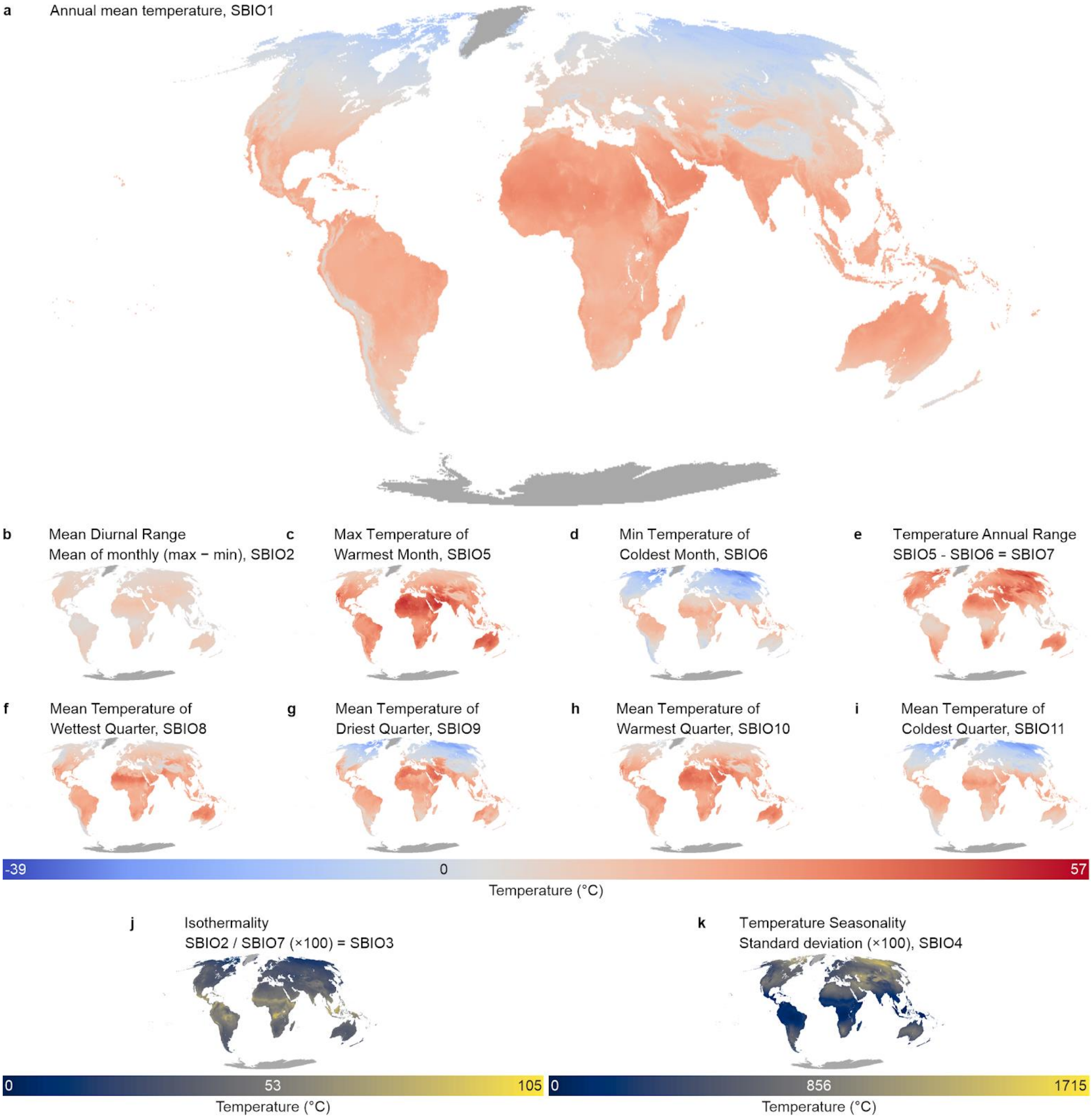

Fig. S9: Bioclimatic variables for the second soil layer. Global maps of bioclimatic variables for the second soil layer (5–15 cm depth) climate, calculated using the maps of monthly temperature offsets (see Fig. 2, Fig. S8) and the bioclimatic variables for air temperature from CHELSA (*4*).

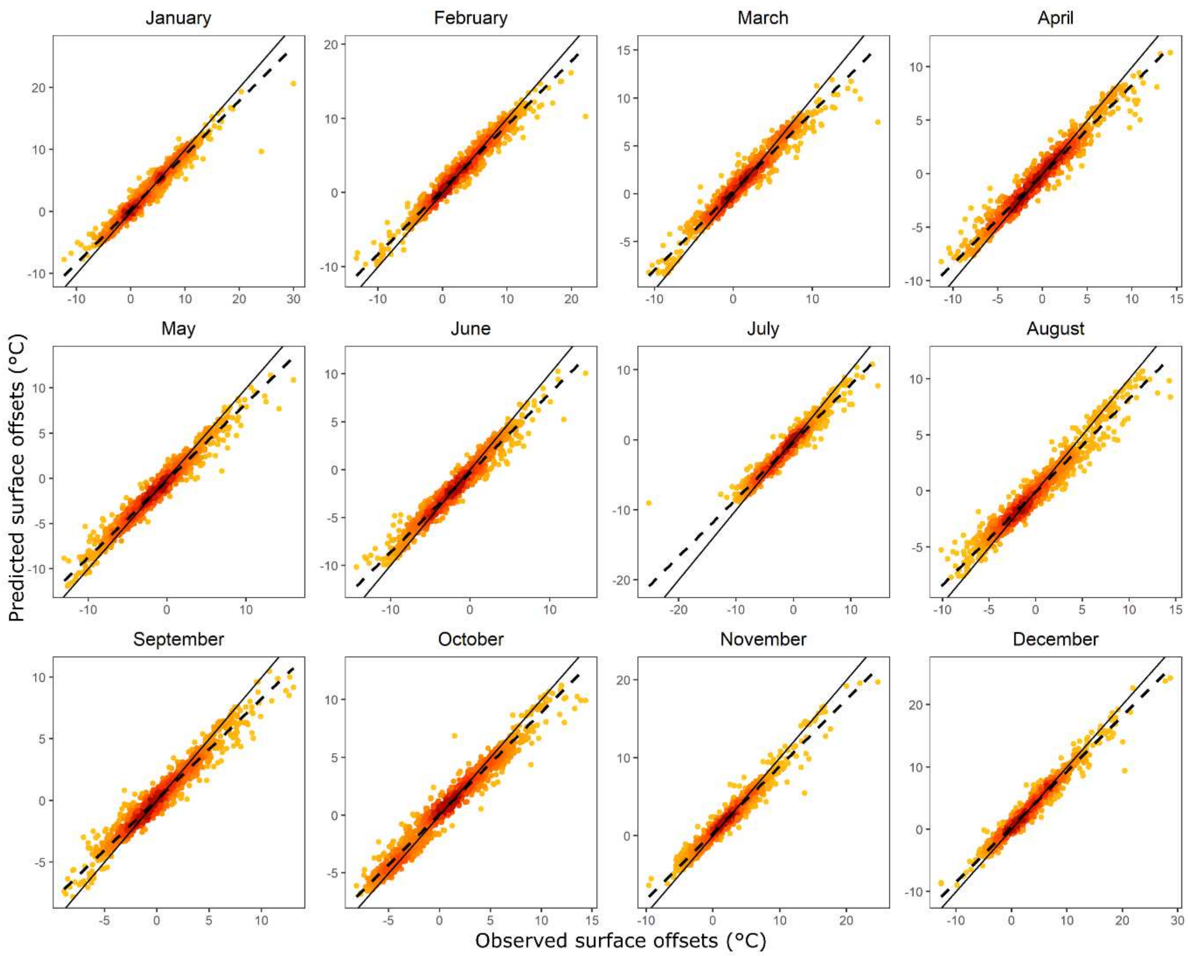

Fig. S10: Observed versus predicted temperature offsets. Correlative plots showing temperature offsets – averaged at a 1 × 1 km resolution – as observed in the field, versus those as predicted by the models, separately for each month. Colours show density of points (darker = higher point density). Dashed lines from linear regressions; solid lines refer to the 1:1-line of perfect correlation between predicted and observed offsets.

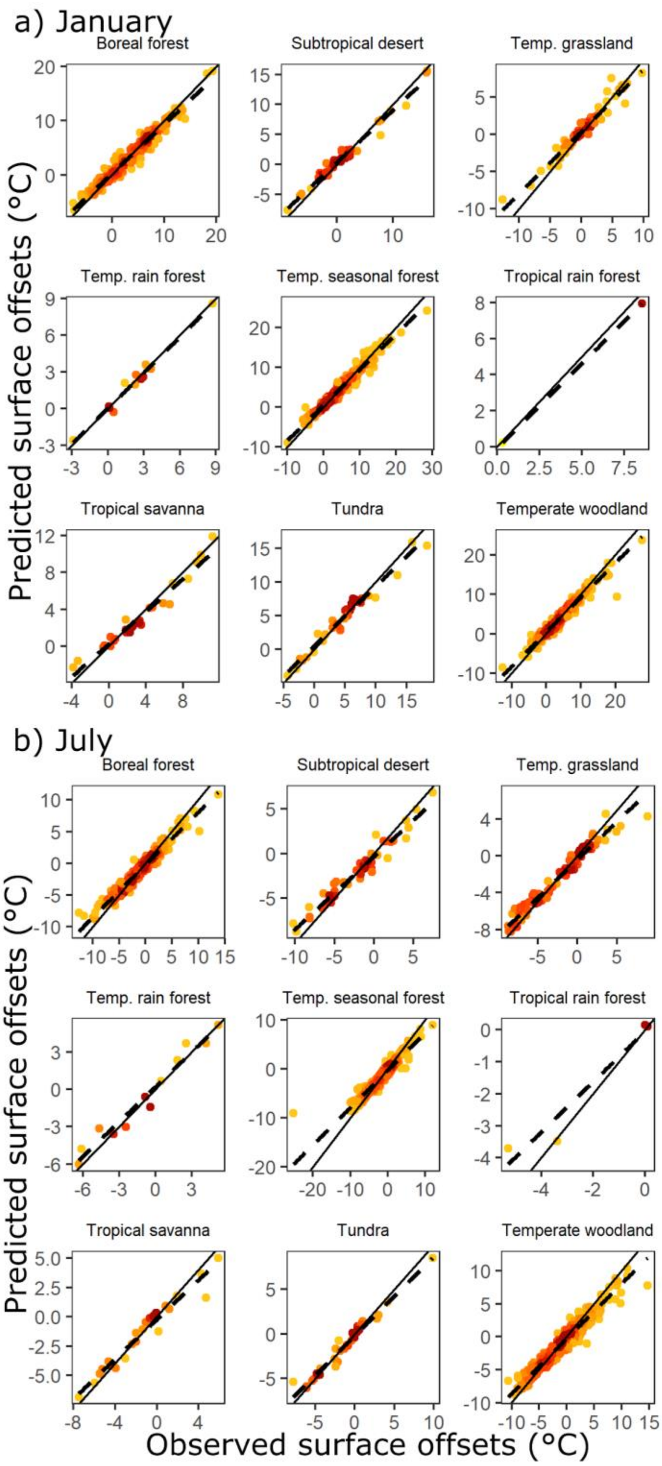

Fig. S11: Observed versus predicted temperature offsets per biome. Correlative plots showing temperature offsets – averaged at a 1 × 1 km resolution – as observed in the field, versus those as predicted by the models, separately for each biome, for January (a) and July (b). Colours show density of points (darker = high point density). Dashed lines from linear regressions; solid lines refer to the 1:1-line of perfect correlation between predicted and observed offsets.

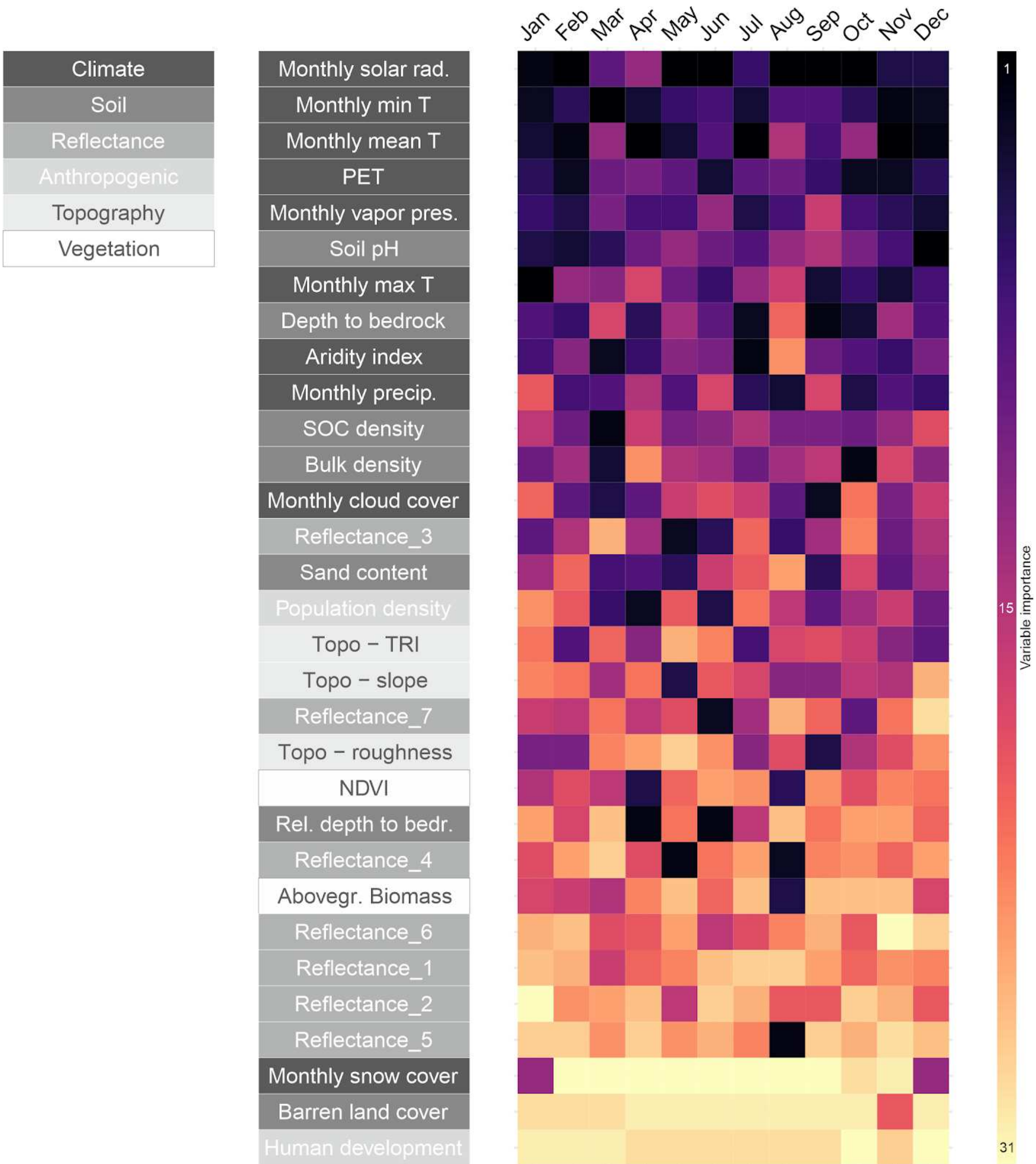

Fig. S12: Relative importance of explanatory variables. Explanatory variables in all twelve monthly analyses sorted by mean Variable Importance (computed based on the summed decrease of impurity over all trees in the forest that results from the variable used at a node; higher for variables with a higher importance) across all models of the first soil layer (0–5 cm depth) (first variable = ranked on average most importantly across all twelve monthly models). Colours represent relative variable importance (ranked from 1 to 31, with 1 the highest importance) within each monthly model for the topsoil (0–5 cm depth). T = temperature, PET = potential evapotranspiration, SOC = soil organic carbon, TRI = topographic roughness index, NDVI = normalized difference vegetation index. For full details on all explanatory variable layers, see Data S1.

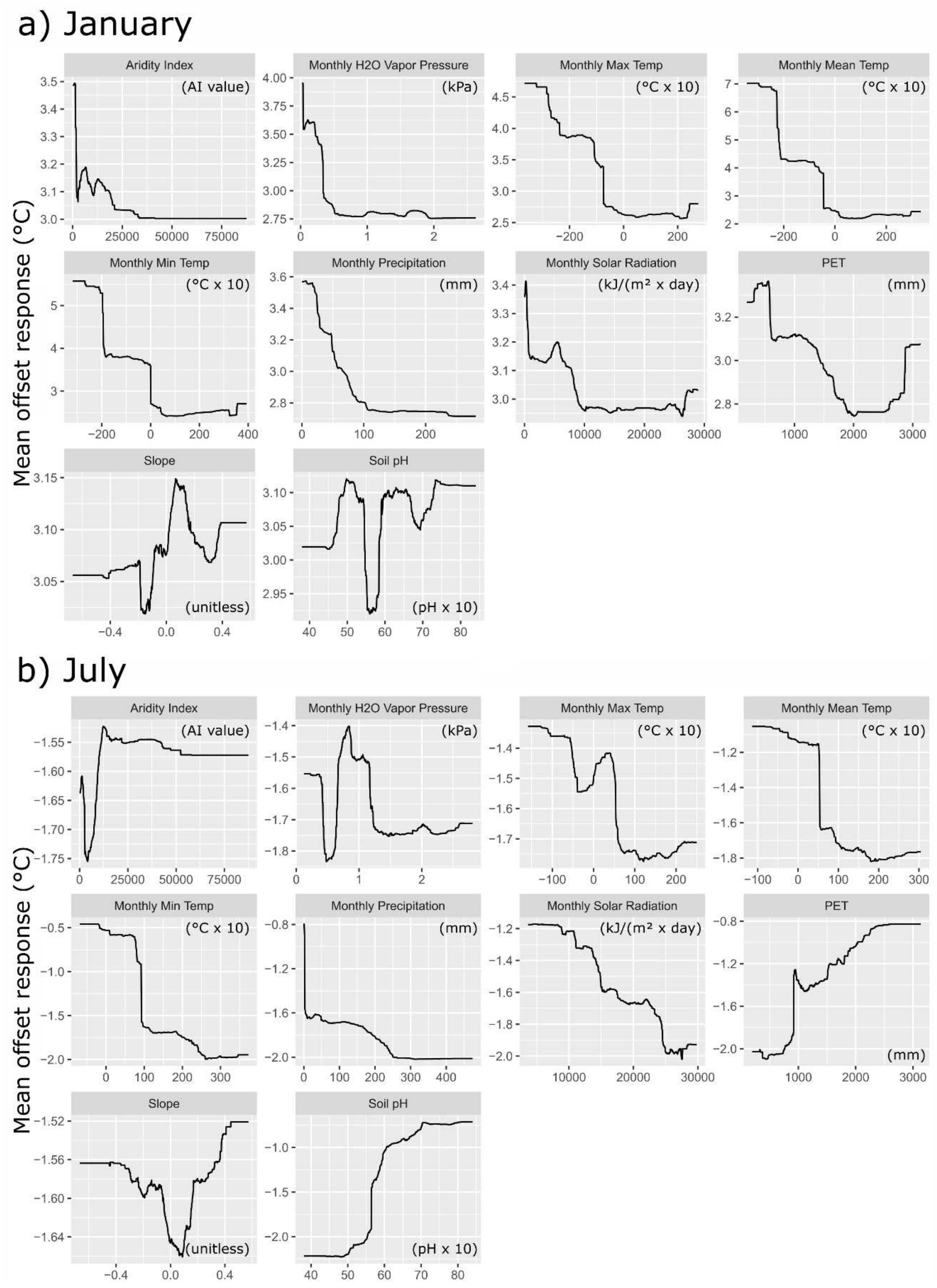

Fig. S13: Partial dependency plots of main effects. Partial dependency plots of the 10 most important variables (selection based on the mean Feature Importance from Fig. S12) for January (a; top) and July (b; bottom), as examples of the two most contrasting months. Results for the first soil layer (0–5 cm depth).

Supplementary Tables

Table S1: Number of sensors from the most common logger brands in the top soil (left, 0–5 cm depth) and the second soil layer (right, 5–15 cm depth). Other sensors include among others Decagon devices, GeoPrecision data loggers, thermocouples and TinyTags.

Logger brand	Number of sensors	
	0–5 cm	**5–15 cm**
iButton	1840	1685
TOMST	512	1090
HOBO	689	491
Lascar	247	0
Others	1025	587

Table S2: Number of sensors in each soil layer

Depth of soil layer (cm)	Number of sensors
0–5	4530
5–15	3989
15-30	484
30-60	294
60-100	54
100-200	11

Table S3: Number of data points (in brackets the number of unique pixels after averaging at 1 × 1 km pixel resolution) for each month as used in the models.

Month	N° of data points (0–5 cm)	N° of data points (5–15 cm)
January	6674 (1212)	10130 (977)
February	6649 (1223)	10214 (986)
March	6527 (1184)	10345 (979)
April	6439 (1093)	10266 (989)
May	6611 (1150)	10510 (1003)

June	6537 (1154)	10546 (1011)
July	6874 (1352)	10515 (1141)
August	6960 (1383)	10950 (1098)
September	6690 (1317)	10484 (1019)
October	6991 (1299)	10429 (1018)
November	6995 (1215)	10683 (996)
December	6846 (1193)	10607 (988)

Table S4: Number of unique pixels after averaging the annual data at 1 × 1 km pixel resolution for each biome, as used in Fig. 1. The number of individual annual averages on which this number is based is shown between brackets.

Biome	N° of pixels (0–5 cm)
Boreal forest	240 (10168)
Sub-tropical desert	37 (802)
Temperate grassland	66 (9558)
Temperate rainforest	10 (27)
Temperate seasonal forest	245 (21566)
Tropical rainforest	2 (299)
Tropical savanna	13 (2062)
Tundra	29 (1584)
Temperate woodland	224 (16952)

Table S5: Number of unique pixels after averaging the monthly data at a 1 × 1 km pixel resolution for each biome as used in the models, averaged across all months.

Biome	N° of pixels (0–5 cm)	N° of pixels (5–15 cm)
Boreal forest	284	323
Sub-tropical desert	46	4
Temperate grassland	82	63
Temperate rainforest	12	2
Temperate seasonal forest	349	304
Tropical rainforest	5	9
Tropical savannah	26	31
Tundra	35	34
Temperate woodland	466	353

Table S6: Biome-specific quantile distribution of the estimated aboveground biomass at the 1 x 1 km pixel level (unit: tons/ha i.e., Mg/ha, for the year 2010, Santoro, 2018) for each sensor identified as either measuring in forests (top) or open vegetation (bottom), for all sensors for which the latter information was available (numbers between brackets). Numbers in green indicate sensors under aboveground biomass of 1.00 tons/ha or higher, here identified as forested.

Biome	1%	5%	25%	50%	75%	95%	99%
Forests							
Boreal forest (18)	53.70	60.50	77.50	84.50	106.00	114.15	114.83
Subtropical desert (3)	2.00	2.00	2.00	2.00	38.00	66.80	72.56
Temperate grassland (12)	3.00	3.00	16.00	45.00	86.00	98.00	98.00
Temperate rain forest (7)	53.12	53.60	63.50	76.00	220.00	296.60	322.52
Temperate seasonal for. (227)	17.00	32.50	63.00	101.00	177.00	291.00	431.00
Tropical rain forest (6)	149.50	167.50	245.50	277.50	284.00	313.75	321.15
Tropical savanna (17)	186.00	186.00	186.00	186.00	207.00	224.00	224.00
Tundra (3)	8.04	8.20	9.00	10.00	12.00	13.60	13.92
Temperate woodland (145)	0.00	0.20	8.00	24.00	120.00	218.00	242.36
Open vegetation							
Boreal forest (463)	0.00	0.00	0.00	0.00	53.00	53.00	105.00
Subtropical desert (13)	0.00	0.00	0.00	0.00	0.00	0.00	0.00
Temperate grassland (44)	0.00	0.00	0.00	0.00	0.00	32.00	107.00
Temperate rain forest (0)	-	-	-	-	-	-	-
Temperate seasonal for. (89)	0.00	0.00	0.00	0.00	32.00	223.00	248.08
Tropical rain forest (0)	-	-	-	-	-	-	-
Tropical savanna (0)	-	-	-	-	-	-	-
Tundra (75)	0.00	0.00	0.00	0.00	0.00	6.00	10.00
Temperate woodland (93)	0.00	0.00	1.00	19.00	66.00	171.00	172.00

Table S7: Difference in temperature offset between forested and unforested habitats. Mean and standard deviation of offsets per Whittaker biome for all sensors, and for sensors in forested and non-forested habitats separately. All values averaged at a 1 × 1 km resolution (number between brackets = number of unique 1 × 1 km pixels), only biomes with sufficient number of loggers in forested habitats are shown. Habitat assessment at the location of the sensor based on observations by the contributors, whenever available (60% of sensors).

Biome	All	Forested	Non-forested
Boreal forest	2.47 ± 2.01 (240)	3.40 ± 1.64 (41)	3.12 ± 1.77 (105)
Temperate grasslands	0.92 ± 2.13 (66)	1.39 ± 2.79 (4)	1.30 ± 2.79 (27)
Temperate seasonal forests	0.46 ± 2.79 (245)	-0.82 ± 2.21 (53)	1.00 ± 3.95 (20)
Temperate woodland	-0.12 ± 3.38 (224)	-0.71 ± 3.11 (31)	1.22 ± 4.31 (35)

Data S1. (separate file)

Final selection of global covariate layers used for geospatial modelling. A total of 31 global covariate layers was used in our modelling approach.